Vol. V. No.4 Editor : B.S. Tomar October 2006

Editorial

Computational methods in chemistry have in recent times acquired an important role in understanding the physico-chemical properties of a chemical system both under static and dynamic conditions. This is evident from the award of Nobel prize in chemistry for the year 1998 to professor walter Kohn for his development of density functional theory and to John Pople for his development of computational methods in quantum chemistry. Thus, while the power of computational methods is being used to optimize the synthesis route for a compound of desired property (combinatorial chemistry), it is also providing explanation to the observed phenomena such as stability of a particular species, unusual properties of clusters and nanomaterials, etc. It is to the credit of computational methods that chemists now seek explanation of the observed phenomena through first principles than qualitative arguments. The present bulletin is aimed at highlighting the role of computational methods in unraveling the phenomena that occur in chemical systems. I am grateful to Dr. Swapan K.Ghosh, a theoretical chemist of international repute, who has kindly agreed to be the guest editor of this bulletin. I thank all the authors of the articles for timely submission of their articles but for which this bulletin would not have been published in time. Lastly I hope this thematic bulletin would inspire the young chemists to seek the quantitative explanations of their experimental observations through computational methods.

B.S. Tomar

CONTENTS

From the Secretary's Desk 258

Guest Editorial 261

Quantum Simulations of Water Cluster Anions: Electron Solvation and Hydrogen Bonds 262
Subha Pratihar and Amalendu Chandra

Ab initio Treatment of Large Molecules : Cut-and-Stitch the Tailor's Way 267
Shridhar R. Gadre, Anuja Rahalkara and V. Ganesh

Prediction of Novel Molecular Species with ab initio Quantum Chemical Methods 277
T. K. Ghanty

Fluids at Interfaces – A Theoretical Chemist's Perspective 286
Chandra N. Patra

Excitement at the Bottom: Tuning the Electronic Properties of Clusters through First Principle Calculations 300
Chiranjib Majumder

Chemical Reactivity and Conceptual Density Functional Theory 307
Pratim Kumar Chattaraj and Debesh Ranjan Roy

Electro-Hydrodynamic approach to Study the Rate of Excitation Energy Transfer from a Dye to a Metal Nanoparticle 316
Sangeeta Saini, Somnath Bhowmick, Vijay B. Shenoy and Biman Bagchi,

Nucleus 324

From the Secretary's Desk

IANCAS has so far conducted 62 National Workshops at many universities in the country and more than 300 one-day workshops in schools and colleges. The association's mission is to popularize the subject of radiochemistry and thus enhance the nation's nuclear education infrastructure to meet the manpower requirements of the Nation's energy, environmental, healthcare and security sectors. There is an acute long term shortage of nuclear engineers and scientists to mitigate the forthcoming retirement of nuclear workforce. University Grants Commission (UGC) has not been able to shore up the teaching of nuclear and radiochemistry in university curriculum and many institutes are on the verge of closing this branch of science. It has missed the initiative in visualizing the emerging acceptance of nuclear technology in meeting the energy demand of the nation and the need to promote teaching of this subject.

In most countries including India the science curriculums offered at undergraduate levels do not take sufficient consideration of the basic courses and laboratory studies on nuclear chemistry. As an unavoidable reflection, the attention of graduate level students do not show enough interests to research areas which has resulted in a significant drastic decline in availability of the number of qualified teaching professionals in the nuclear chemistry field in the recent decades.

If the sad situation in the chemistry curriculums continues, it will also not be further possible to find qualified teaching stuff including professors to teach the required courses in any university in the country in the near future. For this reason, the decline should be reversed as soon as possible by revising the existing curriculums to include basic nuclear chemistry courses and laboratory studies in the undergraduate chemistry programs. We need to foster an active nuclear R&D partnership among power utilities, research and regulatory agencies, governments and universities.

Action is a process to reach a goal; action may reflect tumult but when measured and focussed, will yield its objective of stability and peace.

We welcome active participation by scholars and individuals who share our sense of the urgent need to launch such a Nuclear Education Project at this critical and dangerous moment in world history. Readers are requested to write their views through our website.

G.A. Rama Rao

Computational Chemistry

Guest Editor

Swapan K. Ghosh

Theoretical Chemistry Section
Bhabha Atomic Research Centre
Mumbai 400 085

Guest Editorial

Dr. Swapan K. Ghosh

It gives me immense pleasure to present a collection of articles in this Special Issue on "Computational Chemistry". Computation has invaded almost all branches of chemistry, playing a major role in microscopic understanding of the structure, properties and reactivity of molecules, reaction mechanisms, and many other physicochemical phenomena. Theoretical and Computational Chemistry forms an integral component of research in chemistry and is now also emerging, through its interface with other subjects such as materials science, condensed matter physics, chemical engineering and biological sciences, as a major contributor to frontier areas of interdisciplinary research. With the availability of powerful computational resources, it may no longer be a dream to predict the structure and dynamics of complex systems, and to design novel molecules and materials with desired properties for various applications.

A major challenge one faces in this endeavor arises from the need to use different tools for different length and time scales inherent in the description of materials and phenomena. In the microscopic domain, the electronic structure obtainable through the solution of Schrodinger equation of quantum mechanics is relevant, while in the intermediate mesoscopic length scale, classical equations of motion, statistical mechanical description and atomistic simulation are commonly used and in the larger macroscopic length scale, continuum mechanics might suffice.

In this issue, there are articles covering electronic structure to atomistic description and from molecules, clusters, nanoparticles, to liquids. Gadre et al have presented novel methodologies for the ab-initio quantum chemical treatment of large molecules. Prediction of novel molecular species through ab initio calculation has been reported by Ghanty. Elemental clusters have been treated through electronic structure calculation by Majumder, while Chandra et al have investigated molecular clusters using quantum simulation method, the focus being electron solvation and hydrogen bonding in water. Chattaraj et al provides a view of the concepts of chemical reactivity through the window of density functionals. The energy transfer from molecules to nanoparticles through a novel electro-hydrodynamic approach has been investigated by Bagchi et al. The behaviour of fluids at interfaces has been discussed by Patra.

As portrayed in this broad canvas, the range of diversity of applications of computational chemistry is quite evident. It is of course not sufficient to have computation alone and a proper blend of computation with experiment, theory, analysis and modeling can only provide a vivid picture of the chemical world.

I am extremely grateful to the colleagues who contributed articles to this Special Issue. I am also thankful to IANCAS for deciding to bring out this special issue and Dr B.S. Tomar for giving me an opportunity to be associated with it.

Dr. Swapan K. Ghosh *received his Ph.D. in Chemistry from Indian Institute of Technology, Bombay in 1982. At present, he is Head of the Theoretical Chemistry Section, Bhabha Atomic Research Centre, Mumbai and is also Dean-Academic (BARC), Chemical Sciences, Homi Bhabha National Institute (Deemed University). His current research interests include density functional theory, multiscale materials modeling, computational materials science, dynamics in condensed phase and soft condensed matter physics. He is a Fellow of the Indian Academy of Sciences, Bangalore, Indian National Science Academy, New Delhi and National Academy of Sciences, India, Allahabad.*

Quantum Simulations of Water Cluster Anions: Electron Solvation and Hydrogen Bonds

Dr. Subha Pratihar *was born in 1977. She obtained her B.Sc and M.Sc. from the University of Calcutta in 1999 and 2001, respectively. She is currently working for her Ph.D. at IIT Kanpur with a research fellowship from the Council of Scientific and Industrial Research. Her Ph.D. work involves both quantum chemical and finite temperature quantum simulation studies of electron and metal atom solvation in hydrogen bonded clusters, liquids and supercritical fluids.*

Dr. Amalendu Chandra *was born in India in 1963. He received his B.Sc. and M.Sc. in Chemistry from the University of Burdwan, India, in 1984 and 1986, respectively, and his Ph.D. in Chemistry from Indian Institute of Science, Bangalore, in 1991. He was an Izaak Walton Killam postdoctoral fellow at the University of British Columbia before joining Indian Institute of Technology Kanpur as an Assistant Professor in 1993. He is currently a Professor in the Department of Chemistry at IIT Kanpur and a Fellow of the Indian Academy of Sciences. He was a Visiting Assistant Professor at Washington State University in 1997 and a Visiting Professor at Ruhr-Universitaet Bochum in 2002—2003 with a research fellowship from the Alexander von Humboldt Foundation. His research interests include theoretical and computational studies of liquids, interfaces,lusters and supercritical fluids using both classical and quantum methods.*

Abstract

We discuss the role of hydrogen bonds in the solvation of an excess electron in small water clusters at finite temperatures. In addition to a brief overview of recent experimental and quantum chemical studies of the structure, energetics and vibrational spectra of these cluster anions, we also present some preliminary quantum simulation results from our own laboratory. The quantum simulations are performed employing the Car-Parrinello molecular dynamics method where the forces on the nuclei are obtained directly from 'on the fly' quantum electronic structure calculations. We focus on the localization structure of the excess electron, arrangement of solvent molecules around the excess electron, the changes of the overall hydrogen bonded structure of the clusters as compared to those of the neutral ones and vertical detachment energies of the anionic clusters. It is found that the hydrogen bonded structures of the anionic clusters are very different from those of the neutral clusters and dynamically evolves from one conformer to other during the finite temperature simulations. The spatial distribution of the singly occupied molecular orbital shows where and how the excess electron is primarily localized. The results of vertical detachment energies of the anionic clusters provide an insight into the stability of the different isomeric forms of the clusters with the bound excess electron.

Introduction

A free electron can be solvated by polar solvents, such as ammonia [1] and water [2]. The aqueous electron, e^-_{aq}, has been the subject of intense study since its discovery [2] in 1962 but still our understanding of its solvation structure and dynamics is far from complete. A microscopic understanding of solvated electrons in dipolar solvents such as ammonia, water or methanol is extremely important in many areas of chemistry, physics and biology. Although a single water or an

Dr. Subha Pratihar and Dr. Amalendu Chandra, Department of Chemistry, Indian Institute of Technology, Kanpur 208016;
E-mail: amalen@iitk.ac.in

ammonia molecule does not bind an excess electron, yet it is readily solvated by the bulk solvents and clusters of sufficient number of these molecules. This implies that the association of excess electrons with such solvents is a many-body effect requiring a collection of solvent molecules. Over the past few decades, there have been a number of studies on electron solvation in liquid water and ammonia [3-9]. Electron immersed in liquid water, e^-_{aq}, is believed to be trapped in a cavity space bounded by six water molecules [3]. From spin echo modulation analysis, Kevan [3] concluded that an electron is hydrated by six water molecules in an octahedral configuration with one O-H bond of each water molecule oriented toward the electron and referred to it as a wet electron. In recent years, there have been a number of studies on the localization properties of an excess electron in water and ammonia clusters [10-12] and these studies have provided important information on the dependence of electron solvation on cluster size. For example, anionic water clusters $(H_2O)_n$ have been prepared for n 2 [13]. Apart from this size dependence, another important issue of these anionic clusters has been the surface versus internal state of localization of the excess electron. The absorption peaks observed at different vertical electron-detachment energies (VDE) in photoelectron spectra have shown vibrational features that confirm the existence of isomers for n=2, 6, and 7 [14-15]. Very recently Coe and co-workers have shown the presence of three groups of electron-water clusters: dipole bound like states, seen from n=2 - 16; intermediate states, found from n=6 - 16; and bulk embryonts, starting at n=11 and continuing up through the largest cluster studied [14]. The surface-bound states are considered to be more stable than the internal-bound states for small electron-water clusters [16]. However, this has not been fully verified by experiments. Even for large clusters, recent experiments have found both surface and internal states of the excess electron [17]. More recent theoretical studies report that two types of cluster isomers are present (both surface bound and interior bound) rather than one type for the cluster size [18] as small as $(H_2O)_{14}$. For n= 21 and 24, internal states were predicted with significant VDEs [19]. Herbert and Head-Gordon have presented some benchmark calculations of VDEs of $(H_2O)_n$ and $(HF)_n$ in their recent quantum chemical studies [20]. They have inferred that the second-order MÖller-Plesset perturbation theory (MP2), coupled with a basis set containing extra diffuse functions, is sufficient to get VDEs that are within 0.05 eV of the experimental results. Hammer et at have addressed the structure of the $(H_2O)_6$ by using vibrational spectroscopy of lower energy bending modes [21]. They have found presence of mainly two different electron-binding motifs which are reflected through the IR spectra of the H-O-H intramolecular bending modes.

It may be noted that majority of the existing theoretical calculations of these cluster anions were done at zero temperature using quantum chemical methods. The temperature of these systems under experimental conditions is reported to be between 100-200 K. Thus, it is important to investigate these clusters theoretically at finite temperatures by using methods that go beyond the zero temperature quantum chemical methods. In the following section, we discuss finite temperature quantum simulation studies of these clusters that we are currently carrying out in our laboratory.

Quantum simulations of water cluster anions

In this section, we discuss quantum simulations of a particular water cluster anion: $(H_2O)_6$. Our simulations started from the structure 1 (b) [See Fig. 1] which was reported earlier as the most stable structure of this cluster anion [22]. In this structure, the excess electron is attached in the vicinity of a water molecule that accepts two hydrogen bonds (AA-site). The structure of the corresponding neutral cluster (Fig. 1a) is discussed in the later part of this section. The simulations of the anionic cluster are performed by using the Car-Par!inello method [23] and the CPMD code [24]. The cluster was kept in the central region of a cubic box with enough empty space around the cluster in all directions. Plane wave basis within local spin density (LSD) functional theory with an energy cutoff of 80Ry and BLYP functionals are used. The core electrons were treated via the Troullier-Martins normconserving pseudopotentials [25]. A fictitious electron mass was assigned to 400 a.u and the coupled equations of

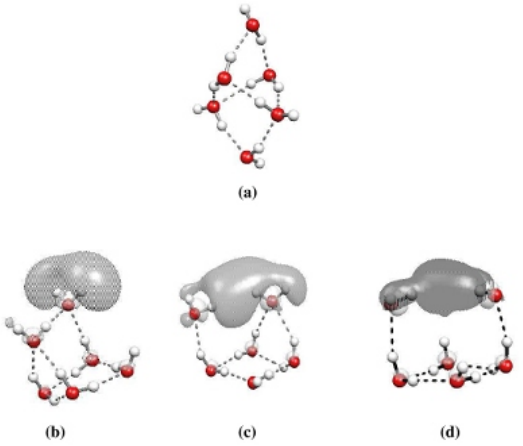

Fig. 1 The structures of neutral (a) and anionic (b–d) clusters $(H_2O)_6$ and $(H_2O)_6^-$ respectively. The SOMO state which holds the excess electron are also shown for the anionic clusters.

motion describing the system dynamics were integrated by using a time step of 3 a.u. The system was equilibrated for about 3 ps at 150K in NVT ensemble using Nose-Hoover chain method and, thereafter, the simulation was continued for another 7.5 ps with the Nose-Hoover thermostating switched off, for calculation of different structural and dynamical quantities. All-electron quantum chemical calculations of the neutral and anionic counterparts have also been carried out to determine energies and dipole moments of different conformers for both neutral and anionic forms. In our quantum chemical calculations of the dipole moments and energies, we have mainly employed the 6-311(1 +3+)g** basis sets. This implies one diffuse sp function on each heavier atom like O, and three diffuse s functions on each H atom [20]. These calculations were performed using the Gaussian03 program [25]. Vertical detachment energies (VDE) for anionic clusters were calculated from the supra molecular approach using the following relationships: VDE = E(neutral at optimized anion geometry) - E(anion).

From the finite temperature simulation trajectories, we have seen the real time evolution of the water cluster with the solvated electron. The structure as well as hydrogen bond network of the water cluster change with time. This gives rise to change in the number of dangling hydrogens. Three different representative configurations taken from the simulation trajectory of the cluster are illustrated in Fig. l (b-d), where the bound-electron charge distributions of the singly occupied molecular orbitals (SOMO) can be clearly visualised. The density of the excess electron is mainly found to be in the vicinity of the dangling hydrogens of water molecules. We started the simulations from structure l (b) and found that l (d) was mostly prevailing structure during the simulations. Structure l (c) was found only for short time periods. 1 (b) has three single acceptor and double donor ADD-sites, one single acceptor single donor AD-site, one double acceptor single donor AAD site and one double acceptor AA-site. The nonbonded hydrogens of the AA-type water molecule are completely surrounded by the diffuse electron cloud. From vibrational spectroscopic analysis Hammer et al showed this type of diffuse electron binding motif [22]. l (c) has four single acceptor double donor ADD-sites, one single acceptor single donor AD-site, one single acceptor A-site, and one double acceptor AA-site. The excess electron is mainly attached to the AA and A type water molecules. l(d) has two AD-sites, two ADD-sites, and two A-sites. The excess electron is trapped in the molecular bowl. Specifically, the free OH groups of the A-type water molecules (two tweezers) hold the electron. This structure is very similar to the tweezers-like structure predicted by Kim et al [26]. They referred to it as partially internal and partially surface state. So it is clearly seen that both H-bond network and the electron binding motifs evolve with time. The time averaged hydrogen-bonding environment of the water molecules are illustrated in Fig. 2. The population of single acceptor (A)type is significant and amount of free (NIL) type and double acceptor (AA) type are very little. For neutral $(H_2O)_6$ cluster, the cage structure (Fig. 1a) has been reported to be the most stable from both experimental and theoretical points of view [27-29]. It has two single acceptor and single donor sites (AD), two at single acceptor double donor sites (ADD) and the rest two at double acceptor and single donor (AAD) sites with total seven hydrogen bonds. Single acceptor or double acceptor or free (A or AA or NIL) type arrangements are energetically unfavourable for the neutral clusters. Their predominance in negatively charged

TABLE 1. The calculated energies (E), dipole moments (ì), vertical detachment energies (VDE) of different conformers of anionic clusters $(H_2O)_6$. The single point calculations are done with 6-311(1+3+)g basis set at BLYP level. The codes of different structures are as in the Fig. 1.**

Cluster	Conformer code	E (Hartree)	(D)	VDE (eV)
$(H_2O)_6$	1 (a)	-458.56378	1.98	-
$(H_2O)_6$	1 (b)	-458.58456	10.242	0.701
	1 (c)	-458.56534	8.58	0.781
	1 (d)	-458.56555	7.17	0.796

clusters shows how the excess electron disrupts the H-bonding network. Dipole moment of the neutral cluster (la) is 1.98 D at the BLYP level of calculations, but that of the anionic structures are very high (see Table 1). There is a substantial increase in the VDE (See Table 1) from l (b) to l (d) which indicate a stronger binding of the excess electron in the cluster l (d). A calculation of the power spectra of hydrogen atom velocity correlations (not shown here) also reveals the presence of hydrogen atoms in different hydrogen bonding environments which is consistent with the time-averaged distributions of Fig. 2.

In summary, there are many different conformers possible for the anionic clusters. These structures tend to have large dipole moments to hold the excess electron and also have large vertical detachment energies. An excess electron disrupts the hydrogen-bonding network of the neutral clusters. It is found that the motif of electron binding changes with time at finite temperature. Significant population of single acceptor (A) type, free (NIL) type, and double acceptor (AA) type water molecules were found from the quantum simulation study. There are signatures of these type of water molecules in the power spectrum of hydrogen atoms. In general, the hydrogen bonds are found to play a significant role in determining the solvation structure of the excess electron in water clusters.

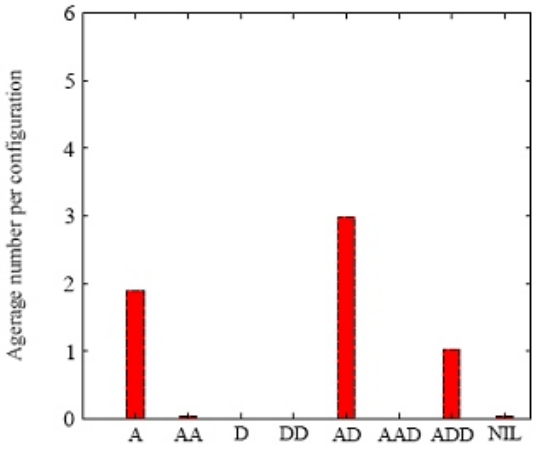

Fig. 2 The time- averaged population of water molecules in different hydrogen-bonding environment along the simulation trajectory.

Acknowledgment

We thank Council of Scientific and Industrial Research (CSIR), Government of India, for a research fellowship to S.P. We also gratefully acknowledge the financial support from Department of Science and Technology (DST), Government of India.

References

1. W. Weyl, Poyg. Ann. 123, 350 (1864).
2. E. J. Hart and J.W. Boag, J. Am. Chem. Soc. 84, 4090 (1962).
3. L. Kevan, Acc. Chem. Res. 14, 138 (1981).
4. F.-Y. Jou and G.R. Freeman, J. Phys. Chem. 83, 2383 (1979).
5. B. Baron et al. J. Chem. Phys. 68, 1997 (1978).
6. P. Han and D. M. Bartles, Phys. Rev. Lett. 64, 1469 (1990).
7. P. Krebs, V. Giraud and M. Wantschik, Phys. Rev. Lett. 44, 211 (1980).
8. J. Schnikter and P. J. Rossky, J. Chem. Phys. 86, 3471 (1987).

9. M. Boero, M. Parrinello, K. Terakura, T. Ikeshoji and C.C. Liew, Phys. Rev. Lett. 90, 226403 (2003).

10. J. Kim, J. M. Park, K. Oh, J. Y. Lee, S. Lee, and K. S. Kim, J. Chem. Phys. 106, 10207 (1997); S Lee, J. Kim, S. L. Lee, and K. S. Kim, Phys. Rev. Lett. 79, 2038 (1997); H. M. Lee, S. B. Suh, P. Tarakeshwar, K. S. Kim, J. Chem. Phys. 122, 400309 (2005).

11. T. Tsurusawa, S. Iwata, Chem. Phys. Lett. 287, 553 (1998).

12. S. A. Kulkarni, L. J. Bartolotti, R. K. Pathak, J. Chem. Phys. 113, 2697 (2000).

13. H. Haberland, C. Ludewigt, H. -G. Schindler and D.R. Worsnop, J. Chem. Phys. 81, 3742 (1984).; H. Haberland, C. Ludewigt, H.-G. Schindler and D. R. Worsnop, B.Bunsenges, J. Chem. Phys. 88, 271 (1984).

14. J. V. Coe, G. H. Lee, J. G. Eatson, S. T. Arnold, H. W. Sarkas, K. H. Bowen, C. Ludewigt, H. Heberland, and D. R. Wornshop, J. Chem. Phys. 92, 3980 (1990); J. V. Coe, S. T. Arnold, J. E. Eaton, G. H. Lee, K.H. Bowen, J. Chem. Phys. 125, 014315 (2006)

15. M. Armbruster, H. Haberland, and H.-G. Schindler, Phys. Rev. Lett. 47, 323 (2001); L. A. Posey and M. A. Johnson, J. Chem. Phys. 89, 4807 (1988); P. J. Campagnola, D.M. Cry, and M. A. Johnson, Chem. Phys. Lett. 181, 206 (1991); J. Kim, I. Becker, O. Cheshnovsky and M. A. Johnson, Chem. Phys. Lett. 297, 90 (1998); P. Attoye, G. H. Weddle, C.G. Bailey, M. A. Johnson, F. Vila, and K.D. Jordon, J. Chem. Phys. 110, 6268 (1999).

16. R. N. Barnett, U. Landman, C. L. Cleveland and J. Jortner, J. Chem. Phys. 88, 4421, 4429, (1988).

17. J . R. R. Verlet, A. E. Bragg, A. Kammrath, O. Cheshnovsky and D. M. Neumark, Science 307,93 (2005).

18. A. Khan, J. Chem. Phys. 125, 024307 (2006).

19. A. Khan, J. Chem. Phys. 121, 280 (2004); A. Khan, Chem. Phys. Lett. 401, 85 (2005); A.. Khan, J.Chem. Phys. 121, 280 (2004).

20. J. M.Herbert and M Head-Gordon, J. Phys.Chem. A 109, 5217 (2005); J. M.Herbert and M Head-Gordon, Phys. Chem. Chem. Phys. 8, 68 (2006)

21. N. I. hammer, J. R. Roscioli, and M. A. Johnson, J. Phys. Chem. A. 109, 7896 (2005)

22. N. I. hammer, J-W Shin, J. M. Headrick, E. G. Diken, J. R. Roscioli, G. H. Weddle and M. A. Johnson, Science 306, 675 (2004); K. D. Jordan, Science 306, 618 (2004)

23. R.Car and M. Parrinello, Phys. Rev. Lett. 55, 2471 (1985); D. Marx and J. Hutter, Ab initio Molecular Dynamics: Theory and Implementation in Modern Methods and Algorithms of Quantum Chemistry, Ed. J. Grotendorst (NIC, FZ Jülich, 2000).

24. CPMD Program, J.Hutter, A. Alavi, T. Deutsch, M. Bernasconi, St. Goedecker, D. Marx, M. Tukerman, and M. Parrinello, MPI fur Festkorperforschung and IBM Zurich Research Laboratory.

25. M. J. Frisch, G. W. Trucks, H. B. Schlegel et al. GAUSSIAN 03 (gaussian Inc. Pittsburgh, PA, 2003).

26. K.S. Kim, S. Lee, J. Kim, and J. Y. Lee, J. Am. Chem. Soc. 119, 9329 (1997)

27. K. Liu, J. D. Cruzan, R. J. Saykally, Science 271, 929 (1996)

28. K. Miiller-Dethlefs, P. Hobza, Chem. Rev. 100, 143 (2000)

29. S. Maheshwary, N. Patel, N. Sathyamurthy, A. D. Kulkarni and S. R. Gadre, J. Phys. Chem. A. 105, 10525 (2001)

30. H. M. Lee, S. Lee, and K. S. Kim, J. Chem. Phys. 119, 187 (2003)

Ab initio Treatment of Large Molecules : Cut-and-Stitch the Tailor's Way

Prof. Shridhar R. Gadre *received his Ph. D. from IIT, Kanpur in 1978. After his post-doctoral research with Professor Robert G. Parr and Robert L. Matcha, he joined University of Pune as a lecturer and was promoted to Professorship in 1988. He has authored over 165 publications mostly in high-impact journals, guided 15 Ph.D. students and completed over 10 research projects sponsored by government agencies and industries. Professor Gadre is a Fellow of the Indian Academy of Sciences, Bangalore and the Indian National Science Academy, New Delhi and a recipient of the prestigious Shanti Swarup Bhatnagar award (1993) in Chemical Sciences.*

Ms. Anuja Rahalkar *has completed her bachelor's degree in chemistry and master's degree in inorganic chemistry from the University of Pune. She was awarded a scholarship from Torrent Pharmaceuticals and she has topped her class in M.Sc. She has cleared CSIR-NET and was within the top 10 per cent of the NET-awardees in July 2006. She has joined Professor Gadre as a CSIR-JRF to pursue her Ph.D.*

Shri V. Ganesh *obtained a bachelor's degree in Computer Science in Bharati Vidyapeeth and was awarded a gold medal. After competing MCS degree from the Interdisciplinary School of Scientific Computing, he joined Professor Gadre's group for a Ph. D. degree. Ganesh has been developing linear scaling algorithms for handling large molecular systems at ab initio level of theory. He also actively participates in small open source programs. See http://tovganesh.blogspot.com for more information.*

Introduction

In modern days, science has progressed a lot from one of its own beautiful creations: the computing machine. The raw speed of digital electronic computer has been a constant companion of the computational scientist for the past few decades. Scientific computing methods have been applied to (but certainly not limited to) many diverse areas, such as fluid dynamics; computational chemistry, physics and biology; data mining; business and financial analysis etc. In the recent past, enormous interest has been generated in computational chemistry and allied fields such as computer-aided drug designing and bio-informatics, partly due to the commercial aspects involved in these areas. The basic work involved in these studies revolves around the understanding of electronic energies, properties and reactivity of the molecules of interest.

At the same time, the studies in scientific computing are getting enormous impetus from the way the hardware technology is growing, as aptly described by Moore's law [1]: "the transistor density of integrated circuits, with respect to minimum component cost, doubles every 18 months". In simple terms, this means that the computational power of a new chip doubles every 18 months, in

Prof. Shridhar R. Gadre, Ms. Anuja Rahalkar and Shri V. Ganesh, Department of Chemistry, Interdisciplinary School of Scientific Computing, University of Pune, Pune 411007; E-mail: gadre@chem.unipune,ernet.in

turn providing more computing power with passage of time. Computational studies of the properties of molecules have not only helped provide deep insights into their behavior, but have also made it possible to explore chemical reaction pathways. Over the years, a number of theories have been developed to aid *in silico* studies of many chemical phenomena. These methods have varying degree of chemical accuracy and computational requirements. With more accurate methods, the required computational resources (e.g. the CPU time, main memory and secondary storage requirements) keep increasing non-linearly.

A pivotal contribution to computational quantum chemistry was made by Pople and co-workers [2], which ultimately led to a state-of-the-art electronic structure calculation package. This package has eventually reached all the areas of chemistry including the old-fashioned divisions of physical, organic, inorganic and biochemistry, which are now getting integrated in a seamless manner. Application of elaborate quantum chemical methods is able to accurately describe electronic properties of atoms, molecules and clusters. However, with increasing sophistication, the computational effort [3-7] required to perform these calculations also grows very rapidly. The scaling of these methods is typically given in terms of power of the number of basis functions involved, viz. $O(N^m)$. The parameter m is dependent on the method of quantum chemistry used. These methods range from Hartree-Fock (HF) [typical value for large molecules being m=3], Density functional theory (DFT) [m=3-4], Møller-Plesset second order perturbation theory (MP2) [m=5] and Coupled cluster methods (CC) [m=6]. This points to tremendously increasing computational requirements with the desired accuracy and also the size of the molecular system under study. Computational chemists around the world are looking into reducing this computational complexity of ab initio methods by applying some ingenious techniques. Of such numerous attempts made during the past decade or so, the divide-and-conquer algorithms are very popular and easy to implement. These algorithms are also able to provide an effective solution for computing the energies and other properties of large molecules and clusters. The application of most of these methods has so far been mostly limited to energy and property evaluation at a fixed geometry [8-15]. It is only in the recent years that some attempts have been made for applying these methods to geometry optimization [16-23] of a variety of large molecules containing more than say, 100 atoms.

Zhao and Yang [16] reported one of the earliest attempts in applying DC-type methodology for geometry optimization with density functional theory (DFT). Although the results obtained by them were reported to be close to the actual computations when applied to small molecules like -tetrapeptide comprising of glycine, there was no apparent advantage in terms of CPU time when benchmarked with the full Kohn-Sham calculation. Using molecular fractionation with conjugate caps (MFCC) approach, Li et al. [17] have proposed that geometry optimization can be done using divide-and-conquer method. However, most of the systems reported by the previous researchers are either small or linear except for the case of crambin molecule [21]. Our group [10, 23] has independently developed a molecular tailoring approach (MTA) which has recently been modified to a form termed as cardinality guided MTA (CG-MTA) [23(c)]. MTA has been applied for the computation of one-electron properties such as electron density (ED) and electrostatic potential (ESP) of large nonlinear molecules such as silicalite and ibuprofen cluster. Further, CG-MTA has also been applied for partial geometry optimization, of a small albumin binding protein [1prb] containing 851 atoms, at the HF/6-31G level using PC resources [23(b, c)]. In the following Section, we discuss the CG-MTA algorithm and how it can be applied for computing one-electron properties, energetics and structures of large molecules of chemical and biological interests. The acronyms MTA and CG-MTA are used interchangeably in the following text and, most of the times, it essentially refers to CG-MTA.

The Tailoring Approach

MTA closely resembles the way a tailor stitches clothes form cut pieces of a large cloth, by keeping some overlaps among them. The MTA analogously divides a large molecule into a set of overlapping fragments that are the means to mimic the chemical environment of atoms of the parent

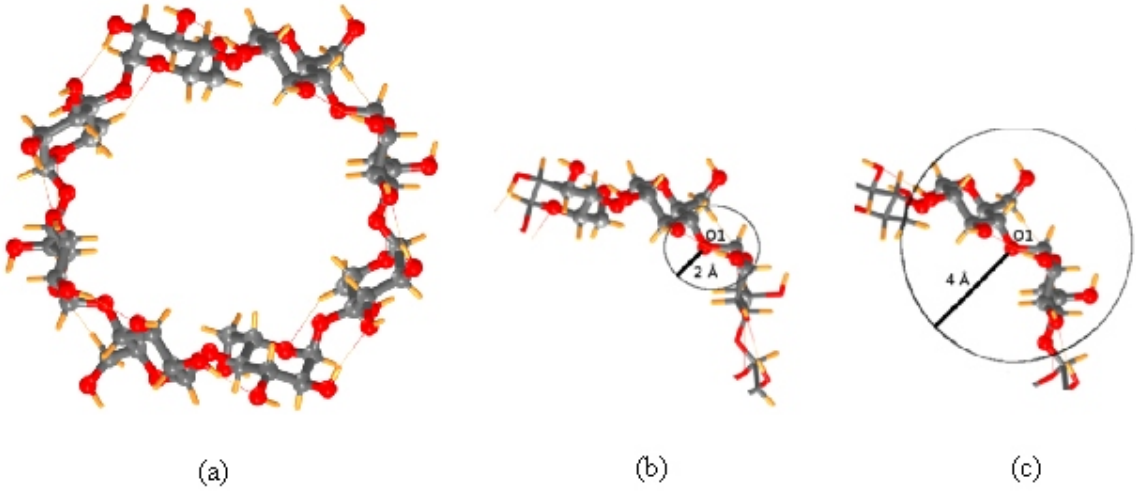

Fig. 1 *-cyclodextrin (a) and two of its fragments (b) and (c). For fragments, ball-and-stick model represents the atoms included a fragment, while the rest are shown in stick model. see text for details.*

supermolecule. The overlapping is necessary because if we scissor the fragments in such a way that there are no overlaps, then the boundary atoms will have a poor representation of their chemical environment. During the fragmentation process, care is taken so that no multiple bonds or planar ring structures are broken. At those places where the bonds are cut, appropriate substitution of hydrogen atoms is generally made along the bond vector so as to preserve the valencies. In other words, MTA is a divide-and-conquer (D&C) methodology, which decomposes a problem (SCF for the parent molecule) into subproblems (SCF only for the overlapping fragments), which can be individually solved. Later the results of these subproblems are combined (stitch the DM, or estimate the energy and its derivatives) together to arrive at the result of the original problem. Before we proceed, we define a few terms that will be used for assessing the fragmentation procedure. The first and the foremost important term used is the R-goodness of an atom in the fragment, and the minimum R-goodness of the fragmentation scheme.

R-goodness of an Atom in a Fragment

It is defined as the minimum radius of a sphere centered at the atom i, so that all the atoms falling within this sphere are also a part of the fragment F (containing the atom i). An atom present in more than one fragment will have different R-goodness values therein. The maximum of all these R-goodness values represents the R-goodness for that atom in the given fragmentation scheme. As an example, consider Fig. 1, which depicts two fragments for -cyclodextrin molecule (Fig. 1b and Fig 1c). The atom labeled O1 is present in both fragments 1b and 1c, albeit with different R-goodness: 2.0 and 4.0 Å respectively. Thus the R-goodness for atom O1 is 4.0 Å in this fragmentation scheme. In other words, atom O1 is best represented in fragment 1c.

Minimum R-goodness of the Fragmentation Scheme

The minimum of all atomic R-goodness values is taken to be the R-goodness of the fragmentation scheme. Larger R-goodness implies better accuracy, although at a higher computational cost. Table 1 summarizes a few fragmentation schemes for -cyclodextrin (Fig. 1) and taxol (Fig. 4). By providing different initial maximum fragment size and R-goodness one can obtain different sets of fragments. The best fragmentation scheme is the one that provides better accuracy (read R-goodness) and

TABLE 1. Analysis of 5 different fragmentation schemes of taxol and -cyclodextrin molecules (see Fig. 1 and 4 for geometries). N_f, N_a, R, S are the number of fragments, average number of atoms in fragments, minimum R-goodness of the scheme and scaling factor (the ratio of total number of atoms in all the fragments together to the number of atoms in the parent molecule) respectively. See text for details.

-cyclodextrin, 168 atoms				
Scheme #	N_f	N_a	R	S
1	21	32	2.6	3.4
2	27	32	3.3	4.4
3	20	40	3.8	4.3
4	16	46	3.8	3.9
5	10	50	4.0	2.7
Taxol, 113 atoms				
Scheme #	N_f	N_a	R	S
1	15	37	2.5	4.0
2	10	40	2.5	3.1
3	14	48	2.8	5.3
4	9	52	2.8	3.7
5	8	54	3.0	3.4

most time (and memory) advantage. These typically are the ones with lower scaling factor (i.e. the ratio of the total number of atoms in all fragments to the number of atoms in the parent molecule). Thus, while choosing the best set of fragments, one must take into account the computational resources available at the disposal as well as the desired accuracy. A fragmentation scheme with better R-goodness value generally has better ability of mimicking the chemical environment of the supermolecule.

Algorithm for Fragmentation

(i) Identify connectivity of the atoms using the molecular graph generated form the input co-ordinates. (ii) Place a sphere of radius R (typically 3 to 5Å) along each atom positions, by a breadth-first traversal of the molecular graph. (iii) For each such sphere, collect all the atoms that fall within this sphere and form a fragment. (iv) During the formation of a fragment, check if it violates any 'common sense' criterion such as a double bond been broken or an aromatic ring being cut, and correct for these. Include or exclude depending on the maximum fragment size criterion. (v) Merge the fragments according to the nearness to each other. (vi) Do a general merge recursively depending on the maximum overlaps between the fragments and their nearness. This recursive procedure stops when the fragments can no longer be merged because of the maximum size constraint. (vii) The final set of fragments is then checked for its R-goodness.

If the purpose is to construct a density matrix (DM) for computing the one-electron properties, then these fragments are subjected to standard self-consistent field (SCF) procedure and the fragment DMs are stitched together to form the DM of the parent system. The DM elements are appropriately picked from the information about atomic R-goodness indices, which are indicative of the fragment where a given atom is best represented. For performing geometry optimization (cf. Fig. 2), it is necessary to compute the energy along with its first derivative (and sometimes second derivative). Then a cardinality-based expression [23(c)] is set up using which the energy and its derivatives are computed employing only the fragment energies and gradients. In general the expressions for energy, E and its derivatives then can be written in terms of the fragment energies, E^{fi} and the overlap fragment energies $E^{fi\ fj}$ etc. as :

$$E \quad E^{fi} \quad E^{fi\ fi} \ \dots \ (\ 1)^{k\ 1} \quad E^{fi\ fi\ \dots\ fk} \tag{1}$$

and

$$\frac{E}{X} \quad \frac{E^{fi}}{X^{fi}} \quad \frac{E^{fi\ fj}}{X^{fi\ fj}} \ \dots \ (\ 1)^{k\ 1} \quad \frac{E^{fi\ fj\ \dots\ fk}}{X^{fi\ f\ \dots\ fkj}} \tag{2}$$

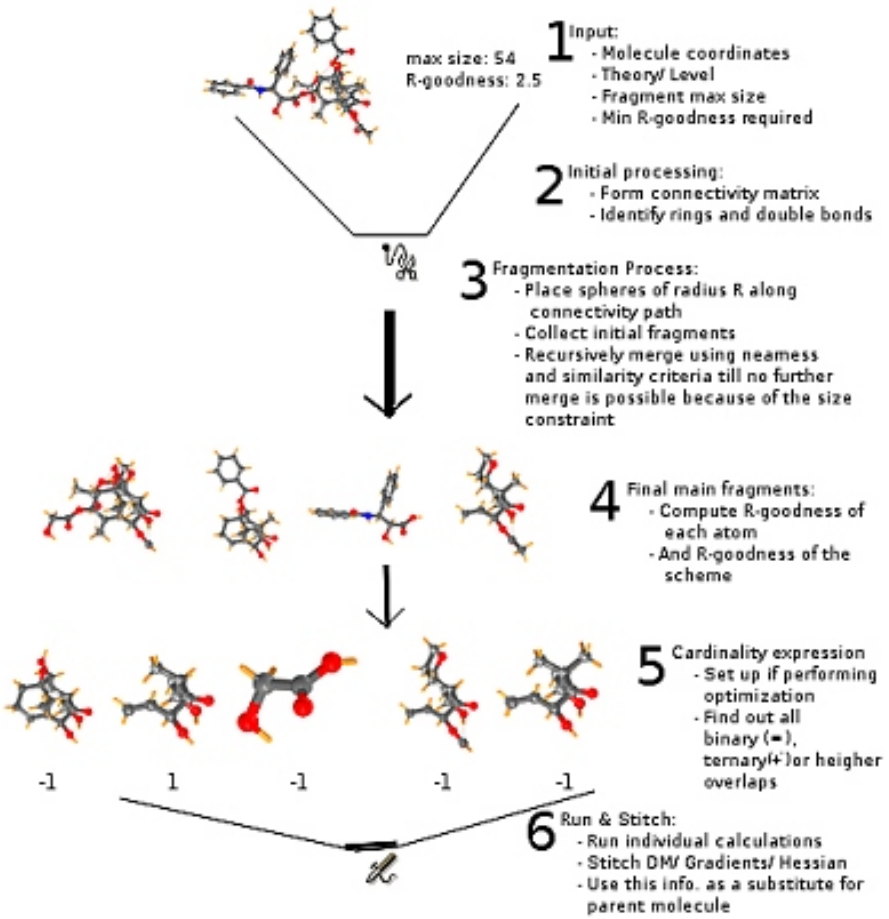

Fig. 2 The flow of the CG-MTA fragmentation process. See text for details.

Applications to Large Molecular Systems

Algorithm described in the preceding section has been implemented in a locally modified version of GAMESS [27] package and some details are presented in Ref. 23(c). Some new results of energy evaluation and geometry optimization are presented here. A more exhaustive set of test applications can be found elsewhere [10, 23]. Accuracy of energy and gradients of a few test molecules at HF and DFT level (using B3LYP [25] functional) are presented in Table 2. A few of the geometries presented in Table 2 are taken from Ref. 23(b, c). It is clear from Table 2 that the maximum error in the energy at any geometry using CG-MTA is only of the order of 0.1 to 0.2 millihartrees. A few test runs of full optimization of a few large molecules are presented in Table 3 (also Ref. 23(c)). The largest calculation that we tested on a single PC (Pentium 4, 2.8 GHz with 1GB RAM) was that for an albumin binding protein (PDB ID: 1prb) with 851 atoms at HF/6-31G level of theory. A single cycle of optimization using CG-MTA took about 600 minutes. At the same time, a single cycle of actual calculation was not at all possible on the same set-up because of the large amount of memory (estimated to be over 2GB) required by the actual calculation. This job clearly indicates what CG-MTA could enable: calculations otherwise not possible on PC resources are now actually accomplished!

As a test case of property evaluation, MESP isosurfaces of -cyclodextrin molecule, computed using CG-MTA (Fig. 3) and the actual one obtained

TABLE 2. A comparison of the actual and CG-MTA energy and gradients (in a.u.) for four molecules (see Fig. 1 and 4) at some randomly selected geometries. N, N' and R are number of basis functions for the parent system, largest number of basis functions for the fragments and the R-goodness of the fragmentation scheme respectively. G_{max} and G_{rms} are maximum gradient norm and RMS gradient respectively. T_r is the ratio of time taken for the actual calculation to that for CG-MTA calculation.

System (level/ basis)	N, N', R	Actual (G_{max}, G_{rms})	CG-MTA (G_{max}, G_{rms})	T_r
-cyclodextrin B3LYP/6-31G(d, p)	1480, 485, 4.1	-4883.54609 (0.00166, 0.00042)	-4883.54567 (0.00150, 0.00031)	3.1
taxol B3LYP/6-31G(d, p)	1185, 715, 4.0	-2927.89660 (0.00304, 0.00051)	-2927.89652 (0.00252, 0.00043)	2.3
folic acid HF/6-31G(d)	518, 226, 2.2	-1560.90939 (0.08511, 0.02158)	-1560.90931 (0.08671, 0.02174)	3.6
folic acid B3LYP/6-31G(d)	518, 226, 2.2	-1569.24737 (0.05449, 0.01282)	-1569.24720 (0.05507, 0.01292)	5.4
-carotene HF/6-31G(d)	712, 333, 4.0	-1547.14197 (0.03431, 0.01403)	-1547.141929 (0.03429, 0.01404)	2.1
-carotene B3LYP/6-31G(d)	712, 333, 4.0	-1556.76983 (0.02555, 0.00913)	-1556.76966 (0.02554, 0.00910)	2.6

Table 3: A few test cases of CG-MTA-based geometry optimization. See text and captions of Table 2 for the notation and other details. G_{max} and G_{rms} are maximum gradient norm and RMS gradient respectively. The jobs are run for a few cycles of optimization (typically 20 to 50).

System (level/ basis)	N, N', R	Initial geometry (G_{max}, G_{rms})	Final geometry (G_{max}, G_{rms})
-cyclodextrin B3LYP/6-31G(d, p)	1480, 485, 4.1	-4883.34370 (0.17812, 0.01891)	-4883.55609 (0.00047, 0.00014)
taxol B3LYP/6-31G(d, p)	1185, 715, 4.0	-2927.83639 (0.6280, 0.01320)	-2927.89656 (0.00264, 0.00070)
1prb * HF/6-31G	4635, 628, 3.0	-20162.81113 (0.14024, 0.00114)	-20164.04792 (0.00932, 0.00130)

*Initial Coordinates of 1prb obtained from RCSB Protein Data Bank site: http://www.pdb.org/

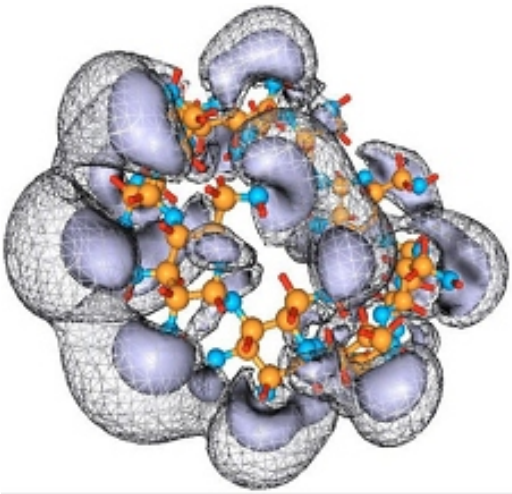

Fig. 3 MESP isosurfaces of -cyclodextrin plotted at -0.012 a.u. (chickewire) and -0.030 a.u. (blue) at HF/6-31(d) level of theory. See text for details.

from a full calculation were compared. The calculations for the property were performed at HF/6-31G(d) level of theory. The accuracy of MTA-based MESP is very high and the difference with the actual one is visually not discernible. Hence only the MTA-based MESP isosurfaces are presented. The major features of the actual MESP are well replicated in the CG-MTA calculation, although with much less effort. Numerically, a maximum of 1% error was observed in computed MESP values. However, 95-98% points (usually the most significant ones) had less than 0.1% error [10, 23(a, b)].

Using Commodity PC-Cluster to Speed up Computation

The calculations on individual fragment-subsystems being completely independent of each other, CG-MTA presents a case of an embarrassingly parallel implementation with minimal communication cost. The parallelization schemes used in CG-MTA implementation are detailed out in Ref. 23(b, c). But in a nutshell, the commonly used parallelization scheme for commodity PC cluster is a distributed scheme that involves sending one fragment job per PC, so as to perform the tasks simultaneously. This allows for the completion of jobs faster, and, many a time, just adding one more PC in the cluster makes calculation faster. In an alternative set-up, simple desktop PCs could be combined together over a local area network (LAN) for executing a large CG-MTA job. This enables usage of existing resources for performing calculations that are otherwise impossible without a supercomputing facility. Also nowadays, it is relatively easy to procure an off-the-shelf PC with the necessary networking hardware at a cost that is affordable even to an individual working in the area of computational chemistry. This means that a "home-made" cluster would suffice for doing quantum chemical calculations on large molecules/ molecular clusters using CG-MTA.

When a large number of nodes are tagged together to perform a single CG-MTA task (of geometry optimization or property calculation), load balancing of the fragment jobs becomes an important issue. As the sizes of the fragments, and many a time, the power of machines (PCs) involved in computation can vary widely, it becomes important for the job scheduler to have maximum utilization of the computing resources. However, these issues are beyond the scope of this article and a detailed discussion on the scheduling schemes used in CG-MTA and its scalability can be found in Ref. 23(c).

It is clear that in coming years, with the advent of faster CPU's and large storage capacity disks, there will be more and more applications of ab initio methods, guided by linear scaling methods such as CG-MTA to address some grand challenge problems in chemistry, chemical physics and molecular biology. In their seminal article "Broken Bottlenecks" [28], Roothaan and Mulliken had effectively summed up the whole theme behind exploring ideas such as the one presented in this paper: "Looking towards the future, it seems certain that colossal rewards lie ahead for large scale quantum mechanical calculations of the structure of matter..."

Acknowledgements

The authors thank C-DAC, Pune and the CAS program of the UGC for financial and computational support.

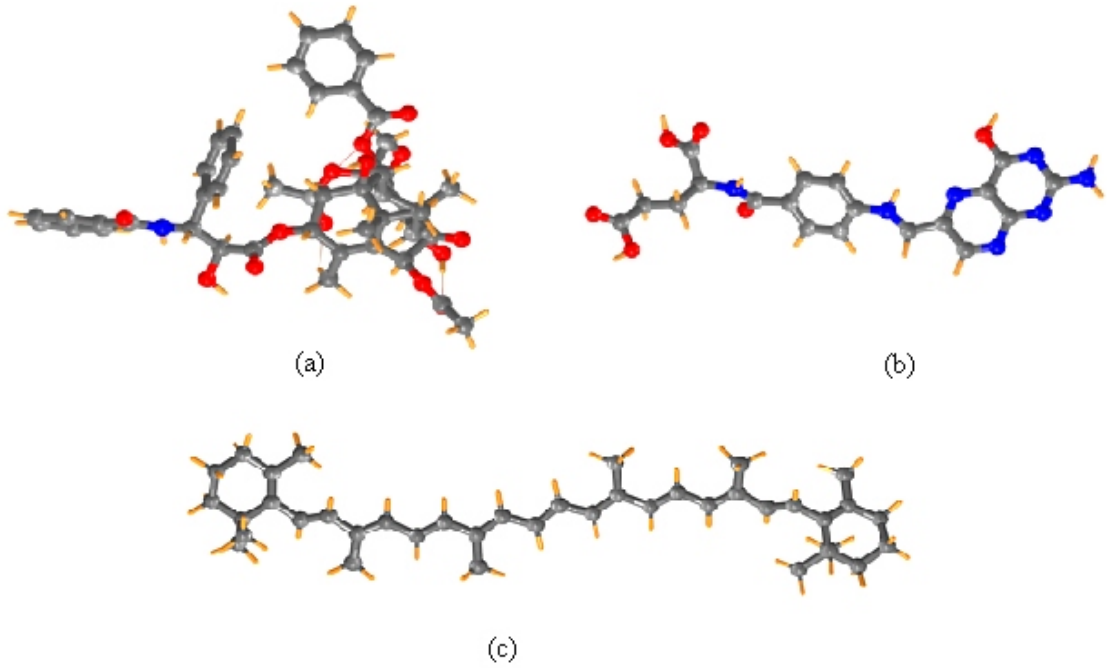

Fig. 4 Structures of some of the molecules used for CG-MTA calculation : (a) Taxol (b) Folic acid (c) -carotene. See text for details.

References

1. G. E. Moore, Electronics, 8 (1965) 38.
2. M. J. Frisch, G. W. Trucks, H. B. Schlegel, G. E. Scuseria, M. A. Robb, J. R. Cheeseman, J. A. Montgomery, Jr., T. Vreven, K. N. Kudin, J. C. Burant, et al., Gaussian 03, Revision C.02, Gaussian, Inc., Wallingford, CT, 2004.
3. A. Szabo and N. S. Ostlund, Morden Quantum Chemistry (McGraw-Hill, New York, 1989).
4. W. J. Hehre, L. Random, and P. V. R. Schleyer, Ab Initio Molecular Orbital Theory (John Wiley, New York, 1986).
5. J. AlmlÖf, K. Faegri, and K. Krosell, J. Comp. Chem., 3 (1982) 385.
6. D. L. Strout and G. E. Scuseria, J. Chem. Phys., 102 (1993) 8448.
7. H. F. Schaefer, III and C. J. Barden, Pure App. Chem., 72 (2000) 1405 .
8. W. Yang, Phys. Rev. Lett., 66 (1991) 1432.
9. W. Yang and T. S. Lee, J. Chem. Phys., 103 (1995) 5674.
10. (a) S. R. Gadre, R. N. Shirsat and A. C. Limaye, J. Phys. Chem., 98 (1994) 9165. (b) K. Babu and S. R. Gadre, J. Comput. Chem., 24 (2003) 484. (c) K. Babu, V. Ganesh, S. R. Gadre, and N. E. Ghermani, Theoret. Chem. Accts., 111 (2004) 255.
11. T. E. Exner and P. G. Mezey, J. Phys. Chem. A, 108 (2004) 4301.
12. W. Li and S. Li, J. Chem. Phys., 122 (2005) 194109.
13. V. Deev and M. A. Collins, J. Chem. Phys., 122 (2005) 154102 .
14. X. Chen, Y. Zhang, and J. Z. H. Zhang, J. Chem. Phys., 122 (2005) 184.
15. (a) T. Ijegami, T. Ishida, D. G. Fedorov, K. Kiraura, Y. Inadomi, H. Umeda, M. Yokokawa, and S. Sekiguchi, Proc. of Supercomputing, IEEE Computer Society p. 10 (2005). (b) D. G. Fedorov and K. Kitaura, J. Chem. Phys., 121 (2004) 2483.

16. Q. Zhao and W. Yang, J. Chem. Phys., 102 (1995) 9598.

17. S. Li, W. Li, and T. Fang, J. Am. Chem. Soc., 127 (2005) 7215.

18. (a) T. Nakano, T. Kaminuma, T. Sato, Y. Akiyama, M. Uebayasi, and K. Kitaura, Chem. Phys. Lett., 318 (2000) 614. (b) K. Kitaura, S. Sugiki, T. Nakano, Y. Akiyama, and M. Uebayasi, Chem. Phys. Lett., 336 (2001) 163.

19. M. A. Collins and V. A. Deev, J. Chem. Phys., 125 (2006) 104104.

20. R. P. A. Bettens and A. M. Lee, J. Phys. Chem. A, 110 (2006) 8777.

21. C. V. Alsenoy, Y. Ching-Hsing, A. Peters, J. M. L. Martin, and L. Schafer, J. Phys. Chem. A, 102 (1998) 2246.

22. K. S. Byun, K. Morokuma, and M. J. Frisch, J. Mol. Struct. (Theochem), 462 (1999) 1.

23. (a) S. R. Gadre, K. Babu, and V. Ganesh, in Recent Trends in Practice and Theory of Information Technology: Proceedings of NRB Seminar, Edited by S. N. Maheshwari, p86 (Viva Books, New Delhi, 2005). (b) S. R. Gadre and V. Ganesh, J. Theoret. Comp. Chem. (in press 2006). (c) V. Ganesh, R. K. Dongare, P. Balanarayan, and S. R. Gadre, J. Chem. Phys., 125 (2006) 104109.

24. T. Vreven, K. Morokuma, O. Frakas, H. B. Schlegel, and M. J. Frisch, J. Comput. Chem., 24 (2003) 760.

25. C. Lee, W. Yang, and R. G. Parr, Phys. Rev. B, 37 (1988) 785.

26. J. J. Vincent, S. L. Dixon, and K. M. Merz, Jr., Theor. Chem. Acc., 99 (1998) 220.

27. M. S. Gordon, The GAMESS package (2003), URL http://www.msg.ameslab.gov/GAMESS/GAMESS.html.

28. R.S. Mulliken and C.C.J. Roothaan, Proc. Natl. Acad. Sci. (USA), 45 (1959) 394.

Glossary of Terms

Ab initio calculation
Ab initio is Latin for "from the beginning". An ab initio calculation involves no empirical or experimental parameters except for very few fundamental constants such as the charge and mass of an electron, Planck's constant etc.

Hartree-Fock (HF) theory
A type of ab initio calculation method, which is a self-consistent iterative procedure to calculate the so-called "best possible" single determinant solution to the time-independent Schrödinger equation of a many-electron system with fixed nuclei. As a consequence, it incorporates the exchange energy exactly, but does not include the effect of electron correlation.

Density functional theory (DFT)
Uses electron density as the main variable and not the many-body wavefunction. The governing principles of DFT are called the Hohenberg-Kohn (H-K) theorems, valid for the ground state of a many-electron system.

Variation principle
It states that the expectation value of energy obtained from a trial wavefunction for a given system is always greater than or equal to its true ground state energy.

Gaussian basis sets
These are constructed as linear combinations of primitive Gaussian functions of the general form below which are normally centered on the nuclei at $\{R_A\}$ in the molecule.

$$(r \quad R_A) \quad (x \quad x_A)^l (y \quad y_A)^m (z \quad z_A)^n e^{|r \quad R_A|^2}$$

Parallel computing
Parallel computing is the method of simultaneously executing many independent parts of a given task leading to a solution of the task in a faster way.

Divide-and-conquer (D&C)
Divide-and-conquer is an algorithm design paradigm that works by recursively breaking down a problem into two or more sub-problems of the same (or related) type, until these become simple enough to be solved directly. The solutions to the sub-problems are then combined to give a solution to the original problem.

Density matrix (DM)
The elements of the first order density matrix, P are given in terms of the occupied MO coefficients $\{C_{ia}\}$ and the MO occupancies $\{n_a\}$ as :

$$P_{ij} \quad \sum_{a}^{occ} n_a C_{ia} C_{ja}$$

Molecular electron density (MED) is obtained by integration of the absolute square of the many-particle wavefunction over all the

electronic coordinates except one.

$$(r) \quad N \qquad | \quad (x, x_2, \ldots, x_{N)}|^2 d^3 r_2 \ldots . d^3 r_N$$

Molecular electrostatic potential (MESP) is defined as the work done to bring a unit test positive charge from infinity to the reference point, r.

MESP due to a molecular charge distribution at a point is r is the sum of the nuclear and electronic contributions (first and second terms respectively) :

$$V(r) \qquad \frac{Z_A}{|r \quad R_A|} \qquad \frac{(r')}{|r \quad r'|} d^3 r'$$

Slater determinant

It is a determinantal form of the wave function for a many-electron system, which by construction, satisfies the antisymmetry requirement and the Pauli exclusion principle.

Geometry optimization

A calculation to find a minimum energy configuration for a molecular system. The calculation adjusts atomic coordinates in steps to find a configuration in which net forces on each of the atoms are reduced to zero.

Self consistent field theory

The self consistent field method is a numerical algorithm for solving the Schrödinger equation for many electron atoms and molecules. It starts with a set of guess atomic/ molecular orbitals and keeps improving it via an iterative scheme till convergence.

Fock matrix

The matrix elements of the effective one-electron operator for a many electron system constitute the Fock matrix.

Overlap matrix

The overlap matrix element S_{ij} is given by :

$S_{ij} =$ $^*_i(r)$ $_j(r) d^3 r$

where $_i$ and $_j$ represent molecular orbitals.

Orbital

A wavefunction that explicitly depends on the coordinates and spin of a single electron.

Energy gradients

The first order partial derivatives of the energy expression with respect to Cartesian coordinates of the nuclei.

Cardinality of a set

The number of elements in a set is termed as its cardinality. For a set A the set cardinality is generally represented as |A|.

Molecular graph

A graph is collection of vertices and edges. Similarly, a graph depicting a molecule as a collection of atoms (vertices) and bonds (edges: connections between vertices) is termed as a molecular graph.

Prediction of Novel Molecular Species with ab initio Quantum Chemical Methods

After obtaining his M.Sc. degree in Physical Chemistry form Burdwan University, ***Dr. T. K. Ghanty*** *joined BARC in 1988 through 32nd batch Training School and received Homi Bhabha Award. He obtained his Ph.D. degree in Chemsitry from Bombay University in 1996 for his work on density functional theory of chemical binding and chemical reactivity on molecular systems. He has spent two years (1997-99) at Chemistry Department, Indiana University, USA as a postdoctoral fellow. His research interests include theoretical prediction of novel rare-gas compounds, computational investigation of structure and properties of hydrogen-bonded systems, supramolecular chemistry, electronic excited states, clusters and cluster assembled materials. He is also involved in the study of structure and bonding in lanthanide and actinide complexes relevant to nuclear waste management. Dr. Ghanty has co-authored more than 55 papers in peer reviewed*

Abstract

Quantum chemical methods can today be employed to invent new molecules and to characterize them through prediction of their structure and various physico-chemical properties. In this article an overview of some of our ongoing work along this direction is described. In particular, the prediction of chemical compounds formed by rare gas atoms is discussed. Also, the scope of computational techniques in predicting and rationalizing the structure and properties of molecular species containing heavy atoms are presented briefly, with a special emphasis to lanthanide chemistry.

Introduction

Computational chemistry plays a central role in the prediction of structure and various physico-chemical properties of atoms, molecules and clusters with the results obtained through quantum chemical calculations using computers. The potential role of quantum chemistry has been recognized through the award of the 1998 Nobel Prize in chemistry to Walter Kohn and John Pople jointly. With the advancement of high-speed computers and efficient algorithms, in principle ab initio quantum chemistry [1] now allows the investigation of molecular species containing any atoms in the periodic table. The properties that are most commonly calculated include molecular geometry in ground and excited states, charge and spin density distributions, potential energy surfaces, spectroscopic properties, reaction rate constants, thermodynamic properties, details of the dynamics of a process etc. Computational quantum chemical methods can also be employed for the prediction of the existence of novel chemical species. Particularly, computational chemistry is very useful in investigating potentially hazardous compounds that are difficult to handle in laboratory or inaccessible experimentally. It can also be used in combination with experiment to corroborate or complement experimental results. Although the underlying principles and the concerned quantum mechanical equations describing a many electron systems were known long back, however, solutions of those equations were not achieved successfully. Only in the fifties numerical solution of the SchrÖdinger equation for a many electron system has been possible [2] using the self-consistent-field theory of Hartree and Fock (HF) [3,4] within the framework of linear combination of atomic orbital (LCAO) approach. One major drawback of HF theory is the missing of electron correlation energy. Although the contribution of correlation energy to the total energy of a system is very small, it is nevertheless very important in the prediction of any molecular property. In the mid sixties, with the introduction of

Dr. Tapan K. Ghanty, Theoretical Chemistry Section, Chemistry Group, Bhabha Atomic Research Centre, Mumbai 400 085; E-mail: tapang@barc.gov.in

orbital-based density functional theory (DFT) [5] by Hohenberg, Kohn and Sham [6,7], the electron correlation problem has been solved exactly, at least in principle. They showed that electron density at all points in space is enough to uniquely determine the energy, and hence all of the other properties of the system. To achieve this goal one has to assume a relationship between the total energy and the electron density function, which is popularly known as the "density functional". One component of this density functional, viz., exchange-correlation term is not known explicitly for a real system with inhomogeneous electron density distributions. However, the corresponding functional form for a homogeneous electron gas was known, which forms the basis of the local density approximation. Subsequently, many approximate exchange-correlation energy density functionals corresponding to inhomogeneous electron density distribution have been proposed within the framework of the homogeneous electron gas expression in the last two decades. In 1992, John Pople and his team have introduced DFT in the Gaussian program. Here it is important to mention that Pople has been the founder leader of the Gaussian Program, initiated in seventies. Nowadays several such functionals are incorporated in all most all the standard quantum chemistry programs like GAMESS, Gaussian etc. Because DFT includes corrections to HF energies for correlation energy, it is possible to obtain the structures and energies accurately with DFT methods. It is also important to note that computations using DFT is much less expensive as compared to that using other correlated methods based on Møller-Plesset perturbation theory, configuration interaction or multi-configuration approaches [1]. Thus, various chemical systems and processes can be modeled quite accurately using correlated quantum-chemical techniques for interpretation and rationalization of experimentally observed results. In the following sections we discuss two specific areas, viz., (1) rare gas (noble gas) containing chemical compounds, and (2) chemical species involving lanthanide ions.

Theoretical Prediction of New Noble Gas Chemical Compounds

It is well known that the noble gas elements helium, neon, argon, krypton, and xenon are chemically inert due to their closed shell stable electronic configurations in the ground state. However, search for the rare-gas compounds started way back in late thirties when Pauling predicted [8] the possibility of chemical bonding of heavier rare-gas elements due to the less shielding effect of the outer valence electrons from the nucleus. This prediction became a reality through the synthesis of the first rare-gas compound, xenon hexafluro-platinate [$Xe^{+}(PtF_6)^{-}$] by Bartlet in 1962 [9]. This was followed by the preparation of various krypton, xenon, and radon compounds. The synthesis of noble gas compounds proves the unusual examples of chemical bonding; therefore their exploration unravels new bonding mechanism and expands our understanding of a chemical bond. In recent years, several novel rare-gas compounds are predicted theoretically as well as prepared and identified experimentally [10]. The most notable development among them is the preparation and characterization of the molecules of the type HNgX (where Ng is a rare-gas atom such as Ar, Kr, and Xe, and X is an electronegative atom or group) at low temperature by RÄsÄnen and co-workers [11]. Recently Seidel and Seppelt reported [12] the existence of first bulk compound containing a noble gas-noble metal bond ($AuXe_4^{2+}$ $[Sb_2F_{11}^{-}]_2$). It is in contrast to the conventional behavior of noble gas and noble metal atoms that have nearly covalent bonds between gold and xenon. If one considers gold as a truly noble metal and xenon a truly noble gas, such an Au-Xe bond would be impossible. However, noble metal such as gold has a very rich and unusual chemistry with varying physico-chemical properties. It is mostly due to the strong relativistic effects, which considerably decreases the size of the valence 6s orbital and lead to the expansion of the 5d orbital resulting in this kind of unusual behavior [13,14].

We now consider [15] altogether a new class of rare gas compounds containing noble gas-noble metal bond where a noble gas atom (Ng) is inserted into a noble metal molecule (AuX) resulting into the formation of Au-Ng-X species. Essentially, the hydrogen atom in H-Ng-X has been replaced by a gold atom to form Au-Ng-X species. The origin of this development has been the behavior [16,17] of a gold atom as a hydrogen atom in various gold compounds. In the spirit of this behavior of a gold

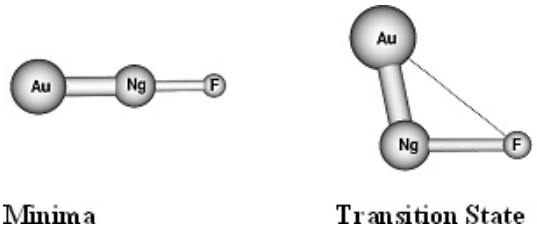

Fig. 1 Minimum energy and transition state structures of AuNgF species

atom as a hydrogen atom we have been motivated [15] to investigate the bonding between a noble gas atom and a noble metal atom in the insertion compounds Au-Ng-X (Ng=noble gas atom and X= electronegative atom or group), e.g. AuKrF and AuXeF. Thus, here our objective is to investigate the structure and properties of the Au-Ng-F compounds with the aid of quantum chemical calculations and to explore whether they are stable or not with reference to their corresponding dissociated products on the respective potential energy surface. We have also considered [18] Cu-Ng-F and Ag-Ng-F compounds for the purpose of comparison with the corresponding Au-Ng-F species (with Ng=Ar, Kr and Xe).

Ab initio molecular orbital calculations within the framework of density functional theory (DFT) using B3LYP exchange-correlation energy density functional and also Møller-Plesset second order perturbation theory (MP2) have been performed employing the GAMESS [19] electronic structure program. Standard 6-311++G(2d,2p) basis sets have been used for the H, F and Ar atoms. For the Kr and Xe atoms we have used Gaussian (6s6p1d1f)/[4s4p1d1f], (6s6p1d1f)/[4s4p1d1f] basis sets [20] along with the Stutgart effective core potentials (ECP). For Cu, Ag and Au atoms also we have used quasi-relativistic Stutgart ECPs along with the corresponding (8s7p6d1f)/[6s5p3d1f] basis sets [20]. The harmonic vibrational frequencies have been calculated to characterize the nature of the stationary points on the respective potential energy surface of different species.

The optimized structures of the AuNgF species (Ng=Ar, Kr and Xe) shown in Figure 1 reveal that the AuXeF and AuKrF are linear. The structures of CuNgF and and AgNgF are also found to be similar to that of the corresponding AuNgF structure. The MP2 calculated geometrical parameters corresponding to the optimized structures of MNgF (M=Cu, Ag, Au) species are reported in Table 1. The Cu-Ng bond lengths in CuArF, CuKrF and CuXeF have been found to be 2.161 Å, 2.253 Å and 2.451 Å, respectively. A similar trend is observed in the Ag compounds, where the calculated Ag-Ng bond lengths are 2.433 Å, 2.506 Å and 2.651 Å for AgArF, AgKrF and AgXeF, respectively. However, the Ng-F bond lengths in CuNgF species are almost the same for all the three systems and the corresponding values are 2.281 Å, 2.267 Å and 2.280 Å for CuArF, CuKrF and CuXeF respectively. Analogous bond lengths in AgNgF systems are also almost the same. Thus, the Ng-F bond lengths are in the range of 2.27-2.28 Å and 2.29-2.32 Å for the Cu and Ag species as compared to the range of 2.06 Å to 2.14 Å in the case of AuNgF molecules. The calculated Ng-F bond length values in HNgF compounds are also found to be smaller than that in CuNgF or AgNgF molecues and ranges from 2.0 to 2.1 Å. The M-Ng-F bond angle is 180 degree for all the systems considered here. It is interesting to compare the noble metal-noble gas bond lengths as obtained in the present work with that of earlier reports for different class of noble-gas compounds, viz., MNgF [15,18] containing noble metal-noble gas bonding. The reported results in Table 2 reveal that the present calculated M-Ng bond length in MNgF species are always smaller than that in NgMF systems published in the literature [21,22] (also calculated here for the sake of consistency in methods, basis sets etc.). It is interesting to note that the deviations in the M-Ng bond lengths in the two classes of compounds, viz., MNgF and NgMF are more for the Cu-Ar, Ag-Ar and Ag-Kr bonds, and the respective differences are 0.071, 0.181 and 0.103 Å. However, for the Au-Ng bond the two sets of values are found to be almost the same. It indicates that the M-Ng bonds in MNgF (with M=Cu and Ag, and Ng=Ar and Kr) are relatively shorter than that in NgMF as compared to the Au-Ng bonds in the two classes of species. As a consequence, the M-Ng interaction in MNgF species is likely to be stronger than that in NgMF systems. Also, the larger Ng-F bond length in CuNgF and AgNgF as compared to that in AuNgF indicates that the Ng atom interacts rather weakly with F atom in

TABLE 1. MP2 calculated values of the optimized geometrical parameters and dipole moments of MNgF (M=Cu, Ag and Au; Ng=Ar, Kr and Xe) systems (bond length R in Å , bond angle in degree and the dipole moment in Debye).

Parameter	systems					
	CuArF		CuKrF		CuXeF	
	Minima	TS	Minima	TS	Minima	TS
R(Cu-Ng)	2.161	2.162	2.253	2.247	2.411	2.388
R(Ng-F)	2.281	2.364	2.267	2.432	2.280	2.505
(Cu-Ng-F)	180.0	138.4	180.0	123.7	180.0	112.4
	15.8	16.0	14.0	14.8	11.7	13.2
	AgArF		AgKrF		AgXeF	
	Minima	TS	Minima	TS	Minima	TS
R(Ag-Ng)	2.433	2.436	2.506	2.505	2.651	2.637
R(Ng-F)	2.325	2.382	2.289	2.445	2.291	2.527
(Ag-Ng-F)	180.0	145.5	180.0	128.6	180.0	114.3
	17.4	17.5	15.2	16.2	12.5	14.4
	AuArF		AuKrF		AuXeF	
			Minima	TS	Minima	TS
R(Au-Ng)			2.448	2.435	2.585	2.555
R(Ng-F)			2.063	2.438	2.140	2.508
(Au-Ng-F)			180.0	112.8	180.0	104.9
			7.5	16.2	6.3	12.2

CuNgF and AgNgF. As a result, the Cu-Ng or Ag-Ng interaction is again expected to be stronger. In view of the interesting reports [21,22] on comparison of the M-Ng bond length with respect to a covalent limit, R_{cov} [r_{cov} (M(I) + r_{cov} (Ng)] and a van der Waals limit, R_{vdw} [r_{ion} (M^+) + r_{vdw} (Ng)] we have tabulated the corresponding limiting values of the bond lengths in Table 2 for the different pairs of M and Ng atoms. From this table it is quite evident that the calculated M-Ng bond lengths in MNgF species are much closer to the covalent limit as compared to the van der Waals limit. In fact, it is important to note that the Cu-Kr bond length in CuKrF is slightly smaller than the corresponding covalent limit. Also, the difference between the calculated Cu-Xe bond length and the corresponding covalent limit is merely 0.041 Å. All these results are somewhat in contrast to the earlier reports [21,22] involving NgMF species where it has been observed that for the Ar compounds the Ar-Ng bond lengths are closer to the van der Waals limit and Kr-Ng bond lengths are in between the two limits. The calculated bond length values also indicate that the Au-Xe bond is closer to the covalent limit as compared to the van der Waals limit and comparable to the corresponding value in XeAuF (2.562 Å), $XeAu^+$ (2.57 Å) and

TABLE 2. Comparison between the MP2 calculated values of the optimized M-Ng bond distance in MNgF and NgMF systems and the corresponding homolytic bond dissociation energy (M=Cu Ag and Au; Ng=Ar, Kr and Xe) (bond distance R in Å and the bond energy D_e in kJ/mol).

Bond	R(M-Ng)		R_{cov}[b]	R_{cov}(TP)[c]	R_{vdw}[b]	D_e(M-Ng)	
	MNgF	NgMF[a]				MNgF[d]	NgMF[e]
Cu-Ar	2.161	2.232 (2.238)	2.04	2.16	2.48	29.2 (17.7)	35.6 (44)
Cu-Kr	2.253	2.300 (2.322)	2.26	2.28	2.60	82.1 (67.0)	50.2 (45)
Cu-Xe	2.411	2.429 (2.459)	2.37	2.42	2.78	153.8 (139.1)	67.9 (59.4)
Ag-Ar	2.433	2.614 (2.590)	2.26	2.33	2.69	-1.2 (-12.7)	12.8 (14)
Ag-Kr	2.506	2.617 (2.609)	2.38	2.45	2.81	42.8 (29.3)	22.6 (17)
Ag-Xe	2.651	2.700 (2.684)	2.58	2.59	2.99	116.2 (101.1)	38.1 (36)
Au-Kr	2.370	2.46	2.45	2.31	2.77	2.0	(58)
Au-Xe	2.585	2.57	2.57	2.45	2.95	109.8	97 (101)

[a]The values of M-Ng bond length in NgMF systems calculated in this work. Within the parenthesis the results from Ref. [21,22] are given.
[b]The terms R_{cov} and R_{vdw} indicate the covalent and van der Waals limits, respectively, of the M-Ng bond; see text for more details.
[c]The terms R_{cov} (TP) refers to the sum of the triple bond covalent radii for the respective atoms corresponding to each M-Ng bond.
[d]The calculated values of the M-Ng bond energies in MNgF systems calculated in this work. Within the parenthesis the BSSE-corrected values are given.
[e]The BSSE-corrected values of the M-Ng bond energies in NgMF systems calculated in this work. The BSSE-corrected values from Refs. [21,22] are given within the parenthesis.

$XeAuXe^+$ (2.66 Å). On the other hand, for $[AuXe_4]^{2+}$ the Au-Xe bond distance is rather large (2.79 Å) and lies in between covalent and van der Waals limit. Now it is interesting to compare the M-Ng bond lengths in MNgF species with the sum of triple bond covalent radii proposed recently [23]. For the AgNgF species the Ag-Ng bond distances are slightly above the corresponding triple bond covalent radii sum (see Table 2). However, the Cu-Ng bond distances in CuNgF species are very close to the respective covalent radii sum. In fact, it is important to note that the Cu-Kr bond length in CuKrF is smaller than the sum of triple bond covalent radii, implying a partial triple bond nature in the noble metal atom and the noble gas atom bonding.

It is important to note that some of the calculated values of the M-Ng bond dissociation energies (with Ng=Kr and Xe) are remarkably larger in MNgF species than that in NgMF systems. For instance, the Cu-Xe bond energy in CuXeF (139.1 kJ/mol) is ~2 times (~105%) larger than the same in XeCuF (67.9 kJ/mol) species. Similarly, the Ag-Xe bond energy in AgXeF (101.1 kJ/mol) is ~2.7 times (165%) larger than the same in XeAgF (38.1 kJ/mol) species. The calculated value of Au-Xe bond energy in AuXeF molecule (109.8 kJ/mol) has been found to compare very well with previous Au-Xe bond energy obtained for other compounds, viz. XeAuF (101.0 kJ/mol), $XeAu^+$ (127.0 kJ/mol) and $XeAuXe^+$ (108.0 kJ/mol). It is also interesting to compare the variation of the M-Ng bond energy along the series Cu-Ag-Au for the two sets of species, viz., MNgF and NgMF. Considering the values reported in Table II it is clearly evident that the M-Ng bond energies in MNgF species (with Ng=Kr and Xe) follow the trend, Cu-Ng>Ag-Ng≥Au-Ng, which is somewhat different than that observed in NgMF species (Au-Ng>Cu-Ng>Ag-Ng). In this context it is important to note that the Au-Xe bonding has been predicted theoretically before its existence has been established experimentally.

TABLE 3. Energies (in kJ/mol) of the various dissociated species relative to the energies of the MNgF (M=Cu and Ag, Ng=Ar, Kr and Xe) systems calculated at the MP2 level of theory.

Molecular Species	Ng=Ar	Ng=Kr	Ng=Xe
CuNgF	0.0	0.0	0.0
CuF + Ng	-397.9	-344.8	-272.6
Cu + F + Ng	30.1	83.1	155.3
Transition State (CuNgF→CuF + Ng)	5.3	19.8	46.8
AgNgF	0.0	0.0	0.0
AgF + Ng	-349.4	-305.2	-231.4
Ag + F + Ng	-0.3	43.9	117.7
Transition State (AgNgF→AgF + Ng)	2.4	14.2	42.3
AuNgF		0.0	0.0
AuF + Ng		-276.0	-166.2
Au + F + Ng		-3.0 (-52.4)	-112.9 (-128.9)
Transition State (AuNgF→AuF + Ng)		74.9 (76.6)	119.1 (126.2)

To assess the stability of the predicted noble gas compounds, we have reported the energies corresponding to the various dissociated products of MNgF molecules in Table 3. It is clear that MKrF and MXeF are less stable than MF + Kr and MF + Xe by 276.0 and 166.2 kJ/mol, respectively at the MP2 level of theory. An alternative channel to decompose MNgF is a direct dissociation of M-Ng and Ng-F bonds leading to the formation of M + Ng + F. The dissociation energies corresponding to this channel indicate that most of these species are metastable and have a local minimum in their respective potential energy surfaces. The kinetic stability of the MNgF species have been assessed through calculations of the transition state corresponding to the MF + Ng dissociation channel. The calculated transition state structures are reported in Figure 2 and the corresponding geometrical parameters are included in Table 1. The calculated barrier heights (Table 3) indicate that most of the species should be kinetically stable with respect to the bending reaction coordinate.

Structure of Lanthanide Complexes

Coordination chemistry of trivalent lanthanides (Ln) and actinides is an important area of research [24-28] because of its significance in the management of nuclear spent fuel. Transmutation of the trivalent actinides will only be possible after separation of the minor actinides from the trivalent lanthanides that are present in large excess. This separation is often difficult because of the great chemical similarity of these two series of f-block elements with similar charge and size. Nevertheless, it is possible to discriminate between the two series of ions because of a small difference in their affinities for a comparatively softer donor ligands containing N or S as donor atoms, e.g., viz. Cyanex-301 (Bis (2,4,4-trimethyl pentyl) dithiophosphinic acid) [25]. Depending on the experimental conditions, the structure and the composition of the ion-ligand complexes have been reported to differ drastically [29]. Therefore, our objective here [30] is to find out the ion-ligand

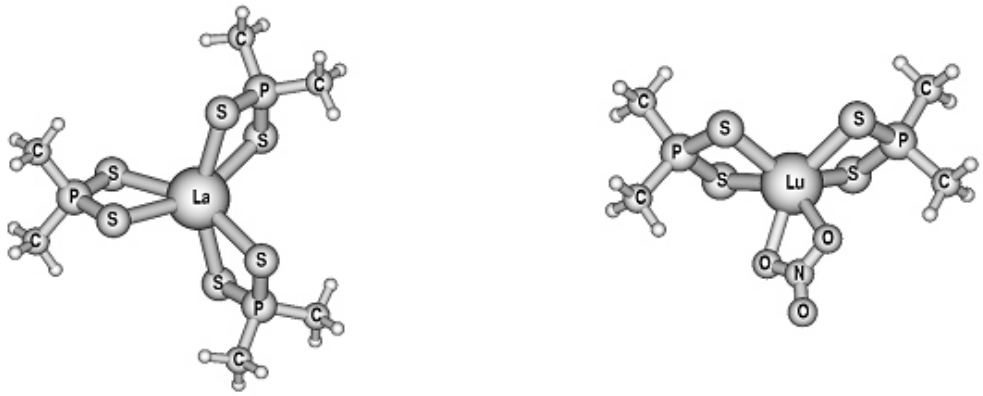

Fig. 2 Minimum energy structures of the $La(Me_2PS_2)_3$ and $Lu(Me_2PS_2)_2NO_3$ complexes

complexes (extracted species) for various lanthanide ions in presence of Cyanex-301 and nitrate ion as ligands, through the calculation of the energy of complex formation using ab initio molecular orbital theory. For computational simplicity we have considered Dimethyl dithiophosphinic acid (Me_2PS_2H) in place of Cyanex-301. Thus, the structures of the possible extractable species with a different number of $Me_2PS_2^-$ and NO_3^- ligands were optimized at the Hartee-Fock level of theory using GAMESS electronic structure program [19]. For the H, C, N, O, P, and S atoms 6-31G** basis sets have been used. Stuttgart quasirelativistic effective core potentials [20] have been used for the lanthanides along with the corresponding (5s/4p/3d) valence basis sets.

We consider the following equation to determine the composition of the complex for different ions.

$$Ln(NO_3)_3 + nMe_2PS_2H \rightarrow Ln(Me_2PS_2)_n(NO_3)_{3-n} + nHNO_3 \quad (1)$$

The energy of complex formation in presence of two different ligands, viz., $Me_2PS_2^-$ and NO_3^- (E_n, with n as the number of $Me_2PS_2^-$ ligand) for various species involving La(III), Eu(III) and Lu(III) have been defined as $E_n = E_P - E_R$, where E_P and E_R indicate the energy of the products and energy of the reactants, respectively. Thus, E_1, E_2 and E_3 correspond to the formation energy of the $Ln(Me_2PS_2)(NO_3)_2$, $Ln(Me_2PS_2)_2(NO_3)$ and $Ln(Me_2PS_2)_3$ species, respectively. Energies of the reactants (E_R) and the products (E_P) have been calculated using ab initio HF level of theory. The complex formation energies reported in Table 1 indicate that the formation of the species with two $Me_2PS_2^-$ and one nitrate ion [$Ln(Me_2PS_2)_2(NO_3)$] is the most preferred one for all the three lanthanides considered here. In the cases of La(III) and Eu(III), E_1 and E_2 values have been found to be closer (difference 1.3-2.0 kcal/mol). It implies that formation of both the species is almost equally probable. However, at higher Me_2PS_2H concentration the formation of $La(Me_2PS_2)_3$ species is more probable because of the closer E_2 and E_3 values. On the other hand, in case of Lu(III), the formation of $Lu(Me_2PS_2)_2NO_3$ is more preferred as compared to the other species due to a comparatively larger energy differences between E_2 and E_1, and also between E_2 and E_3. It indicates that Lu(III) is likely to be extracted as $Lu(Me_2PS_2)_2NO_3$ irrespective of the Me_2PS_2H concentration. The minimum energy structures of the complexes are reported in Figure 2. It is indeed interesting to note that similar kind of behavior has been observed [30] experimentally through solvent extraction experiments with varying Cyanex-301 concentration. From the distribution studies (by slope analysis) of the lanthanides (viz. La(III), Eu(III) and Lu(III)) it has been observed that in case of La(III) and Eu(III) only two molecules of Cyanex-301 were involved in the extractable species at low Cyanex-301 concentration (upto 0.3M), however, it changed to the species with three Cyanex-301 molecules with increase in Cyanex-301 concentration. On the other hand, in case of Lu(III)

TABLE 4. Reaction energies (in kcal/mol) of different species of the lanthanides with one, two and three molecules of Me_2PS_2H

Lanthanides	E_1	E_2	E_3
La^{3+}	-4.3	-6.3	-6.2
Eu^{3+}	-4.4	-5.7	-4.1
Lu^{3+}	-12.4	-16.6	-12.8

the extractable species contained only two Cyanex-301 over the whole concentration range. The charge neutralization of the species with two Cyanex-301 molecules was therefore taken place by the nitrate ion present in excess in the aqueous phase. Density functional calculations on these species are in progress.

Concluding Remarks

Here, we have investigated the structure and the stability of a new class of insertion compounds of noble gas atoms of the type MNgF (M=Cu, Ag and Au; Ng=Ar, Kr and Xe) using ab initio techniques. For most of the predicted species, the noble metal-noble gas bond (M-Ng) distances are calculated to be comparable with the corresponding covalent limit. The predicted stability of these species would widen the scope of the field of rare gas chemistry containing noble metal-noble gas moiety. The results presented here suggest that among all the species considered here CuXeF is sufficiently stable and may be a likely candidate to be prepared experimentally in analogy with the experimentally observed rare gas hydrides (HNgF). Further investigations to predict new noble gas compounds are in progress [31-33] in our laboratory.

Because of its importance in nuclear industry the selective extraction of lanthanides and actinides has received considerable attention. In an attempt to rationalize the experimental results obtained from solvent extraction experiments (viz., different extractable species corresponding to different trivalent lanthanides), we have employed ab initio methods to determine the structure and energy of formation for a selective number of lanthanide complexes in presence of Cyanex-301 and NO_3^- ligands. At lower concentration, $Ln(Cyanex\text{-}301)_2NO_3$ is the most favored extractable species for all the lanthanides considered here. However, for higher concentration of Cyanex-301, the extractable species found experimentally [$Ln(Cyanex\text{-}301)_3$] for the La and Eu ions can be rationalized from the small difference in complex formation energy . Also, the experimentally predicted most favored Lu complex, viz., $Lu(Cyanex\text{-}301)_2NO_3$ over whole range of Cyanex-301 concentration can be explained from a relatively larger energy difference in the energy of complex formation. More work is in progress along this direction. Thus, we have briefly demonstrated the potential role of computational chemistry in the prediction and rationalization of structure and properties of two different type of chemical systems.

Acknowledgments

I would like to thank Dr. B. S. Tomar for giving me an opportunity to write an article in this special issue of IANCAS bulletin. I am very much thankful to Arunasis Bhattacharyya and Dr. T. Jayasekharan for many helpful discussions. It is a pleasure to thank Dr. Swapan K. Ghosh and Dr. Tulsi Mukherjee for their kind interest and constant encouragement.

References

1. (a) W. J. Hehre, L. Radom, P. v. R. Schleyer and J. A. Pople, "Ab Initio Molecular Orbital Theory", John Wiley & Sons, New York, 1986; (b) F. Jensen, Introduction to Computational Chemistry, Wiley, Chichester, (1999).
2. C. C. J. Roothaan, Rev. Mod. Phys. 32 (1960) 179.
3. D. R. Hartree, The Calculation of Atomic Structures, Chapman and Hall, London (1957).
4. V. Fock, Z. Phys 61 (1930) 126.
5. R. G. Parr and W. Yang, Density Functional Theory of Atoms and Molecules , Oxford University Press: New York, (1989).
6. P. Hohenberg and W. Kohn, Phys. Rev. B136 (1964) 864.

7. W. Kohn and L. Sham, Phys. Rev. A140 (1965) 1133.
8. L. Pauling, J. Am. Chem. Soc. 55 (1933) 1895.
9. N. Bartlett, Proc. Chem. Soc. 218 (1962).
10. M. Pettersson, L. Khriachtchev, J. Lundell and M. Räsänen, in Inorganic Chemistry in Focus II, edited by G. Meyer, D. Naumann and L. Wesemann (Wiley, Weinheim, 2005), pp 15-34. See also, R. B. Gerber, Annu. Rev. Phys. Chem. 55, 55 (2004).
11. L. Khriachtchev, M. Pettersson, N. Runeberg, J. Lundell, M. Räsänen, Nature 406 (2000) 874.
12. S. Seidel and K. Seppelt, Science 290, 117 (2000).
13. P. Pyykkö and J. P. Desclaux, Acc. Chem. Res. 12 (1979) 276.
14. P. Pyykkö, Chem. Rev. 88 (`1988) 563.
15. T. K. Ghanty, J. Chem. Phys. 123 (2005) 074323.
16. P. Pyykkö, Angew. Chem., Int. Ed. 43 (2004) 4412.
17. T. K. Ghanty, J. Chem. Phys. (Communication) 123 (2005) 241101.
18. T. K. Ghanty, J. Chem. Phys. 124 (2006) 124304.
19. M. W. Schmidt, K. K. BalDridge, J. A. Boatz, S. T. Elbert, M. S. Gordon, J. H. Jensen, S. Koseki, N. Matsunaga, K. A. Nguyen, S. J. Su, T. L. Windus, M. Dupuis, and J. A. Montgomery, Jr., J. Comput. Chem. 14 (1993) 1347.
20. D. Andrae, U. Haussermann, M. Dolg, H. Stoll and H. Preuss, Theor. Chim.Acta 77 (1990) 123.
21. J. M. Thomas, N. R. Walker, S. A. Cooke, and M. C. L. Gerry J. Am. Chem. Soc., 126 (2004) 1235.
22. S. A. Cooke and M. C. L. Gerry, J. Am. Chem. Soc., 126 (2004) 17000; and references therein.
23. P. Pyykkö, S. Riedel and M. Patzschke, Chem. Eur. J. 11 (2005) 3511.
24. N. Kaltsoyannis, Chem. Soc. Rev. 32 (2003) 9.
25. M.A. Denecke, Coord. Chem. Rev. 250 (2006) 730.
26. Y. Zhu, J. Chen, and R. Jiao; Solv. Extr. Ion Exch. 14 (1996) 61.
27. M. P. Jensen, and A. H. Bond, J. Am. Chem. Soc. 124 (2002) 9870.
28. L. Petit, C. Adamo and P. Maldivi, Inorg. Chem. 45 (2006) 8517.
29. A. Bhattacharyya, P. K. Mohapatra and V. K. Manchanda, Solv. Extr. Ion Exch., 24 (2006) 1.
30. A. Bhattacharyya, P. K. Mohapatra, T. K. Ghanty and V. K. Manchanda NUCAR-2007 (accepted).
31. T. Jayasekharan and T. K. Ghanty, J. Chem. Phys. 124 (2006) 164309.
32. T. Jayasekharan and T. K. Ghanty, J. Chem. Phys. 125 (2006) 234106.
33. T. Jayasekharan and T. K. Ghanty, J. Chem. Phys. (Manuscript in preparation).

Fluids at Interfaces – A Theoretical Chemist's Perspective

Dr. Chandra N. Patra *is working as a senior scientist in the Theoretical Chemistry section of Bhabha Atomic Research Centre. He graduated in Chemistry discipline from the 33rd batch of BARC Training School in 1989. Since then he is actively engaged in research and development work on the theoretical chemistry of soft condensed systems including designing of efficient methodologies and application to the areas of current interest. He obtained his Ph.D. in Chemistry from Bombay University in 1996 and has a large number of publications in his credit. He has pursued his postdoctoral research at the University of Wisconsin, Madison, USA during 1997-1999. He was a visiting professor at the Universidad de Guanajuato, Mexico in 2002 and an associate at the University of Utah, USA in 2005.*

Abstract

A clear and efficient understanding of the microscopic structure and macroscopic properties of condensed phase systems from a molecular standpoint is important for both classical and modern chemistry. Statistical mechanics provides the same by bridging the gap between molecular events and the structural and physicochemical properties of macroscopic systems. With exponential rise in computational capabilities coupled with robust methodologies, molecular simulations and ab initio quantum mechanics are promising to provide a nearly exact route for utilizing the full potential of statistical mechanics. However, phenomenological and semiempirical methods still remain relevant in the forthcoming days because of their simplicity and versatility for solving problems involving multiple length and time scales that are yet unreachable by direct methods. Amalgamation of analytical theories and computer simulation offers a serious compromise: on the one hand, it is able to retain the theoretical rigor of statistical mechanics and, on the other hand, similar to an approximate method, it demands only modest computational cost for modeling the properties of macroscopic systems. Recent advances on such approximate methods are summarized with emphasis on applications to quantitative modeling of the interfacial behavior of fluids and soft materials, including simple fluids, electrode-electrolyte interface, polymer solutions, and polyelectrolytes. Attention is also given to some potential applications of these methods to nanomaterials and self-assemblies.

Introduction

The goal of statistical mechanics is to interpret and predict the properties of macroscopic systems in terms of their microscopic counterparts [1,2]. It provides the basis for understanding numerous natural phenomena and for design and optimization of chemical processes [3,4]. The importance of statistical mechanics in many different branches of basic and applied chemistry has long been realized, although its tunability to specific structural and dynamical problems has become feasible only in recent times [5-8]. The obvious reason for such a systematic development is its versatile applicability and suitability to cover the entire spectrum of physicochemical problems, thereby providing an inherent proximity to real experimental data [9-12]. As a corollary, a number of approximate and semiempirical methods [13-15] emerge which use ingenious combinations of basic concepts from statistical mechanics.

The quanta of sophistication in statistical mechanical methods are naturally driven by the specificity of problems used to represent various physicochemical systems. So far a number of more rigorous theoretical methods have been devised [16], which are based on molecular simulations [17], liquid-state theories [18], self-consistent field theory [19], and classical density functional theory [20].

Dr. Chandra N. Patra, Theoretical Chemistry Section, Chemistry Group, Bhabha Atomic Research Centre, Mumbai 400 085, E-mail:chandra@barc.gov.in

Thus, efficient lattice-Boltzmann methods have been developed [21] for predicting the structure and dynamics of charged colloidal systems, integral equation theory has been established [22] for equilibrium phase behavior of fluids involving virtually any system of practical interest, density functional theory in various versions has been formulated [23] to study the conformational behavior of polymer solutions at interfaces. With the rapid increase of computational capabilities, molecular simulation [24] and ab initio quantum mechanics [25] started providing the major impetus for statistical mechanics. However, simulation itself has a long way to go for the actual realization of the fundamental concepts in chemistry, not only because significant progress has yet to be made about the strategies for modeling multiple length and time scale phenomena but, more importantly, interpretation of simulation data, much like experimental results, often requires theoretical tools for analysis and representation. Thus the present and the next decade are going to have an amalgamation between the analytical and simulation methodologies for predicting the molecular constituents of a system with "tailored" properties, commonly used in practical applications including control of gene expression [26], synthesis of biomacromolecules [27] and fabrication of nanomaterials [28].

The goal of materials design is the optimization of specific properties such as high strength and low density together with a number of other critical aspects including manufacturing cost and environmental acceptability. Computational materials design should help in addressing all these aspects. The present decade is passing through an evolution of methodologies [29-31] for designing new materials through multiscale materials modeling [32], ranging from the quantum, atomistic or molecular, and mesoscales. At the quantum scale, computations seek to solve the SchrÖdinger equation and describe the ground state (and sometimes the excited state) energies as well as other properties (e.g., molecular geometry, vibrational and NMR spectroscopic data, multipolar moments, etc.) of chemical species. Currently, ab initio molecular orbital theory [33] provides the most accurate prediction of molecular properties. The results of quantum mechanical calculations are often used in the design of molecular force fields providing a connection to the next scale, that of atomistic simulations. The atomistic or molecular scale encompasses a wide variety of computations. Calculations are usually done by molecular dynamics or Monte Carlo methods using classical "ball and spring" force fields. Using statistical mechanics, the results of atomistic or molecular scale calculations can then be applied to describe behavior at the mesoscopic and macroscopic scale (e.g., process or bulk properties). Mesoscale computations describe behavior and properties of systems that reflect the molecular composition of materials, but consist of far too many atoms to compute atom by atom. Quantitative, predictive methods for dealing with such systems are only now on the horizon. Some current approaches include linear statistical modeling, fractal models, re-normalization models, lattice-Boltzmann approaches, wavelets, homogenization solutions of partial differential equations, self-consistent mean field theory, dynamic mean-field density functional methods, and dissipative particle dynamics. Current models rely heavily on either atomic-scale or continuum assumptions.

The rich variety of equilibrium and dynamical phenomena associated with the solid-fluid interface has been investigated through a number of theoretical approaches from time to time. In recent years there has been an upsurge of interest in this field due to significant progress in computer simulation as well as availability of sophisticated tools in the theoretical formulations. Most of the earlier developments, however, have been based on simple model systems to mimic the characteristics of the real complex systems. The purpose of this article is to review, along with illustrative examples, recent progress in the modeling of interfacial properties of fluids and soft materials. Following a brief introduction to the basic concepts and new developments, the main text is concerned with applications of these methodologies to (1) interfacial behavior of simple fluids and their mixtures, (2) bulk fluids, (3) electric double layers, (4) solvation, and (5) structure of polymeric materials. This article concludes with a brief discussion of some possible future applications of theoretical chemistry to fabrication of novel materials, biomolecular engineering, and molecular self assembly. No

attempt has been made to cover all aspects of methodologies and techniques in the recent literature.

Basic Concepts and New Developments

Statistical mechanical description of classical systems [18] involves the concept of an ensemble, which is an arbitrarily large collection of imaginary systems, all of which are characterized by the same macroscopic parameters, but each member of the ensemble has different sets of coordinates and momenta of the particles. The system dealing with an interface is an open system in general, and is characterized by fixed values of volume V, temperature T and chemical potential . An ensemble of systems of this type is called a grand canonical ensemble, which is represented by a cloud of phase points distributed in space according to the probability density

$$f_0(r^N, p^N; N) \quad \frac{h^{3N}}{N!} \frac{\exp(N \quad) \exp([\quad H_N(r^N, p^N)]}{(\quad, V, T)}$$

where, the grand partition function is defined as

$$\sum_{N \quad 0} \frac{z^N}{N!} \quad \exp \quad U_N(r^N) \; dr^N$$

with z as the activity, (=2/k_BT)as the inverse temperature and $U_N(r^N)$ representing the total potential energy. The link between the statistical mechanics and thermodynamics is made through the relation

$$= -\exp[- \quad (\quad, V, T)] = \exp(\quad PV)$$

where, (= F-N) is the grand potential, and P is the pressure. The equilibrium n-particle density, $^{(n)}(r^n)$, which represents the probability of any particle being in dr_1 at r_1, . . . , another particle in dr_n at r_n, is defined as

$$^{(n)}(r^n) \quad \frac{1}{N \quad n} \frac{z^n}{(N \quad n)!} \exp[\quad U_N(r^N)] dr^{(N \quad n)}$$

and is normalized according to the relation

$$^{(n)} dr^n \quad \left\langle \frac{N!}{(N \quad n)!} \right\rangle$$

In particular, for one and two particle densities, one has

$$^{(1)}(r) dr \quad \langle N \rangle$$

$$^{(2)}(r_1, r_2) dr^2 \quad \langle N^2 \rangle \quad \langle N \rangle$$

which imply that for a homogeneous system, the single particle density is

$$^{(1)}(r) \quad \frac{\langle N \rangle}{V} \quad 0$$

which is nothing but the bulk density of the fluid. In the case of an ideal gas [where $U_N(r^N)=0$],

$$^{(n)}(r^n) \quad \frac{\sum_{N \quad n} \frac{z^N}{(N \quad n)!} V^{N \quad n}}{\sum_{N \quad 0} \frac{z^N}{N!} V^N} \quad z^n \quad \begin{matrix} n \\ 0 \end{matrix}$$

Therefore, it seems quite appropriate to introduce the corresponding n-particle distribution function $g^{(n)}(r^n)$ as

$$g^{(n)}(r^n) \quad \frac{^{(n)}(r^n)}{\prod_{i \quad 1}^{n} {}^{(1)}(r_i)}$$

which defines the fractional deviation from the ideal gas limit (complete randomness). In fact, $g^{(n)}(r^n)$ 1 for all n at large separations. For an isotropic and homogeneous system, the pair distribution function $g^{(2)}(r_1,r_2)$ is a function of the interparticle separation $r_{12}=|r_1-r_2|$ only, and is called the radial distribution function (RDF) g(r). One can also define a pair correlation function (PCF)

$$h(r_1-r_2) = g^{(2)}(r_1-r_2) - 1$$

which vanishes in the limit $|r_1-r_2|$ and gives a measure of the total correlation between particles 1 and 2. The RDF, g(r) is a very important quantity in the liquid state theory as it can be directly accessible from scattering experiments and also most of the thermodynamic properties of the liquid can be expressed in terms of g(r). The single particle density $^{(1)}$(r) can also be conveniently expressed in terms of instantaneous density as

$$^{(1)}(r) \quad (r) \quad \langle \hat{}(r) \rangle \quad \left\langle \sum_{i\ 1}^{N} (r \quad r_i) \right\rangle$$

which, however, for a molecular fluid will be dependent on the individual position of all the atoms [R=(r_1,r_2,…,r_n)].

The starting point in a density functional theory [34] is an expression for the grand potential as a functional of the density profile (r) of the fluid

$$[\ ] \quad {}^{1} \ dr \ (r)\{\ln[\ (r)\ ^{3}] \ 1\} \ F_{ex}[\ ] \\ dr \ (r)[U_{ext}(r) \quad]$$

which attains a minimum value at the true equilibrium density

$$\frac{\quad}{(r)} \quad 0$$

This gives rise to the fundamental equation for the density distribution (r)

$$(r) \quad z\exp[\quad U_{ext}(r) \quad c^{(1)}(r;[\ ])]$$

where $c^{(1)}$(r;[ ]) represents the one-particle direct correlation function (DCF), the first in the hierarchy of DCFs, the n-particle being defined as

$$c^{(n)}(r_1, r_2, \ldots\ldots, r_n;[\ ]) \qquad \frac{^{n}F_{ex}[\ ]}{(r_1)\ldots \quad (r_n)}$$

The exact functional form of the excess free energy functional F_{ex}[ ] for a nonuniform distribution is, however, not known in general, and therefore the crux of the problem lies in finding a suitable approximation to express this functional in terms of density. The same is often known for homogeneous systems with some model interparticle potentials and this knowledge is usually used for approximating them for the corresponding nonuniform systems. The simplest approach is the perturbative approach [35] where F_{ex}[ ] is obtained through functional Taylor expansion about the bulk density $_0$

$$F_{ex}[\ ] \quad F_{ex}[\ _0] \quad \sum_{n\ 1} \frac{1}{n!} \ dr_1 \ldots dr_n \tilde{c}^{(n)}(r_1,\ldots,r_n) \prod_{i\ 1}^{n} [\ (r_i) \quad _0]$$

where $\tilde{c}^{(n)}$ denotes the DCF for the uniform fluid. The second approach is the nonperturbative approach, where the effect of higher order terms are

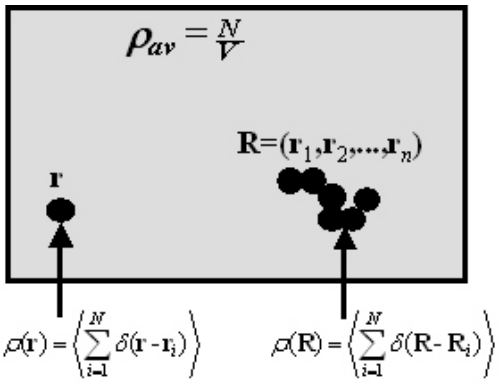

*Fig. 1 Definitions of average density $_{av}$, local atomic density (**r**) and local molecular density (**R**) in a system containing N polyatomic molecules in volume V.*

incorporated in an average manner by involving the concept of weighted density approximation (WDA) [36]. It relies on mapping the nonuniform fluid locally into an uniform fluid at some effective density, constructed from the actual nonuniform density using a coarse graining procedure, viz.,

$$^{-}(r) \quad dr' \ (r')w(r,r')$$

with a nonlocal weight function w(r,r), which may in general be density dependent and is normalized to unity so that $^{-}(r)$ reduces to the bulk density $_0$ in the uniform limit.

Another class of theories that made significant progress over the recent years in the calculation of structure and thermodynamic properties of bulk fluids as well as fluids at interfaces belong to the integral equation theory (IET) [37]. Although several versions are available, in most cases, IET starts with the Ornstein-Zernike (OZ) equation,

$$h(r_{12}) \quad \tilde{c}^{(2)}(r_{12}) \quad _0 \quad dr_3 \tilde{c}^{(2)}(r_{13})h(r_{32})$$

which indicates that the PCF, $h(r_{12})$ consists of a direct part and an indirect part, which incorporates the influence propagated directly to a third particle 3. The OZ equation is essentially a constitutive equation and requires a closure relation for calculation of PCF or RDF, the commonly used one being the Percus-Yevick (PY) approximation

$\tilde{c}^{(2)}(r_{12}) \quad g(r_{12})\{1 \quad \exp[\ u(r_{12})]\}$

and the hypernetted chain (HNC) approximation

$\tilde{c}^{(2)}(r_{12}) \qquad u(r_{12}) \quad h(r_{12}) \quad \ln g(r_{12})$

where $u(r_{12})$ represents the pair potential between particles 1 and 2 and the total potential energy, $U_N(r^N)$ is assumed to be given as a sum of pair terms

$$U_N(r^N) \quad \sum_{i\ j}^{N} u(r_{ij})$$

Since both PY and HNC closures do not generate a thermodynamically consistent equation of state for any specified interparticle potential, a number of new closures are found to be useful in a number of applications. This has resulted into a number of hybrid methods in recent times that consist of both DFT and IET, the notable among these is the self-consistent density functional approach (SCDFA) [38], which is based on the universality of the free energy density functional.

Alongside the developments of versatile theoretical tools, the past two decades have seen a phenomenal growth in computer experiments [39] mainly because they provide essentially exact, quasi-experimental data on well defined models, and hence theoretical results can be tested unambiguously in a manner that is generally impossible with data obtained in experiments on real liquids. It is also possible to obtain information on quantities of theoretical importance that are not readily measurable in the laboratory. Although several versions of computer simulation methods exist in the literature, all methodologies are mainly dependent on two major techniques, viz. Molecular Dynamics (MD) and Monte Carlo (MC) simulation methods. In a conventional molecular dynamics simulation, a system of N particles is placed within a cell of fixed volume, frequently cubic in shape. A set of velocities is also assigned, usually drawn from a Maxwell-Boltzmann distribution appropriate to the temperature of interest, viz.

$(v_i) \quad (\ m_i / 2\ )^{3/2} \exp(\quad m_i |v_i^2|/2)$

and selected in such a way so as to make the net linear momentum $P = m_i v_i = 0$. The subsequent trajectories of the particles are then calculated by integration of the classical equations of motion

$m\ddot{\boldsymbol{r}}_{\boldsymbol{i}} \qquad {}_iV_N(r^N)$

The particles are assumed to interact through some prescribed force law and the bulk of the computational labor is concerned with the calculation at every step of the forces acting on each particle. The static and dynamic properties of the system are then obtained as time averages over the dynamical history of the system

$$A_{obs} \quad \langle A \rangle_i \quad \lim_{r} \ \frac{1}{-} \ dt\, A[\ (t)]$$
$$0$$

where represents a particular point in phase space. Apart from the choice of initial conditions, a molecular dynamics simulation is, in principle, entirely deterministic in nature. By contrast, as the name suggests, a probabilistic element is an essential part of any Monte Carlo computation. In a classical Monte Carlo simulation, a system of N particles interacting through some known potential is again assigned a set of arbitrarily chosen initial coordinates; a sequence of configurations of the particles is then generated [(t) (t+1)] by successive random movements with the probability density $_{ens}(\ )$ of the ensemble. Any reasonable initial distribution should lead to the same average value

$A_{obs} \quad \langle A \rangle_{ens} \quad \langle A| \ _{ens} \rangle \qquad A(\ )\ _{ens}(\ )$

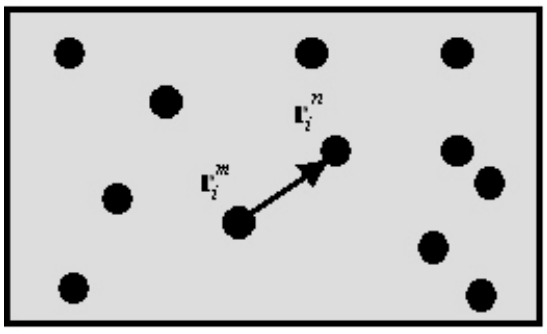

Fig. 2 Monte Carlo translational move of a particle. State n is generated from state m by displacing a particle from r_i^m to r_i^n.

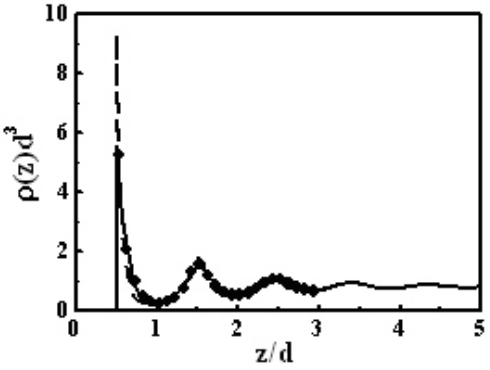

Fig. 3 Density profile of a hard sphere fluid ($_0d^3$ =0.715) near a hard wall. The solid curve refers to the results from SCDFA and the dashed curve refers to the results obtained using the PY approximation. Simulation results are shown as circles.

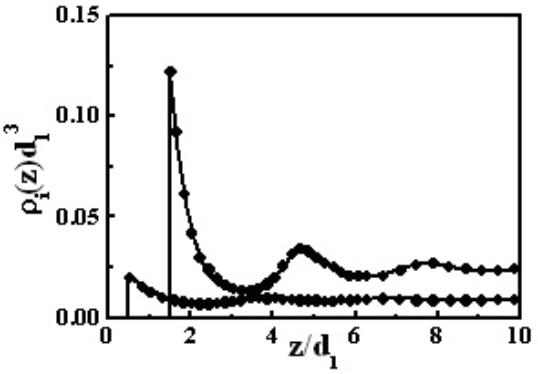

Fig. 4 Density profiles of a binary hard-sphere mixture (=0.3435) near a hard wall for the parameters d_1/d_2=1/3, and x=0.7144. The bottom and the top curves refer to $_1$(z) and $_2$(z), respectively. Simulation results are shown as circles.

with the ergodicity holding good for the specified system of interest.

Applications

As indicated in Section 1, there have been numerous applications of the newer theoretical developments and computer simulation methods discussed above to the calculation of various interfacial properties of fluids that are essential for industrial operations involving thin liquid films, micelles, microemulsions, adsorption-based separations, and heterogeneous chemical reactions and in technological developments involving specialty chemicals, paints, detergents, liquid polymer alloys, and DNA technology. Rather than attempting to review the entire field, which is rather cumbersome, we select a few topics that illustrate the usefulness and shortcomings of the recent developments in these fields.

Hard Sphere Hard Wall Interface

The simplest system studied so far is the hard sphere fluid in presence of a smooth hard wall. This model system has been the subject of intense discussion over last decades because it serves as a test system for the improvement and consolidation of the liquid state theories to more complex systems. Fig. 3 depicts [40] the local density profile at bulk density $_0d^3$=0.715, calculated using the SCDFA formalism alongwith the results obtained using the PY approximation within IET and the simulation results [41]. It is amply evident that SCDFA reproduces the ordering of the fluid particles quite comparable with the simulation results. It should be pointed out that the SCDFA based on the universality of the bridge function B( ) expressed as a function of (r) [= h(r) - $\tilde{c}$(r)] and that of the quantity $\tilde{c}^{(1)}(^{-}(r))$ $\tilde{c}^{(1)}(^{-}_0)$ as a function of $^{-}(r)$ is essentially the same. Thus, SCDFA based on the former approach predicts [42] the density profiles of a binary hard-sphere mixture near a hard wall for diameter ratio d_1/d_2=1/3, concentration x $^0_2$ / $_0$ 0.7144, and bulk packing fraction $^0_1d_1^3$ $^0_2d_2^3$ = 0.3435 in excellent agreement with MC simulation results [43]. Fig. 4 clearly reveals the fact that contrary to usual expectation, the larger spheres segregate near the surface in large numbers as compared to the smaller spheres.

Uniform Fluid

Even in a uniform fluid, the average local density near an arbitrarily tagged molecule is inhomogeneous, an idea which was originally pointed out by Percus [44] and is being currently

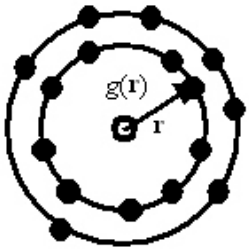

*Fig. 5 Concept of radial distribution function g(**r**) of uniform fluids. It defines the probability of finding a particle at distance **r**, if the other particle is fixed at the origin and is calculated as* $g(\mathbf{r}) = \rho(\mathbf{r})/\rho_0$.

used for calculation of the RDF of uniform fluids. The interacting potential in this case corresponds to the pair potentials. In the case of mixtures, however, the RDF of different components will be different depending on the individual tagged particle. The RDFs of a uniform ternary hard sphere calculated [45] from SCDFA and a simple weighted density approach are shown in Fig. 6 alongwith the corresponding MC results [45]. The success of theoretical approaches in the uniform fluids mainly relies on the prediction of pressure from the virial equation to be consistent with compressibility equation of state. The SCDFA formalism is again found to be the best in this regard.

Electric Double Layers

One of the most widely studied systems involving charged solid-fluid interfaces in recent years is the electric double layers (EDL) [46], which corresponds to the nonuniform ionic distribution arising due to the electric field of the surface charge of the electrode. Theoretical studies of EDL are again mostly based on the simple model, commonly used one is the restricted primitive model (RPM), where the electrolyte is assumed to consist of ions represented by charged hard spheres of equal diameter, the electrode is considered to be a uniformly charged planar hard wall and the solvent is treated as an isotropic dielectric continuum. Although there have been a number of theoretical studies on the ion distributions in EDLs, the notable ones which require mention here are the nonperturbative DFT and the MC simulation

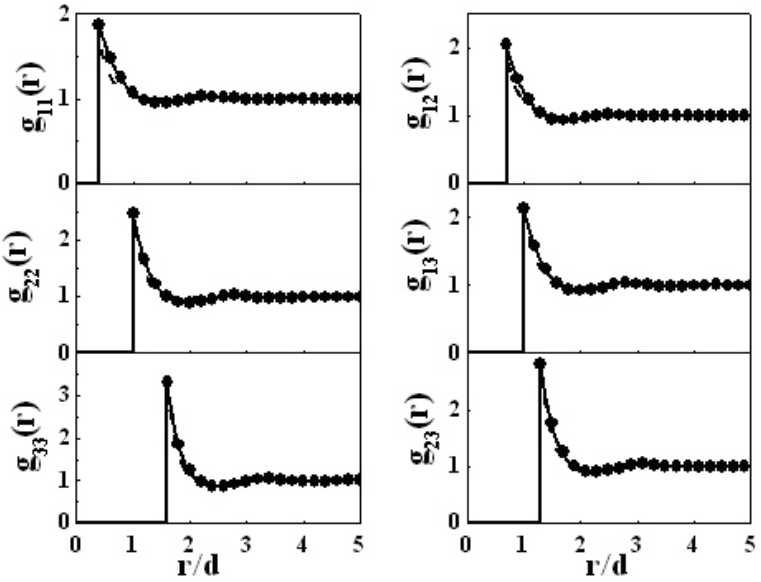

Fig. 6 Radial distribution function profiles $g_{ij}(\mathbf{r})$ *of a uniform ternary hard sphere mixture. The system parameters are: Diameters* $d_1=0.4d$, $d_2=d$, $d_3=1.6d$; *Concentrations* $x_1=x_2=x_3=1/3$, *and bulk packing fraction* $=0.337$. *The solid and dashed curves refer to the results obtained from SCDFA and simple WDA, respectively. Simulation results are shown as circles*

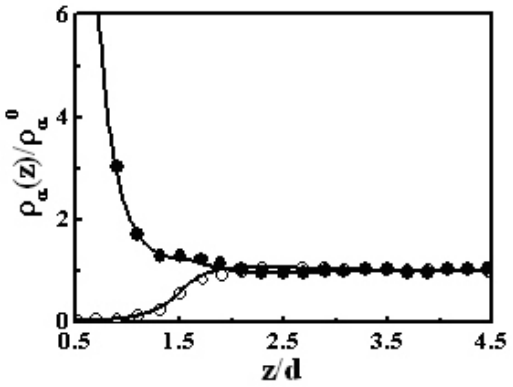

Fig. 7 Ion density profiles for a 1:1 electrolyte at c=2 M and =0.39602. The upper curve refers to counterions and the lower curve to coions. Simulation results are shown as circles (Ref. 47).

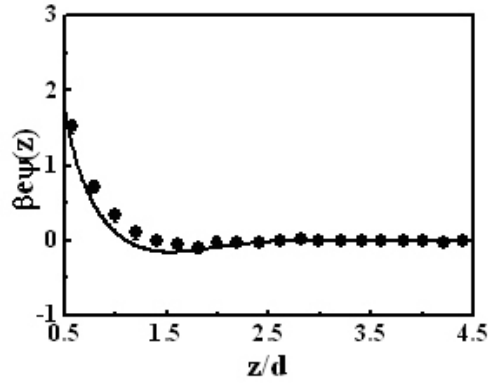

Fig. 8 Mean electrostatic potential for a 1:1 electrolyte at c=2 M and =0.39602. Simulation results are shown as circles (Ref. 47).

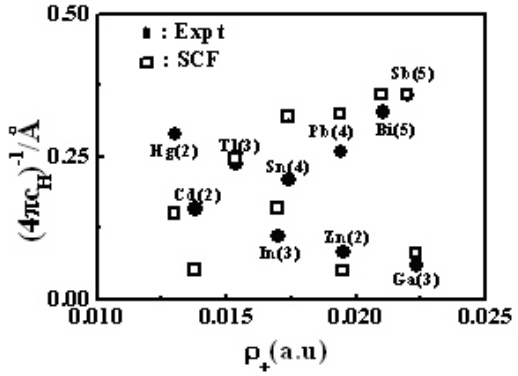

Fig. 9 The inverse inner layer capacitance for various metals immersed in an aqueous solution against the metallic electron density. The experimental results are given as circles and the results from self-consistent calculation are given as squares.

methods. The two most important phenomena experimentally observed in EDL are the layering and the charge inversion effects, which occur at a larger concentration of the bulk electrolyte and at higher surface charges because of the increased electrostatic interactions between the electrode and electrolyte ions. Such effects are clearly revealed [47,48] in Fig. 7, which depicts the ionic density profiles for a 1:1 electrolyte at a concentration c=2M and surface charge density =0.39602. The same effect is also corroborated by the potential inversion as shown [47,48] in Fig. 8 where the positive electrode is found to develop a negative potential at some distance from the electrode surface, where the co-ion density profile crosses the counterion density profile.

The knowledge of the interface between a metal and an electrolyte plays an important role in electrochemical science and technology. The distribution of the ions and the potential drop within the small region of electrochemical interface determine the very nature of electrolysis and adsorption. The behavior of the metal/electrolyte interface changes considerably with change in the nature of the metal as well as the electrolyte. The effect of metallic electron density on the behavior of the metal/electrolyte interface can be readily included in the self-consistent fashion through the overall minimization of the free energy of the whole system with the contribution of the electron density from a quantum mechanical footing. Such a study can in principle predict the experimental inner (c_H) and diffuse layer (c_d) capacitances as well as the electrode potential of various metals at different electrolytes, an open problem to the electrochemists over the years. Fig. 9 compares the results [49] of C_H^{-1} from a self-consistent field theory with the experimental values [50] at the same parameters, i.e., the dielectric constant of water as 80, the diameter of

the molecules (hard spheres) as 7 Å and at a temperature T=298 K. It is clearly seen that the results are extremely good barring Hg(2), Cd(2), and Sn(4) indicating the suitability of such a parameter free calculation.

Solvation and Surface Forces

Solvation force or the structural force [51] refers to the force acting between the two surfaces immersed in a solvent. Depending on the nature and sizes of the solute and the solvent, this force can be repulsive, attractive, or a combination of both and is experimentally measured through a surface force apparatus for a wide variety of liquids. Experimental measurements have revealed that the general qualitative behavior of this force (or the corresponding interaction energy) as a function of the distance between the two surfaces is of decaying oscillatory nature although detailed quantitative aspects differ from system to system. The solvation force arises because the liquid molecules tend to form an integral number of layers between the two surfaces and whenever the separation between them differs from an integral multiple of the molecular diameter, the liquid responds with an excess attractive or repulsive force. The theoretical development in this area started with the studies on the interaction between the charged colloids for which the improvement of the conventional DLVO potential through systematic many body corrections has been worked out. IET as well as DFT are able to confirm its oscillatory nature and both the theories are able to explain the solvent mediated attraction between charged colloids. DFT is also able to predict the interaction energies between two mica surfaces immersed in octamethylcyclotetrasiloxane and also liquid tetradecane, comparable with experiment. As can be seen in Fig. 11, the basic features of experimental results [52] of a real liquid (Fig. 12) are quite well reproduced [53] by DFT.

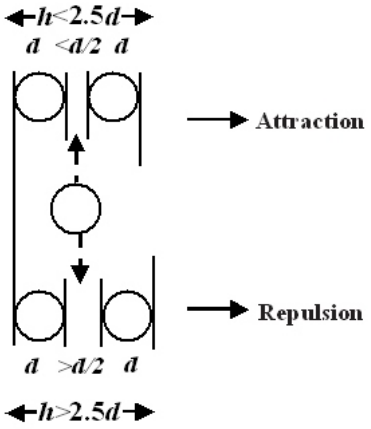

Fig. 10 Pictorial representation of the origin of the solvation force. If the gap between the two solvent molecules (for h > 2d) is less than d/2, the possibility of another molecule entering into this gap is very less, whereas if the gap is greater than d/2, the molecule will try to enter into the gap by pushing them. In terms of interaction, in the former case there will be attraction within the system, whereas the latter situation will lead to repulsion.

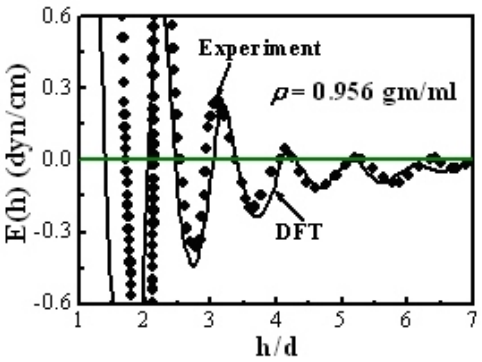

Fig. 11 Interaction energy between two mica surfaces immersed in Octamethylcyclo-tetrasiloxane vs the surface separation.

Polymers at Interfaces

The structure of polymer melts at interfaces [54] is of immense technological importance in diverse applications such as surface finishing, lubrication, nanotechnology, and cybernetics. Unlike the bulk polymer melts where the structure is directly influenced by the short-ranged intramolecular interactions and the long-ranged excluded volume interactions, the properties of polymer melts at interfaces is strongly influenced by the local intramolecular interactions within the length scale of the size of the monomer. The theoretical description of polymer molecules starts with united atom model description, the two most

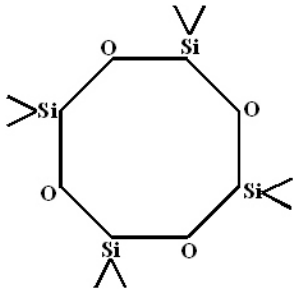

Fig. 12 Octamethylcyclotetrasiloxane molecule (Fig. 13, 14)

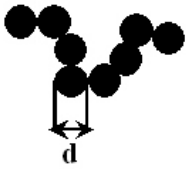

Fig. 13 Freely jointed chain model

Fig. 14 Fused hard chain model

widely studied [55] are the freely jointed chain (FJC) and the fused hard chain (FHC) models.

Computer simulation methods [56] have the advantage that it can be specifically tuned for model systems, although for long chain and high density polymers it becomes prohibitively expensive. In such situations, semianalytic theories like SCF theory, IET and DFT have been found to be quite successful. Quite recently, the behavior of polymer chains confined between surfaces is studied through a canonical Monte Carlo simulation by including different types of monomer-monomer and surface-monomer interactions. Among the various theoretical developments, the notable contribution which warrants mention here is the Monte Carlo density functional theory (MCDFT) [57], where what is required is only the simulation of a single chain in a self-consistent field due to the other molecules and surfaces, which is calculated with a prescribed formulation of DFT.

The MCDFT results are found to be in quantitative agreement with many chain simulation data over a wide range of densities, chain lengths, and interaction potentials. Figure 16 depicts [58] the profiles of 10-mers for =0.2 and at varying interaction potentials. It is amply clear that when both the wall–fluid and fluid–fluid interaction potentials are of comparable strength, the depletion mechanism due to the bulk fluid attraction dominates. The other important prediction is the change of shape of the polymer molecules as they approach the surface, which is clearly visible [59] in Fig. 17, where the semiaxis length profiles indicate that the molecules exist as flattened in shape near the surface. Theoretical developments along the same line for polyelectrolyte systems [60] have predicted many interesting observations for binding interactions including the negative total electrostatic free energy in presence of multivalent salt.

Concluding Remarks and Future Directions

Application of statistical mechanical theories in physicochemical problems has opened a new vista in understanding microscopic structural and dynamic properties and linking the same to macroscopic phenomena occurring in real time. Over the decades, the theoretical developments have given birth to many generic analytical approaches like SCF, IET, DFT and computer simulation methods like MC and MD as well as combination of these methods like SCDFA and MCDFT. The practical value of all these developments is reflected not only by its generality but also by its versatility for solving problems that may not be attained by conventional theories. This review gives some specific examples of recent developments hovering around these methods and also some glimpse of the physical problems, where the application is extremely useful. It is not necessary to apply these more sophisticated theories to problems where conventional theories are sufficient, as the usefulness of many phenomenological theories has been well established and they remain valuable as long as the underlying approximations can be adequately justified for a specific problem. The applicability of the present methods demands the scope for new methodologies as well as versatile numerical algorithms.

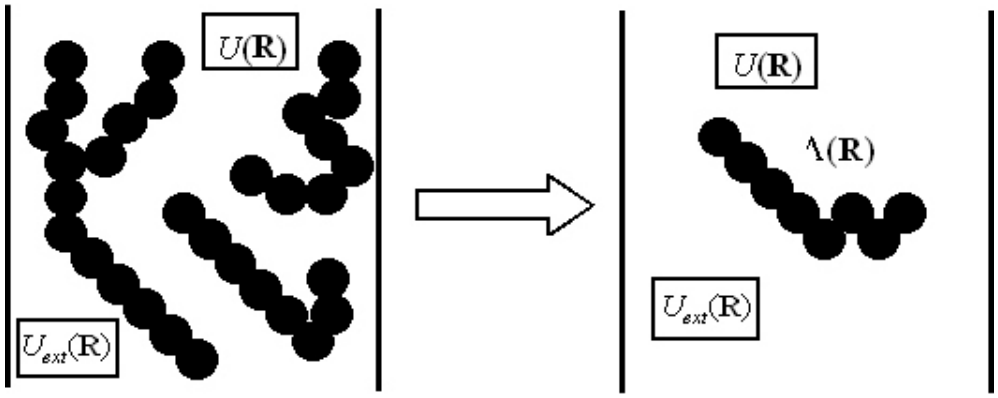

Fig. 15 Single chain simulation. The effective field due to the other molecules is $(\mathbf{R}) = c^{(1)}(r_i;[\ ])$. $U_{ext}(\mathbf{R})$ *and* $U(\mathbf{R})$ *represents the external and intramolecular potentials respectively.*

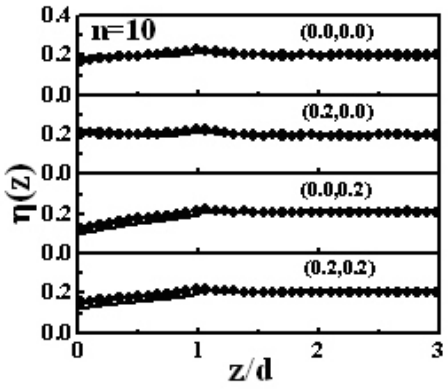

Fig. 16 Comparison between DFT predictions (lines) and Monte Carlo simulations (symbols) for the density profiles of 10-mers for =0.2 and for various values of interaction potentials $_{wf}$, $_{ff}$ *(as marked).*

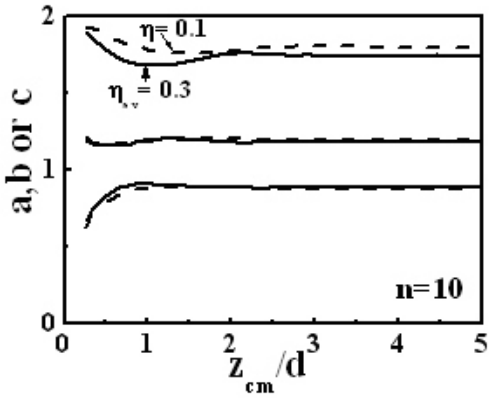

Fig. 17 Average semiaxis vector length profiles for athermal 10-mers.

The contents discussed in the present review are illustrative rather than exhaustive. A number of topics of current interest like the DNA salt binding [61], the molecular self-assembly [62], the solvation dynamics [63], the wetting transition [64] are not covered in the present review. A review of these topics would show that above methods could be reliably applied for studying these systems at a molecular level. Thus, DFT and IET are able to predict [65] the distribution of small ions around the cylindrical polyions and related thermodynamic coefficients in agreement with MC simulation results. Self-assembly of large particles into ordered arrays is supposed to be an efficient way for preparing microstructured materials with interesting versatility of desired properties [66]. The organization of nanostructures within self assembled templates has attracted a great deal of attention in recent years as this method can possibly be used in developing functional hybrid materials [67]. Quite recently, the self-assembly of nano building blocks have been directed through flexible oligomeric tethers with specific and nonspecific interactions. Molecular simulations corroborate the fact that tethering oligomers to specific locations on nanoparticle surfaces could facilitate the self-assembly of nanoparticles into specific structures which will eventually be dependent upon the complex geometry and topology of the tethered

nanoparticles [68]. In the dynamics of solvation of an ion in a dipolar liquid, DFT is able to predict [69] the breakdown of the continuum theory because of the presence of strong local correlations, which could lead to slower solvation due to caging effect. DFT is also able to predict nanodewetting [70] of polystyrene on top of a silicon surface in the presence of an oxide layer, in good agreement with the experimental results.

Future applications of the methods discussed above depend on continuing progress toward more faithful representation of real systems reflecting molecular-level interactions and, more importantly, on their clever implementations. Further, more efficient numerical algorithms and faster processing of vast amount of data are also the need of the hour. Although much current work in the literature concerns relatively simple models with emphasis on the performance of various versions of the theory for representing the qualitative or semiquantitative physiochemical properties in the bulk or near surfaces, much of it in the coming years will depend on the development of more realistic intermolecular force fields for more complex systems. Important advances are already emerging in applications of these methods to material fabrication [71], environmental protection [72], biomolecular engineering [73], transport processes through ion channels [74] and nanotechnology [75] for various high end applications in space, atomic energy, and defence equipments. Modeling and simulation will play an extremely crucial role in all these areas of developments for mankind in the foreseeable future!

Acknowledgments

I am greatly indebted to Swapan K. Ghosh for inspiration and assistance leading to this work and for numerous fruitful discussions. I gratefully acknowledge my collaborators Arun Yethiraj and Grant D. Smith for their helpful guidance at various stages of my research. I am also benefited from insightful discussions from L.B. Bhuiyan, A.L. Benavides, and Teena Goel. It is a pleasure to thank Dr. T. Mukherjee for his kind interest and constant encouragement.

Literature Cited

1. D. Chandler, Introduction to Modern Statistical Mechanics (Oxford University Press, New York, 1987).
2. D.A. McQuarrie, Statistical Mechanics (Harper & Row, New York, 1976).
3. B. Widom, Statistical Mechanics: A Concise Introduction for Chemists (Cambridge University Press, New York, 2002).
4. Molecular Modeling and Theory in Chemical Engineering, edited by A. Chakraborty, (Academic Press, San Diego, 2001).
5. H.T. Davis, Statistical Mechanics of Phases, Interfaces, and Thin Films (VCH, New York, 1996)
6. D. Nicholson and N.G. Parsonage, Computer Simulation and Statistical Mechanics of Adsorption (Academic Press, New York, 1982).
7. Monte Carlo and Molecular Dynamics Simulations in Polymer Science, edited by K. Binder (Oxford University Press, New York, 1995).
8. Fundamentals of Inhomogeneous Fluids, edited by D. Henderson (Dekker, New York, 1992).
9. K. Efimenko, M. Rackaitis, E. Manias, A. Vaziri, L. Mahadevan, and J. Genzer, Nature Materials 4, 293 (2005).
10. S. Link, W.-S. Chang, A. Yethiraj, and P.F. Barbara, Phys. Rev. Lett. 96, 017801 (2006).
11. S.O. Kim, H.H. Solak, M.P. Stoykovich, N.J. Ferrier, J.J. de Pablo, and P.F. Nealey, Nature 424, 411 (2003).
12. D. Cangialosi, A. Alegria, and J. Colmenero, Europhys. Lett. 70, 614 (2005).
13. J. Wu, AIChE J. 52, 1169 (2006).
14. D. Heine, G.S. Grest, and J.G. Curro, Adv. Polym. Sci. 176, 211 (2004).
15. A. Yethiraj, Adv. Chem. Phys. 121, 89 (2002).
16. Handbook of Materials Modeling, edited by S. Yip (Springer, The Netherlands, 2005).

17. R.J. Sadus, Molecular Simulation of Fluids (Elsevier, Amsterdam, 1999).
18. J.P. Hansen and I.R. McDonald, Theory of Simple Liquids (Academic Press, New York, 1990).
19. G. Fredrickson, The Equilibrium Theory of Inhomogeneous Polymers, Oxford University Press, New York, 2006).
20. D.W. Oxtoby, Annu. Rev. Mater. Res. 32, 39 (2002).
21. S. Succi, The Lattice Boltzmann Equation for Fluid Dynamics and Beyond (Oxford University Press, Oxford, 2001).
22. J.A. Barker and D. Henderson, Rev. Mod. Phys. 48, 587 (1986).
23. Chemical Applications of Density Functional Theory, edited by B.B. Laird, R.B. Ross, and T. Ziegler (American Chemical Society, Washington DC, 1996).
24. D. Frenkel and B. Smit, Understanding Molecular Simulation (Academic Press, New York, 2002).
25. Mathematical Models and Methods in ab initio Quantum Chemistry, edited by M. DeFranceschi and C. Le Bris (Springer, New York, 2000).
26. S.C. Harrison and A.K. Aggarwal, Annu. Rev. Biochem, 59, 933 (1990).
27. C. Stan Tsai, Biomacromolecules: Introduction to Structure, Function and Informatics (Wiley-Liss, New Jersey, 2006).
28. Acc. Chem. Res. edited by P.F. Barbara, 34, 409 (2001).
29. A. Leach, Molecular Modelling: Principles and Applications (Prentice Hall, New Jersey, 2001).
30. C.J. Kramer, Essentials of Computational Chemistry: Theories and Models (John Wiley & Sons, New Jersey, 2004).
31. T. Schlick, Molecular Modeling and Simulation (Springer-Verlag, New Jersey, 2002).
32. Multiscale Modelling and Simulation, edited by S. Attinger, and P. Koumoutsakos (Springer, New York, 2004).
33. W.J. Hehre, L. Radom, P.V. Schleyer, and J. Pople, Ab Initio Molecular Orbital Theory (Wiley-Interscience, New York, 1980).
34. R. Evans, in Ref. 8.
35. W.A. Curtin and N.W. Ashcroft, Phys. Rev. Lett. 56, 2775 (1986).
36. P. Tarazona, Phys. Rev. A 31, 2672 (1985).
37. C. Caccamo, Phys. Rep. 274, 1 (1996).
38. C.N. Patra and S.K. Ghosh, J. Chem. Phys. 118, 8326 (2003).
39. M.P. Allen and D.J. Tildesley, Computer Simulation of Liquids (Clarendon Press, Oxford, 1991).
40. C.N. Patra and S.K. Ghosh, J. Chem. Phys. 116, 8509 (2002).
41. R.D. Groot, N.M. Faber, and J.P. van der Eerden, Mol. Phys. 62, 861 (1987).
42. C.N. Patra and S.K. Ghosh, J. Chem. Phys. 117, 8933 (2002).
43. Z. Tan, U. Marini Bettolo Marconi, F. van Swol, and K. E. Gubbins, J. Chem. Phys. 90, 3704 (1989).
44. J.K. Percus, in The Equilibrium Theory of Classical Fluids, edited by H. L. Frisch and J. L. Lebowitz (Benjamin, New York, 1964).
45. C.N. Patra and S.K. Ghosh, J. Chem. Phys. 118, 3668 (2003).
46. W. Schmickler, Interfacial Electrochemistry (Oxford University Press, New York, 1996).
47. G. M. Torrie and J. P. Valleau, J. Chem. Phys. 73, 5807 (1980).
48. C.N. Patra and S.K. Ghosh, J. Chem. Phys. 117, 8938 (2002).
49. C.N. Patra and S.K. Ghosh, J. Chem. Phys. 102, 2556 (1995).
50. S. Trasatti, J. Electroanal. Chem. 123, 121 (1981).
51. J. Israelachvili, Intermolecular and Surface Forces (Academic Press, New York, 1992).

52. H.K. Christenson, D.W.R. Gruen, R.G. Horn and J. Israelachvili, J. Chem. Phys. 87, 1834 (1987).

53. C.N. Patra and S.K. Ghosh, Phys. Rev. E 50, 5123 (1994).

54. R.A.L. Jones and R.W. Richards, Polymers at surfaces and interfaces (Cambridge University Press, Cambridge, 1999).

55. H. Yamakawa, Modern Theory of Polymer Solutions (Harper & Row, New York, 1976).

56. Computer Simulations of Polymers, edited by R. J. Roe (Prentice-Hall, Englewood Cliffs, NJ, 1991).

57. A. Yethiraj and C.E. Woodward, J. Chem. Phys. 102, 5499 (1995).

58. T. Goel, C.N. Patra and S.K. Ghosh, and T. Mukherjee, J. Chem. Phys. 122, 214910 (2005).

59. T. Goel, C.N. Patra and S.K. Ghosh, and T. Mukherjee, J. Chem. Phys. 121, 4865 (2004).

60. R. Chang, C.N. Patra, and A. Yethiraj, J. Phys. Chem. B 108, 9126 (2004).

61. C.F. Anderson and M.T. Record Jr., Annu. Rev. Phys. Chem. 46, 657 (1995).

62. Z. Zhang, M.A. Horsch, M.H. Lamm, and S.C. Glotzer, Nano Lett. 3, 1341 (2003).

63. B. Bagchi and A. Chandra, Adv. Chem. Phys. 80, 1 (1991).

64. D. Bonn and D. Ross, Rep. Prog. Phys. 64, 1085 (2001).

65. C.N. Patra and A. Yethiraj, Biophys. J. 78, 699 (2000).

66. B.A. Grzybowski, A Winkleman, J.A. Wiles, Y. Brumer, and G.M. Whitesides, Nature Materials 2, 241 (2003).

67. Y. Lin, A. BÖker, J. He, K. Sill, H. Xiang, C. Abetz, X. Li, J. Wang, T. Emrick,S. Long, Q. Wang, A. Balazs, and T.P. Russell, Nature 434, 55 (2005).

68. R. K. Saini, I. W. Chiang, H. Q. Peng, R. E. Smalley, W.E. Billups, R. H. Hauge, and J. L.Margrave, J. Am. Chem. Soc. 125, 3617 (2003).

69. A. Chandra and B. Bagchi, J. Phys. Chem. 93, 6996 (1989).

70. M. Muller, L.G. MacDowell, P. Muller-Buschbaum, O. Wunnike, and M. Stamm, J. Chem. Phys. 115, 9960 (2001).

71. Nanomaterials: Research Towards Applications, edited by H. Hosono, Y. Mishima, H. Takezoe, K.J.D. MacKenzie (Elsevier Science, Amsterdam, 2006).

72. J.B. Snape, I.J. Dunn, J. Ingham, and J.E. Pienosil, Dynamics of Environmental Bioprocesses: Modeling and Simulation (Wiley -VCH, New York, 1995).

73. Biomedical Nanotechnology, edited by N.H. Malsch (CRC Press, Boca Raton, 2005).

74. D.J. Aldley and P.R. Stanfield, Ion Channels: Molecules in Action (Cambridge University Press, Cambridge, 1996).

75. J.S. Hall, Nanofuture: What's Next for Nanotechnology (Prometheus Books, New York, 2005).

Excitement at the Bottom: Tuning the Electronic Properties of Clusters through First Principle Calculations

Dr. Chiranjib Majumder *joined Chemistry Division, Bhabha Atomic Research Centre in 1992 after graduating through 35th batch of training school. He has developed an in-house molecular beam experimental facility in tandem with a time-of-flight mass spectrometer. He received his Ph.D. degree in 2000 for the experimental and theoretical studies of metal clusters. Subsequently he has worked on the theoretical aspects of molecular electronics at the Institute for Materials Research, Tohoku University, Japan. He has worked as a visiting scientist at the laboratory of Prof. P. Jena, VCU, USA. His current research interest is to design novel materials for catalysis and to underscore the mechanism of cluster-molecule interactions on a support matrix.*

Introduction

Clusters are defined as the agglomeration of atoms or molecules. During the last two decades there has been considerable interest in understanding the structure and properties of atomic clusters. It is worth mentioning that molecules, which are formed by few atoms and bear all signatures of a magic cluster in their own right, are slightly different due to their fixed stoichiometry and higher stability. Therefore, any molecule can be considered as magic cluster but opposite is not true. Fullerenes are well known example of both magic clusters and molecules.

This new phase of matter, intermediate between atoms and bulk, possesses unique and novel size and composition specific properties. Hence, one of the most interesting aspects of cluster science is the non-monotonous variation of their physico-chemical properties as a function of size [1]. This is essentially due to the discrete nature of the electronic energy levels of such finite size systems, which eventually form the band structure for bulk systems and show material specific properties. For a number of systems the existence of magic clusters, which show higher stability as compared to their nearest neighbors reflected by their larger ion signal intensity in the mass spectra. Fundamental understanding of the electronic and geometric structure of these magic clusters is essential to shed light on their physico-chemical properties at the atomic scale. Based on a large number of studies [2] it has been realized that the stability of metal clusters is governed either by their electronic or the atomic structures. Small alkali metal clusters, which follow Jellium model, show magic behavior for clusters having 8, 20, 40 ……number of atoms [3]. On the other hand covalent clusters, where directional bonding governs the stability, follow atomic structure to decide the relative stabilities [4]. The stability of magic clusters thus synthesized is characterized by their large binding energy, high ionization potential, low electron affinity, low reactivity etc. [5,6].

For small clusters, the physico-chemical properties vary drastically with size and shape. In this regard, computer simulation has been playing an important role as direct spectroscopic determination of geometric shape for even small clusters n = 4 is extremely complicated. Therefore, it is worthwhile to calculate the geometries of small clusters and compare them with the available experimental results. Once good agreements are achieved, the same theoretical techniques can be used to calculate the geometries and electronic structures of larger clusters for which no other direct experimental techniques are available. A large number of theoretical studies have been carried out using different theoretical approaches. Among these, density functional theory formalism [7] and quantum chemical methods based on Hartree-Fock

Dr. Chiranjib Majumder, Chemistry Division, Bhabha Atomic Research Centre, Trombay, Mumbai 400 085;
E-mail:chimaju@barc.gov.in

theory [8] have been used most extensively. An important theoretical development in the electronic structure calculations is the combined electron-ion minimization scheme under the DFT formalism, commonly known as ab-initio molecular dynamics strategy [9]. Throughout our work, we have used plane wave based-pseudo-potential methods within the density functional theory to obtain ground state geometries and energetics. In order to obtain more accurate description of energetics, we have further used quantum chemical methods based on Møller–Plesset perturbation theory incorporating the energy correlation effects truncated at second order (MP2) [10].

In the following sections we have divided our work on small clusters into three sub-sections. In the first part we have described the geometries and energetics homo-atomic clusters. Apart from understanding the relation between structure and chemical bonding at the atomic scale, we have also compared our results with the available experimental data. A good agreement between the experimental and theoretical stability pattern validates the predicted ground state structures of small clusters. In the second part we have discussed the effect of impurity atoms on the structural and electronic properties of host clusters. The results show that a single impurity atom can change the structure significantly and thereby generate different electronic properties. The third part deals with mixed clusters which may be useful to design new materials with tailored properties. We have found that due to surface effects the bulk properties can be altered significantly at the atomic scale. Apart from studies on clusters we have also carried out our research activities towards designing molecular devices based on organic molecules. We have described this work in the fourth section.

Homo atomic Clusters: Si_n, Sn_n, Pb_n

To begin with, we have calculated the structure and energetics of pure homoatomic clusters. The motivation of this work is two fold. Firstly, our theoretical results can be verified with experimental observations and secondly, one can understand how the chemical bonding influences the growth pattern of different elemental clusters. For this purpose we have taken Gr-IV elements as model system as we know that they show different bonding character (from covalent to metallic) in the bulk. Guided by this motivation we have calculated the geometrical and electronic structures of Si_n, Sn_n and Pb_n clusters which are known to exhibit semi-conducting, semi-metal and metallic properties in the bulk, respectively. The accuracy of our calculated results has been verified by a comparison with experimental stability pattern and their respective binding energy and ionization potential values. It is found that the relative stability order calculated through second order difference in energy is in excellent agreement with the mass abundance pattern observed via experiments. Regarding structural growth it has been observed that while Si and Sn clusters favor prolate shape, Pb clusters show compact spherical geometries as the lowest energy isomers. This feature in fact reflects the nature of bonding in the bulk. In figure 1 we have shown a typical example of the ground state geometries of Si_{13}, Sn_{13} and Pb_{13} clusters. While prolate shapes are a manifestation of covalent directional bonding, compact spherical shape bears the metallic character with increased number of coordination. For a detailed discussion on how the ground state geometries evolve from n=2 to larger clusters, readers are requested to go through references published elsewhere [11-18].

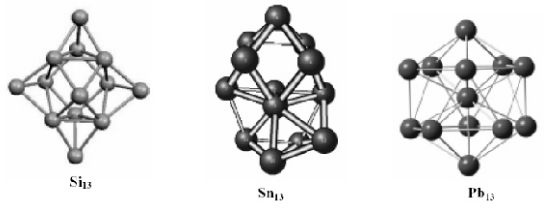

Fig. 1 The ground state structures of Si_{13}, Sn_{13} and Pb_{13} clusters.

Apart from Gr-IV metal clusters, which are important for semiconductor based electronic devices, we have been working on noble metal clusters like Au_n and Pt_n clusters, which are important from the catalysis point of view. The most important observation for this series of clusters is the preference of planar geometries for reasonably larger size clusters. For example, while Gr-IV elemental clusters show three dimensional structures from n =5 onwards, Au clusters adopt planar configurations upto n=13 atoms and Pt clusters show the onset of three dimensional geometries in the

ground state from n =10 onwards. The reason for such preference of heavy noble metal clusters has been attributed to the significant relativistic effects and negligible contribution of p- orbitals to the bonding. The interaction of organic molecules with these noble group elemental clusters is important. The initial results on this study suggest significant improvement of the reactivity in comparison to the respective bulk metals.

Impurity doped Clusters

In bulk materials, a small percentage of impurity doping is known to affect its physico-chemical properties quite significantly. Therefore, in clusters it is expected that the effect of impurities would be more pronounced due to its finite size effects. Doping of clusters can lead to stabilize the cluster by electron shell filling or by breaking its symmetry to another structure with high stability. In our group we have carried out a large number of studies to investigate the effect of impurity doping on the host clusters [19-24]. It is found that when Si clusters were doped with transition metal atoms like Ti, Hf or Zr, the less compact prolate structure of bare Si cluster changes to spherical shape and in particular the $M@Si_{16}$ shows very symmetric fullerene like structure. This cluster has significantly high binding energy and large ionization potential, which are considered to be the reason for higher stability of this cluster. Subsequent to this work, we have used 1st and 2nd row of simple metal (M = Li, Be, B, C, Na, Mg, Al and Si) as the impurity atom and Si_{10} was used as host cluster. The motivation of this work is to find the location of the impurity atom on Si_{10} cluster and its rationalisation based on the atomic size and number of valence electrons which in turn govern the chemical bonding. The ground state structures of MSi_{10} clusters indicate that the location of the impurity atom on the host cluster depends on the atomic size and nature of interaction between the host cluster and impurity atoms. It has been observed that for $BeSi_{10}$ cluster, Be atom goes inside the cage of the Si_{10} cluster and forms highly symmetric close packed structure with large gap between the HOMO and LUMO energy levels. Also for BSi_{10} cluster, B atom can diffuse into the center of the Si_{10} cage, which is 0.12 eV higher in energy than the lowest energy isomer. In contrast to this, the geometries of other MSi_{10} clusters become unstable when M atom is placed inside the Si_{10} cage in spite of having smaller size (C atom) or similar electronic configurations (Mg). The stability of the M doped Si_{10} clusters has been explained through the average binding energies which shows the trend as CSi_{10}> BSi_{10}> $BeSi_{10}$> Si_{11}> $AlSi_{10}$> $LiSi_{10}$> $NaSi_{10}$> $MgSi_{10}$. The interaction energies between the impurity atom and the host cluster also follow the similar trend. Based on these results it is inferred that while the interactions of Li, Na, Mg, Al reduces the stability of the Si_{11} cluster, C, B and Be atoms enhance it more efficiently that Si atom addition.

In order to understand the effect of impurity doping on the energy level ordering we have investigated the influence of an impurity atom in tuning the stability of Pb_{13} cluster. For this purpose we have used C, Al, and Mg atom as an impurity. The results showed that the energy gap between the highest occupied and lowest unoccupied energy levels of Pb_{13} and $MgPb_{12}$ are 0.95 and 2.3 eV, respectively. The significant increase in the energy gap results from the energy level reordering of Pb_{13} by the incorporation of Mg atom as shown in Fig. 2. Further investigations of the stability of MPb_{12} clusters reveal that the interplay between the atomic and electronic structure is crucial to understand the stability of small size clusters.

Recently, we have carried out the atomic and electronic structure calculation of Au_5M (M=Na, Mg, Al, Si, P, S, and Au) clusters. Depending on the nature of interaction with different impurity elements a structural transition from planar to non-planar configuration has been observed in Au_5M. With the exception of S, impurities with p electrons (Al, Si, P) yield non-planar geometries in Au_5M clusters, while those with s electrons (Na, Mg) yield planar geometries. The properties of Au_5S cluster are anomalous. The cluster not only has a planar geometry, but also is chemically most stable albeit an odd electron system. The Au_5S has the highest vertical ionization potential among all the clusters studied as shown in Fig. 3. The origin of these anomalous properties of Au_5S cluster is attributed to the delocalization of electronic wave function associated with the highest occupied molecular orbital.

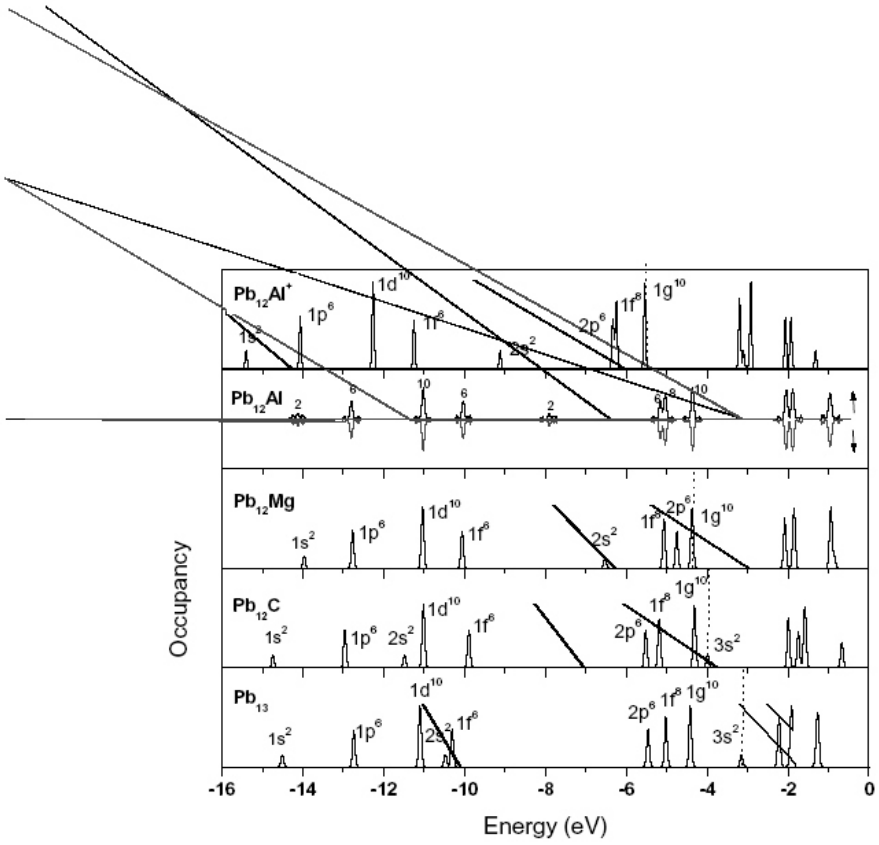

Fig. 2 Energy level reordering and stability of MPb_{12} clusters.

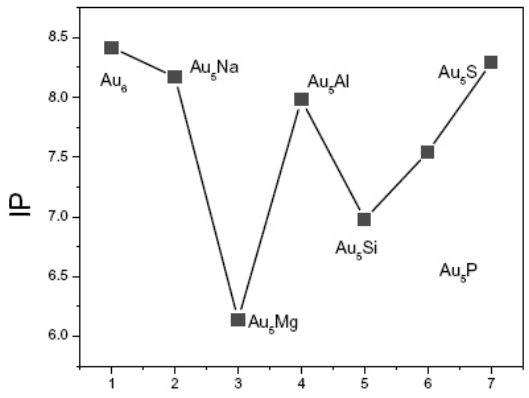

Fig. 3 The vertical ionization potentials of Au5X (X = Na, Mg, Al, Si, P, and S) clusters.

Mixed Clusters: A_4B_4, A_8B_6

Bimetallic nanoclusters have received considerable attention [25] for their peculiar properties, which can be very different from those of pure clusters of their constituents and for a variety of applications, ranging from catalysis to optics What renders bimetallic nanoclusters very attractive is that their properties can vary dramatically not only with size, as happens in pure nanoclusters, but also with chemical composition. Mixing of two or three elements with varying compositions forms bulk alloys. Quite often it has been observed that the two elements, which are not miscible in the bulk, can form small cluster aggregates. This is because of the fact that the strain produced in the alloy formation due to size mismatch is considerably reduced for cluster. Such clusters with significantly high binding energies can be visualized as the building blocks for

the formation of new materials with properties quite different from that of their corresponding alloys. However, predicting geometries of such mixed clusters is difficult due to large number of possible isomers forming rather flat potential energy surface.

We have investigated the equilibrium geometries of mixed clusters with 4:4 and 6:8 composition using molecular dynamics simulation within the orbital free density functional theory formalism. Several isomers of binary clusters consisting of Na, Mg, Al and Si atoms having 4:4 composition have been studied using density functional theory formalism. The stability aspect of such clusters have been discussed in terms of their binding energies, ionization potentials, energy gaps between the HOMO and LUMO energy levels and the charge transfer analysis. From the geometries and energetics it has been found that these binary clusters have a rich variety of local minima in the potential energy surface. Regarding stability of such clusters a direct correlation between the binding energies, ionization potentials and energy gaps has not been observed as is apparent from the results obtained for two binary clusters (Mg_4Al_4 and Na_4Si_4) containing twenty valence electrons. These results suggest that for such binary clusters the definition of the stability should be clearly expressed in terms of the relevant properties. The alkalization of higher valence clusters leads to a decrease in the ionization potential of the mixed cluster. The enhancement of energy gap in Al_4Si_4 binary clusters as compared to the respective energy gaps of the constituent homo-atomic Al_4 and Si_4 tetramers is an interesting observation. This reflects the magic behavior of this cluster with tetrahedral symmetry. The enthalpy of mixing for all these clusters is negative and follows the order Al_4Si_4 > Na_4Si_4> Na_4Al_4> Mg_4Al_4> Mg_4Si_4 > Na_4Mg_4. Finally, the Al_4Si_4 cluster, which has higher values of binding energy, ionization potential, energy gap and energy of mixing suggest that it is the most stable cluster in this series which can further be used as building block to synthesize cluster assembled materials [26].

Although several attempts have been made to search for empty cage fullerene like Si clusters, no report is available to look for a cage structure of a mixed cluster consisting of Si and other metal atoms. Al and Si atoms belong to the same period with one and two electrons in their outermost 3p orbital, respectively. This difference in their electronic configuration has led to significant difference in the bulk properties. While Al is metallic with close packed cubic structure, Si is semiconductor with diamond like structure having 1.12 eV energy gap between the conduction and valence bands. It is therefore of interest to investigate what happens to their geometrical and electronic properties when they are mixed at atomic scale. In this work we report the formation of face centered cubic structure of Al_8Si_6 cluster where Si_6 forms an octahedron whose eight triangular faces are capped by Al atoms forming a cube. In order to generalize the stability of this structure for III-IV mixed clusters additional calculations have been performed for few other A_8B_6 clusters (A = Al, Ga, In and B = Si and Ge). In this context it is important to note that III-IV mixed clusters of 8:6 composition is a mixture of two homoatomic clusters, which are iso-electronic in nature. In all these cases an empty cubic cage structure was found to be stable with large energy gaps. However, when similar studies were carried out for I-IV and II-IV mixed clusters, the face centered cubic geometry was found to be unstable. The stability of this geometry has been verified from vibrational analysis, finite temperature simulation, higher ionization potentials or smaller relaxation in the charged, larger energy gaps etc. In fact the energy gaps of the mixed clusters are even larger than pure Si_6 or Ge_6 clusters, which favor crossed rhombus geometry with D_{4h} symmetry. Contrary to the knowledge of bulk behavior it has been found that the energy gap increases as the capping atom becomes heavier. The predicted an energy gap of 2.66 eV (GGA) for In_8Si_6 cluster is the largest energy gap so far obtained for a metal capped-Si clusters having polyhedral symmetry. Thus these mixed clusters have higher density of state on the surface and a large optical gap responsible for the inner core [27].

Nanoelectronics: Importance of metal-molecule interactions

Organic molecules with delocalized -electrons are materials of great interest because of their unique electronic transport properties. Molecular scale electronics promises to utilize single molecules as the basic operational elements to

design molecular wires, rectifiers, two terminal diode switches and assembling them into more complicated electronic devices like molecular logic gates. In order to understand the molecular properties at the fundamental level we have carried out theoretical investigation of the geometrical and electronic structures of conjugated organic molecules substituted with different donor and acceptor groups [28,29]. This work is required to primarily screen some of the suitable molecules which could be most promising candidates to show device properties at very low cost. To measure electrical properties experimentally, the molecule has to be attached with a non-interacting metallic electrode. Therefore, it is required to understand the interface structure of the metal-molecule junction. We have carried out theoretical investigations on the electronic and structural aspects of the metal-molecule interface considering gold as an electrode and thiophene as a potential organic molecule. The Au (111) surface was modeled by a finite size cluster and periodic slab model [30-32]. The results suggest that the adsorption geometry strongly depends on the surface models as well as the local electronic environment of the terminal sulfur atom. While the interaction energy decreases for Au_3, Au_{24} to the periodic slab models, it increases from thiophene-2-thiolate to thiophen-2-yl-methanethiolate. The charge transfer analysis reveals that the interfacial bonding is strongly directional. Apart from playing the major role in the adsorption site it does not affect the chemical nature of the adjacent thiophene rings, bearing an important implication towards the engineering of metal-molecule interactions for the synthesis of new molecular devices.

Future Direction

Although considerable progress has been made in understanding the structure and bonding of small clusters, they are limited to gas phase model systems. However, in practice they need to be deposited on a support which may cause significant distortion in the structure of free clusters and their chemical properties. Therefore, efforts are being made to calculate the properties of deposited clusters. Another important area where cluster studies can contribute significantly is their applications in bio-medical sciences. An ideal nanoparticle for this application should be a strong magnet, biocompatible, and resistant to corrosion as well as aggregation. Small transition metal clusters have large magnetic moment. However, they are prone to get oxidized. Therefore, encaging these magnetic particles inside an insulator would have significant advantage for application for industrial or medicinal purpose. In recent times, it has been reported that clusters, made of all metal atoms, could behave like aromatic molecules. We also know that molecules having delocalized -electrons are materials of great interest because of their unique electronic transport properties. Therefore, it would be interesting to investigate the electrical transport behavior of metal clusters which show aromatic behavior.

References

1. W. A. de Heer, Rev. of Mod. Phys. 65 611(1993); M. Brack, Rev. of Mod. Phys. 65 677(1993).
2. H. Haberland, Clusters of Atoms and Molecules: Theory, Experiment (Springer Verlag, New York, 1994).
3. W. D. Knight , K.Clemenger, W. A. de Heer, W. A. Saunders, M. Y. Chou, M. L. Cohen :. Phys. Rev. Lett., 52 2141(1984).
4. D. W. Arnold, S. E. Bradforth, T. N. Kitsopoulos, and D. M. Neumark, J. Chem. Phys. 95, 8753 (1991).
5. S. N. Khanna and P. Jena, Phys. Rev. Lett. 69, 1664 (1992)
6. H. Hakkinen and M. Manninen, Phys. Rev. Lett. 76, 1599 (1996).
7. P. Hohenberg, W. Kohn, Phys. Rev. B 136 864(1964). (b) W. Kohn, L. J. Sham. Phys. Rev. A 140 1133(1965).]
8. W. J. Hehre, L. Radom, P. Von R. Schleyer and J. A. Pople, Ab Initio Molecular Orbital Theory (Wiley, New York, 1985).].
9. R. Car and M. Parrinello: Phys. Rev. Lett., 55 2471(1985).
10. M. Haser, J. AlmLof, and G. E. Scuseria, Chem. Phys. Lett. 181, 497 (1991). C. Moller and M. S. Plesset, Phys. Rev. 46, 618 (1934).
11. C. Majumder, V. Kumar, H. Mizuseki, and Y. Kawazoe, Phys. Rev. B, 64 (2001) 233405.

12. C. Majumder, V. Kumar, H. Mizuseki, and Y. Kawazoe, Phys. Rev. B, 64 (2001) 233405.

13. C. Majumder, V. Kumar, H. Mizuseki, and Y. Kawazoe, Chem. Phys. Lett., 356 (2002) 36.

14. Y. Tai, J. Murakami, C. Majumder, V. Kumar, H. Mizuseki, and Y. Kawazoe, J. Chem. Phys., 117 (2002) 4317.

15. C. Majumder, V. Kumar, H. Mizuseki, and Y. Kawazoe, Phys. Rev. B, in press.

16. Y. Tai, J. Murakami, C. Majumder, V. Kumar, H. Mizuseki, and Y. Kawazoe, Euro. Phys. J. D 24 (2003) 295-298.

17. S. Nigam, C. Majumder and S. K. Kulshreshtha, J. Chem. Phys., 121 (2004) 7756.

18. C. Rajesh and C. Majumder, M. G. R. Rajan and S. K. Kulshreshtha, Phys. Rev. B, 72 (2005) 235411.

19. C. Majumder and S. K. Kulshreshtha, Phys. Rev. B, 70, 245426 (2004).

20. C. Majumder and S. K. Kulshreshtha, Phys. Rev. B, 69 (2004) 115432.

21. V. Kumar, C. Majumder, and Y. Kawazoe, Chem. Phys. Lett. 363 (2002) 319,

22. S. Nigam, C. Majumder and S. K. Kulshreshtha, J. Chem. Phys. 125 (2006) 074303.

23. C. Majumder and S. K. Kulshreshtha, Phys. Rev. B., 73 (2006) 155427.

24. C. Rajesh and C. Majumder, Chem. Phys. Lett. 430 (2006) 101.

25. J. Jellinek and E. B. Krissinel, in Theory of Atomic and Molecular Clusters, edited by J. Jellinek (Springer, Berlin, 1999), pp. 277–308.

26. C. Majumder and S. K. Kulshreshtha, Phys. rev. B, 69 (2004) 075419.

27. C. Majumder and S. K. Kulshreshtha, Phys. Rev. B 70, 125416 (2004).

28. C. Majumder, H. Mizuseki, and Y. Kawazoe, J. Phys. Chem. A, 105 (2001) 9454-9459.

29. C. Majumder, T. M. Briere, H. Mizuseki, and Y. Kawazoe, J. Phys. Chem. A, 106 (2002) 7911.

30. C. Majumder, T. M. Briere, H. Mizuseki, and Y. Kawazoe, J. Chem. Phys., 117 (2002) 7669.

31. C. Majumder, T. M. Briere, H. Mizuseki, and Y. Kawazoe, J. Chem. Phys., 117 (2002) 2819

32. C. Majumder, H. Mizuseki, and Y. Kawazoe, J. Chem. Phys., 118 (2003) 9809.

Chemical Reactivity and Conceptual Density Functional Theory

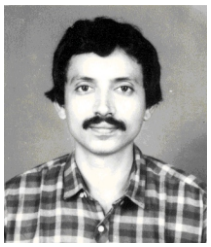

Prof. Pratim Kumar Chattaraj *obtained his Ph.D. degree from Indian Institute of Technology, Bombay. Subsequently he did his postdoctoral research in the University of North Carolina at Chapel Hill. He is currently a Professor of chemistry at the Indian Institute of Technology, Kharagpur. Professor Chattaraj's research interests include density functional theory, nonlinear dynamics, ab initio calculations and the theory of chemical reactivity. He was a visiting faculty at several universities throughout the globe. Professor Chattaraj is a Fellow of the Indian Academy of Sciences, Bangalore. He is a member of the Editorial board of the Journal of Chemical Sciences. A special issue of that journal on Chemical Reactivity is recently edited by Professor Chattaraj.*

Shri Debesh Ranjan Roy *received his B.Sc. (Physics Honours) from the University of Burdwan and M.Sc. (Physics) from the Visva–Bharati University, Santiniketan. Then he joined the research group of Professor P. K. Chattaraj for his Ph.D. degree in the Chemistry Department, Indian Institute of Technology, Kharagpur as a CSIR (Government of India) Fellow.*

Introduction

Conceptual density functional theory (DFT) [1-3] has been quite successful in providing theoretical bases for popular qualitative chemical concepts like electronegativity [4], hardness [5,6] and electrophilicity [7,8]. In DFT the single particle density, $\rho(\vec{r})$, is the basic variable as opposed to the many-particle wavefunction, $\Psi(\vec{r}_1, \vec{r}_2, \ldots\ldots, \vec{r}_N)$. As the number of electrons (N) in a many-electron system (atom, molecule, ion) and the external potential $v(\vec{r})$ completely fix its Hamiltonian, all the properties of this system are supposed to be obtained by the appropriate variations of N and $\rho(\vec{r})$. This approach of analyzing chemical behaviour has been termed as "Conceptual DFT" by Professor Robert G. Parr. In terms of several global and local chemical reactivity and selectivity descriptors a complete theory of chemical reactivity has been envisaged. These descriptors and the associated electronic principles will be presented in this article.

Global Reactivity Descriptors

These descriptors describe the reactivity of the molecule as a whole.

Electronegativity ( ) and Chemical Potential ( )

In order to understand the nature of a chemical bond, Pauling introduced the concept of electronegativity [9] as, 'the power of an atom in a molecule to attract electrons to itself'. Based on thermodynamical data, the calculated electronegativity values of atoms by Pauling follow the general intuition in chemistry.

Later on, the concept of 'absolute' electronegativity which is independent of molecular environment has come into picture as proposed by Mulliken [10]. This 'absolute' electronegativity of any atom or molecule can be expressed in terms of two experimentally measurable quantities,

Shri. D. R. Roy and Prof. P. K. Chattaraj, Department of Chemistry, Indian Institute of Technology, Kharagpur 721 302;
E-mail: pkc@chem.iitgp.ernet.in

ionisation potential (I) and electron affinity (A) as follows:

$$\frac{I \quad A}{2} \tag{1}$$

There are several other definitions of electronegativity. Amongst those definitions, the scale of Allred and Rochow [11] provides a direct physical interpretation of electronegativity as 'the electron-attracting power of atoms'. They measured the electronegativity of atoms as the electrostatic force exerted at the covalent radius (r_{cov}). Their electronegativity can be expressed as:

$$3590\frac{Z^*}{r_{\text{cov}}^2} \quad 0.744 \tag{2}$$

where Z^* is the screened nuclear charge.

Gyftopoulos and Hatsopoulos [12] has considered the atom or a molecule as a member of a grand canonical ensemble with the energy (E) and the number of electrons (N) as the only independent variables. The chemical potential of the ensemble can be expressed as:

$$\frac{E}{N}, \text{ at constant entropy.} \tag{3}$$

As chemical potential implies the escaping tendency of an electron cloud, electronegativity can be expressed as the negative of this quantity, i.e.

$$\frac{E}{N}, \text{ at constant entropy} \tag{4}$$

which is a continuous function of N and the temperature ( ).

According to density functional theory (DFT) [1-3], the Lagrange multiplier associated with the normalisation constraint is identified as the chemical potential ( ), viz.,

$$\frac{E}{N}_{(\vec{r})} \tag{5}$$

where E and $(\vec{r})$ are the total energy and external potential, respectively.

Using the identity

$$d\vec{r} \quad N \tag{6}$$

chemical potential can be shown to be equivalent to the negative of electronegativity as [13]:

$$\frac{E}{N}_{(\vec{r})} \quad \frac{E}{}_{(\vec{r})} \quad \frac{}{N}_{(\vec{r})} \quad d\vec{r} \quad \frac{E}{}_{(\vec{r})} \tag{7}$$

Using the finite difference approximation of $\frac{E}{N}$, Mulliken [10] expressed in terms of I and A as:

$$\frac{I \quad A}{2} \tag{8}$$

In ab initio wavefunction pictures using Koopmans' theorem, I and A can be expressed in terms of the highest occupied molecular orbital energy (ϵ_{HOMO}) and the lowest unoccupied molecular orbital energy (ϵ_{LUMO}) as [14]:

$$I \quad _{HOMO} \quad ; \quad A \quad _{LUMO} \tag{9}$$

Using Koopmans' theorem and can be expressed as:

$$\frac{1}{2} \quad _{HOMO} \quad _{LUMO} \tag{10}$$

Using a SCF finite difference approach, the I and A can be expressed for the N-electron system as follows:

$$I \quad E(N-1) - E(N) \; ; \; A \quad E(N) - E(N+1) \tag{11}$$

where E (N) is the electronic energy of the N-electron system.

Chemical Hardness ( ) and Softness (S)

It is found that, in many cases electronegativity cannot account for the stability of a molecule. To account for the stability of a molecule and the direction of acid-base reactions, Pearson [15] introduced two parameters 'hardness' and 'softness' in chemistry.

For an N-electron system, the second derivative of energy with respect to N, keeping external potential fixed, is considered to be a measure of the chemical hardness:

$$\frac{1}{2}\left(\frac{\partial^2 E}{\partial N^2}\right)_{\vec{r}} \quad \frac{1}{2}\left(\frac{\partial}{\partial N}\right)_{\vec{r}} \tag{12}$$

which would be always positive due to the convex nature of E vs. N curve.

In the Koopmans' framework, can be expressed as:

$$\frac{1}{2}\left(\varepsilon_{LUMO} - \varepsilon_{HOMO}\right) \tag{13}$$

The inverse of hardness [16] can be defined as softness:

$$S \quad \frac{1}{2}\left(\frac{\partial N}{\partial \mu}\right)_{\vec{r}} \tag{14}$$

The softness is closely associated with the polarisability of a system. A larger (more polarisable) chemical system is softer and vice-versa.

As and measure the response of the system when N varies at constant $\vec{r}$), the response function [17] does that job when $\vec{r}$) changes for a fixed N. For weak electric and magnetic fields it is provided by polarisability and magnetisability respectively.

Polarisability ( )

The electric dipole polarisability is a measure of the linear response of the electron density in the presence of an infinitesimal electric field F and it represents a second order variation in energy

$$\alpha_{a,b} \quad \frac{\partial^2 E}{\partial F_a \partial F_b} \qquad a,b \quad x,y,z \tag{15}$$

A soft molecule is more polarisable compared to the corresponding harder counterpart.

Magnetisability ( )

The linear response of the electronic cloud of a chemical species to a weak external magnetic field is measured in terms of magnetisability ( ), as follows:

$$m \quad B; \qquad \frac{\partial^2 E(B)}{\partial B^2}\Big|_{B\ 0} \tag{44}$$

where m refers to the induced magnetic moment and B refers to the external magnetic field.

Electrophilicity Index ( )

Maynard et al [18] have shown that the reaction rate of fluorescence decay experiment on human immunodeficiency virus type-1 (HIV-1) nucleocapsid protein p7 (N C_p7) when interacting with some electrophilic agents, e.g., azodicarbonamide (ADA), N-ethylmaleimide (NEM) etc. gives an almost linear response with the square of electronegativity ( ) to the chemical hardness ( ) ratio. The quantity $^2/$ related to the capacity of an electrophile to promote a soft (covalent) reaction.

Prompted by the work of Maynard and co-workers [18], Parr et al defined electrophilicity index ( ) [7] as:

$$\frac{\chi^2}{2\eta} \quad \frac{\mu^2}{2\eta} \tag{16}$$

which measures the stabilization in energy when the system acquires an additional electronic charge N from the environment.

Local Reactivity Descriptors

These descriptors take care of the site selectivity of an atom in a molecule.

Electron Density ((r))

The most important local descriptor is the electron density itself, in the DFT framework. Electron density $\vec{r}$) is given as [1,2]:

$$\rho(\vec{r}) \quad \left(\frac{\partial E(\ )}{\partial \rho(\vec{r})}\right)_N \tag{17}$$

Fukui function (f (r))

The Fukui function (FF) [19] is one of the widely used local reactivity descriptors in modeling chemical reactivity and site selectivity. Fukui function (FF) is defined as [19]:

$$f(\vec{r}) \quad \left(\frac{\partial}{\partial N}\right)_{\vec{r}} \quad \left(\frac{\partial \mu}{\partial \rho(\vec{r})}\right)_N \tag{18}$$

such that $f(\vec{r})\,d\vec{r}$ 1.

In equation (18) the slope of $(\vec{r})$ vs. N curve is discontinuous at integral N, which provides three types of Fukui functions which account for nucleophilic, electrophilic and radical attacks respectively, at a particular reaction site. By the use of finite difference and frozen core approximations, these three functions can be expressed as [19]:

$$f\ (\vec{r}) \quad \frac{}{N}\ _{(\vec{r})} \quad {}_{N\ 1}(\vec{r}) \quad {}_{N}(\vec{r}) \quad {}_{LUMO}(\vec{r})$$

[for nucleophilic attack] (19a)

$$f\ (\vec{r}) \quad \frac{}{N}\ _{(\vec{r})} \quad {}_{N}(\vec{r}) \quad {}_{N\ 1}(\vec{r}) \quad {}_{HOMO}(\vec{r})$$

[for electrophilic attack] (19b)

$$f^{0}(\vec{r}) \quad \frac{}{N}\ ^{0}_{(\vec{r})} \quad \frac{1}{2}\ {}_{N\ 1}(\vec{r}) \quad {}_{N\ 1}(\vec{r}) \quad \frac{1}{2}\ {}_{HOMO}(\vec{r}) \quad {}_{LUMO}(\vec{r})$$

[for radical attack] (19c)

Equations (19a) to (19c) provide a correspondence between the local parameters and the frontier orbital theory of chemical reactivity [20]. A large value of f^{+}, f^{-}, or f^{0} at any site indicates the probability of respective attacks at that site which would correspond to a large change in chemical potential.

The condensed Fukui functions are proposed by Yang and Mortier [21], considering a finite difference method and the Mulliken population analysis (MPA) scheme as:

$$f_k \quad q_k(N\ \ 1)\ \ q_k(N)$$

[for nucleophilic attack] (20)

$$f_k \quad q_k(N)\ \ q_k(N\ \ 1)$$

[for electrophilic attack] (21)

$$f_k^{0} \quad q_k(N\ \ 1)\ \ q_k(N\ \ 1)/2$$

[for radical attack] (22)

where q_k is the electronic population of atom k in a molecule.

The calculation of the Fukui function (FF) using the variational technique is also prescribed [22]. In this method, using the known electron density $(\vec{r})$ and the hardness kernel [22],

$$\vec{r},\vec{r}' \quad \frac{^{2}F[\ ]}{(\vec{r})\quad(\vec{r}')} \tag{23}$$

a hardness functional is defined as follows:

$$[g] \quad g(\vec{r})g(\vec{r}')\quad \vec{r},\vec{r}'\ d\vec{r}\,d\vec{r}' \tag{24}$$

If we minimise [g] with respect to $g(\vec{r})$ subject to the normalisation condition

$$g(\vec{r})d\vec{r} \quad 1 \tag{25}$$

we obtain the exact Fukui function for the system and the extremum value of $[f]$ can be considered to be the exact hardness of the system.

For an inhomogeneous gas the necessary gradient correction in the Fukui function has been made [23]. For a homogeneous system of N-electrons constrained to move in a cavity of volume V, the Fukui function within the 'local density approximation (LDA)' is given by,

$$f(\vec{r}) \quad \frac{(\vec{r})}{N}\ _{(\vec{r})} \quad \frac{(\vec{r})}{N} \tag{26}$$

where $(\vec{r})$ and $f(\vec{r})$ are constants equal to N/V and 1/V respectively.

For an inhomogeneous gas the necessary corrections are incorporated as [23]:

$$f(\vec{r}) \quad \frac{(\vec{r})}{N}\ 1 \quad (\vec{r};\ ,\ \ ,\ \ ^{2},.....) \tag{27}$$

where is a parameter.

Using an approximation to as a dimensionless quantity, and the normalisation condition of FF, can be expressed as [23]:

$$\frac{1}{}\quad \frac{}{2/3}\quad \frac{^{2}}{5/3}\ \frac{2}{3}\ \frac{}{8/3} \tag{28}$$

Local Softness ($s(\vec{r})$)

In "frontier-controlled" reactions, where frontier orbital densities play an important role, the tendency of a particular site to be involved is given by a local softness parameter. Local softness $s(\vec{r})$ is defined as [24]:

$$s(\vec{r}) \quad — \qquad (29)$$
$$(\vec{r})$$

which is related to the global softness S as:

$$S \quad s(\vec{r})\,d\vec{r} \qquad (30)$$

Local softness is related to FF as follows:

$$s(\vec{r}) \quad \frac{(\vec{r})}{} \quad \frac{}{N} \quad (\vec{r}) \quad \frac{N}{} \quad f(\vec{r})S \qquad (31)$$
$$(\vec{r}) \qquad (\vec{r})$$

Both global and also local softnesses may be expressed as appropriate number fluctuations [16].

Local Hardness ($(\vec{r})$)

The local hardness $(\vec{r})$ is defined as [25]:

$$(\vec{r}) \quad \frac{1}{2} \quad — \qquad (32)$$
$$(\vec{r})$$

which is related to the global hardness as:

$$(\vec{r})\,f(\vec{r})d\vec{r} \qquad (33)$$

which is not a simple integral over as in the case of the local softness [eq. 30].

The definition (32) of local hardness is ambiguous [26] because of the inter-dependence between $(\vec{r})$ and $(\vec{r})$ according to DFT [27]. The situation may improve in an appropriate ensemble like an isomorphic ensemble [28]. While local softness is an electronic reactivity index, the local hardness may be considered to be a nuclear reactivity index and hence together they will take care of variations in N and $(\vec{r})$ which will encompass all possible situations [29].

Philicity ($(\vec{r})$)

Chattaraj et al [30] proposed the generalized concept of philicity which contains almost all information regarding the global as well as local reactivity and selectivity, specially the electrophilic/nucleophilic power of a given atomic site in a molecule. This quantity may be considered as the local variant of the global electrophilicity index, called philicity ($(\vec{r})$) and is defined as [30]:

$$(\vec{r})\,d\vec{r} \qquad (34)$$

Philicity is obtained through the resolution of the identity associated with the normalisation of Fukui function [28], $f(\vec{r})$, as:

$$(\vec{r}) \quad f \quad (\vec{r}) \qquad (35)$$

where = +, -, and 0 refer to nucleophilic, electrophilic and radical reactions respectively. Corresponding condensed-to-atom variants may be written for the kth atomic site in a molecule as

$$_k \quad f_k \qquad (36)$$

In eq. (35) any normalised-to-one quantity (e.g. the shape function, $(\vec{r})$ $(\vec{r})/N$) may be used. But FF is preferred owing to the explicit information of electron addition/removal in it.

Group Philicity

There exists the concept of group philicity ($_g$) which is very useful in unraveling reactivity of various molecular systems. The condensed philicity summed over a group of relevant atoms is defined as the "group philicity". It can be expressed as

$$_g \quad \sum_{k\ 1}^{n} \ _k \qquad (37)$$

where n is the number of atoms coordinated to the reactive atom, $_k$ is the local electrophilicity of the atom k, and $_g$ is the group philicity obtained by adding the local philicity values of the nearby bonded atoms, where (= +, -, 0) represents nucleophilic, electrophilic and radical attacks

respectively. It is allowed owing to the additivity of the Fukui function $\sum_k f_k = 1$.

Nucleophilicity Excess (Net Nucleophilicity)

Recently a new local reactivity descriptor, nucleophilicity excess ($\Delta^{\mp}_g$), is proposed [31] along the line of the dual descriptor [32] as:

$$\Delta^{\mp}_g = \Delta_g = \Delta f_g^- - \Delta f_g^+ \qquad (38)$$

where $\Delta_g = \sum_{k=1}^{n} \Delta_k$ and $\Delta_g = \sum_{k=1}^{n} \Delta_k$ a re the group philicities of the nucleophile in the molecule due to electrophilic and nucleophilic attacks respectively. It is expected that the nucleophilicity excess ($\Delta^{\mp}_g$) for a nucleophile should always be positive whereas it will provide a negative value for an electrophile in a molecule. Essentially this nucleophilicity excess is the net nucleophilicity of a given group [31]. It can be equivalently defined for individual atomic centres which on summation will provide the corresponding group quantity.

Quantum Dissimilarity

When two molecules interact, quantum dissimilarity (Δ^{ij}), which is the minimum quadratic difference in philicity may be defined [33] as:

$$\Delta^{ij} = \left[\Delta_{\max(i)}(electrophile) - \Delta_{\max(j)}(nucleophile) \right]^2 \qquad (39)$$

where $\Delta_{\max}$ and $\Delta_{\max}$ are the maximum philicity values at any atomic site due to nucleophilic and electrophilic attacks respectively.

Electronic Structure Principles

The global and local reactivity descriptors are better appreciated through various related electronic structure principles, such as Sanderson's electronegativity equalisation principle [34], hard and soft acids and bases (HSAB) principle [15,35], maximum hardness principle (MHP) [36,37], minimum polarisability principle [38], minimum magnetisability principle (MMP) [39], etc.

Electronegativity Equalisation Principle (EEP)

The difference in electronegativity plays a major role in chemical reactions. Electrons are transferred from a species of lower electronegativity to a species of higher electronegativity until both possess equal electronegativity values.

Sanderson postulated that [34], during molecule formation the electronegativity of the constituent atoms become equal, yielding a molecular electronegativity (Δ_M) which is roughly the geometric mean of the electronegativities of the isolated atoms,

$$\Delta_M = \left(\Delta_A^0 \; \Delta_B^0 \; \Delta_C^0 \cdots \right)^{1/(a+b+c+\ldots)} \qquad (40)$$

where a, b, c are the number of atoms of a given element (A, B, C, etc.).

As an application of the electronegativity equalisation principle (EEP), Parr and Pearson [40] derived two important expressions to measure the amount of charge transfer ΔN and the energy change ΔE associated with the formation of A:B complex from acid A and base :B. The expressions are:

$$\Delta N = \frac{\Delta_A^0 - \Delta_B^0}{2(\Delta_A + \Delta_B)} \qquad (41)$$

$$\Delta E = \frac{-(\Delta_A^0 - \Delta_B^0)^2}{4(\Delta_A + \Delta_B)} \qquad (42)$$

These expressions are very useful in understanding the acid-base reaction mechanism. It is important to note that the electronegativity difference drives the electron transfer whereas the hardness sum provides a resistance to it. Therefore both Δ and Δ are to be considered in analyzing these processes.

Hard-Soft-Acid-Base (HSAB) principle

The qualitative definitions of the hard and soft acids and bases may be stated as follows:

(a) Hard acids are smaller size acceptor atoms with high positive charge, low polarisability and absence of easily excitable outer electrons, e.g. H^+, Li^+.

Soft acids are large, highly polarisable acceptor atoms with low positive charge having easily excitable outer electrons, e.g. I_2, Pd^{2+}.

(b) Hard bases are smaller size donor atoms with low polarisability, high electronegativity, having empty orbitals with large energy and are hard to oxidise, e.g. NH_3, OH^-.
Soft bases are large, highly polarisable donor atoms with low electronegativity, having low lying orbitals and are easily oxidisable, e.g. H^-, CN^-.

This classification is purely empirical and based on the observations on bond energy, equilibrium constant, rate constant and other experimental data [41] which is in conformity with that obtained from the conceptual DFT definitions of and S provided in eqs. (12) and (14) respectively.

Pearson introduced the hard-soft-acid-base (HSAB) principle [15,35] which in general can describe a variety of acid-base reactions. This principle is stated as, 'hard acids prefer to coordinate with hard bases and soft acids prefer to coordinate with soft bases for both their thermodynamic and kinetic properties'.

In order to quantify the concept of hardness and softness Pearson proposed [42] a relation that correlates the stability of a molecule with the hardness and softness, as well as the inherent strengths of acids and bases. The stability constant of a reaction is given by,

$$\log K \quad S_A S_B \qquad A \quad B \tag{43}$$

where $_A$ and $_B$ are the inherent strengths of acids and bases whereas S_A and S_B are the softness factors. It is expected that $_A$, $_B$ would be related to $_A$, $_B$.

Maximum Hardness Principle (MHP)

Pearson's HSAB principle has been analysed and it has been argued [43] that the hard-hard reactions are governed by the charge-controlled interactions and the soft-soft interactions are of the covalent type. Various studies on the chemical reactivity suggest that soft molecules are more reactive compared to the corresponding harder counterparts. Hence, isomeric molecules with higher chemical hardness are found to be more abundant compared to the molecules with lower hardness values. This fact leads to the principle of maximum hardness. The maximum hardness principle (MHP) is stated [36,37] as 'there seems to be a rule of nature that molecules arrange themselves so as to be as hard as possible'.

Minimum Polarisability Principle (MPP)

As a consequence of the maximum hardness principle (MHP) [36,37] and an inverse relationship [44] between hardness and polarisability, a minimum polarisability principle (MPP) is stated as [38], 'the natural direction of evolution of any system is towards a state of minimum polarisability'.

Both MHP and MPP have been made use of in analyzing molecular vibrations, internal rotations, chemical reactions, aromaticity, atomic shell structure, excited states, dynamical problems etc. [3,8].

Minimum Magnetisability Principle (MMP)

Magnetisability of a system can be decomposed into its diamagnetic component ($_{dm}$) and paramagnetic component ($_{pm}$).

$$_{Total} \qquad _{dm} \qquad _{pm} \tag{45}$$

Very recently, a new electronic structure principle, viz. the minimum magnetisability principle (MMP) [39] has been proposed to extend the domain of applicability of the conceptual density functional theory (DFT) in explaining the magnetic interactions and magnetochemistry. This principle is stated as, "A stable configuration/conformation of a molecule or a favorable chemical process is associated with a minimum value of the magnetisability". It has also been shown that a soft molecule is easily polarizable and magnetizable than a hard one.

Summary

Various global and local chemical reactivity/selectivity descriptors are defined within a conceptual density functional theory framework. They provide important insights into the chemical reaction mechanism when augmented with the associated electronic structure principles.

Acknowledgements

We thank Board of Research in Nuclear Sciences (BRNS), Mumbai for financial assistance. One of us (PKC) would like to thank Drs. B. S. Tomar and S. K. Ghosh for kindly inviting him to contribute this article.

References

1. R. G. Parr and W. Yang, Density functional Theory of Atoms and Molecules, Oxford University Press, New York, 1989; Annu. Rev. Phys. Chem. 46 (1995) 701. Special Issue of J. Chem. Sci. on Chemical Reactivity, 2005, Vol. 117, Guest Editor: P. K. Chattaraj.
2. W. Kohn, A. D. Becke, and R. G. Parr, J. Phys. Chem., 100 (1996) 12974. P. K. Chattaraj, S. Nath, and B. Maiti, "Reactivity Descriptors" in "Computational Medicinal Chemistry for Drug Discovery", J. Tollenaere, P. Bultinck, H. D. Winter, and W. Langenaeker, Eds.; Marcel Dekker: New York, 2003; Chapter 11, p. 295-322.
3. P. Geerlings, F. De Proft, and W. Langenaeker, Chem. Rev., 103 (2003) 1793.
4. Electronegativity: Structure and Bonding; K. D. Sen, and C. K. Jorgenson, Eds.; Springer-Verlag: Berlin, 1987; Vol. 66.
5. Chemical Hardness: Structure and Bonding; K. D. Sen, and D. M. P. Mingos, Eds.; Springer-Verlag: Berlin, 1993, Vol. 80.
6. R. G. Pearson, Chemical Hardness: Applications from Molecules to Solids; Wiley-VCH Verlag GMBH : Weinheim, 1997.
7. R. G. Parr, L. v. Szentpaly, and S. Liu, J. Am. Chem. Soc., 121 (1999) 192.
8. P. K. Chattaraj, U. Sarkar, and D. R. Roy, Chem. Rev., 106 (2006) 2065.
9. L. Pauling, The Nature of the Chemical Bond, 3rd ed., Cornell University Press, Ithaca, New York, 1960.
10. R. S. Mulliken, J. Chem. Phys., 2 (1934) 782; 3 (1935) 573.
11. A. L. Allred, and E. G. Rochow, J. Inorg. Nucl. Chem., 5 (1958) 264. A. L. Allred, J. Inorg. Nucl. Chem., 17 (1961) 215.
12. E. P. Gyftopoulos, and G. N. Hatsopoulos, Proc. Natl. Acad. Sci. USA, 60 (1968) 786.
13. R. G. Parr, R. A. Donnelly, M. Levy, and W. E. Palke, J. Chem. Phys., 68 (1978) 3801.
14. R. G. Pearson, Proc. Natl. Acad. Sci. USA, 83 (1986) 8440.
15. R. G. Pearson, Coord. Chem. Rev., 100 (1990) 403; Hard and Soft Acids and Bases; Dowden, Hutchinson and Ross: Stroudsberg, PA, 1973. R. D. Hancock, and A. E. Martell, J. Chem. Educ., 73 (1996) 654.
16. W. Yang, and R. G. Parr, Proc. Natl. Acad. Sci. USA, 82 (1985) 6723.
17. M. Berkowitz, and R. G. Parr, J. Chem. Phys., 88 (1998) 2554.
18. A. T. Maynard, M. Huang, W. G. Rice, and D. G. Covell, Proc. Natl. Acad. Sci. USA., 95 (1998) 11578.
19. R. G. Parr, and W. Yang, J. Am. Chem. Soc. 106 (1984) 4049; P. W. Ayers, and M. Levy, Theor. Chem. Acc., 103 (2000) 353.
20. K. Fukui, Theory of Orientation and Stereoselection, Springer – Verlag, Berlin, 1975; Science, 218 (1987) 747.
21. W. Yang, and W. J. Mortier, J. Am. Chem. Soc., 108 (1986) 5708.
22. P. K. Chattaraj, A. Cedillo, and R. G. Parr, J. Chem. Phys., 103 (1995) 7645.
23. P. K. Chattaraj, A. Cedillo, and R. G. Parr, J. Chem. Phys., 103 (1995) 10621.
24. W. Yang, and R. G. Parr, Proc. Natl. Acad. Sci. USA, 82 (1985) 6723.
25. M. Berkowitz, S. K. Ghosh, and R. G. Parr, J. Am. Chem. Soc., 107 (1985) 6811. S. K. Ghosh, and M. Berkowitz, J. Chem. Phys., 83 (1985) 2976.
26. M. K. Harbola, P. K. Chattaraj, and R. G. Parr, Israel. J. Chem., 321 (1991) 395. S. K. Ghosh, Chem. Phys. Lett., 172 (1990) 77.
27. P. Hohenberg, and W. Kohn, Phys. Rev. B, 136 (1964) 864.
28. F. De Proft, S. Liu, and R. G. Parr, J. Chem. Phys., 107 (1997) 3000.

29. F. De Proft, S. Liu, and P. Geerlings, J. Chem. Phys., 108 (1998) 7549.

30. P. K. Chattaraj, B. Maiti, and U. Sarkar, J. Phys. Chem. A, 107 (2003) 4973. D. R. Roy, R. Parthasarathi, J. Padmanabhan, U. Sarkar, V. Subramanian, and P. K. Chattaraj, J. Phys. Chem. A, 110 (2006) 1084.

31. D. R. Roy, V. Subramanian, and P. K. Chattaraj, Ind. J. Chem. A, 2006 (In Press).

32. C. Morell, A. Grand, and A. Toro-Labbe´, J Phys Chem A, 109 (2005) 205.

33. D. R. Roy, U. Sarkar, P. K. Chattaraj, A. Mitra, J. Padmanabhan, R. Parthasarathi, V. Subramanian, S. Vandamme, and P. Bultinck, Mol. Div., 10 (2006) 119.

34. R. T. Sanderson, Science, 114 (1951) 670; 116 (1952) 41; 121 (1955) 207; J. Chem. Educ., 29 (1952) 539; 31 (1954) 238.

35. P. K. Chattaraj, H. Lee, and R. G. Parr, J. Am. Chem. Soc., 113 (1991) 1855. P. K. Chattaraj, and P.v.R. Schleyer, J. Am. Chem. Soc., 116 (1994) 1067. P. K. Chattaraj, and B. Maiti, J. Am. Chem. Soc., 125 (2003) 2705.

36. R. G. Pearson, J. Chem. Educ., 64 (1987) 561; Acc. Chem. Res., 26 (1993) 250; J. Chem. Educ., 76 (1999) 267.

37. R. G. Parr, and P. K. Chattaraj, J. Am. Chem. Soc., 113 (1991) 1854. P. W. Ayers, and R. G. Parr, J. Am. Chem. Soc., 122 (2000) 2010.

38. T. K. Ghanty, and S.K. Ghosh, J. Phys. Chem., 100 (1996) 12295. P. K. Chattaraj, and S. Sengupta, J. Phys. Chem., 100 (1996) 16126.

39. A. Tanwar, D. R. Roy, S. Pal, and P. K. Chattaraj, J. Chem. Phys., 125 (2006) 056101.

40. R. G. Parr, and R. G. Pearson, J. Am. Chem. Soc., 105 (1983) 7512.

41. R. G. Pearson, Theoretical Models of Chemical Bonding, Part II, Z. B. Maksic (ed.) Springer Verlag, Berlin, 1990, pp. 45 – 76.

42. R. G. Pearson, Inorg. Chem. 11 (1972) 3146.

43. G. Klopman, J. Am. Chem. Soc., 90 (1968) 223. G. Klopman, Chemical Reactivity and Reaction Paths, G. Klopman (Ed.), Wiley, New York, 1974, Chap. 4. P. K. Chattaraj, J. Phys. Chem. A., 105 (2001) 511.

44. R. G. Pearson, in Ref. 5. P. Politzer, J. Chem. Phys., 86 (1987) 1072. T. K. Ghanty, and S. K. Ghosh, J. Phys. Chem., 97 (1993) 4951.

Electro-Hydrodynamic approach to Study the Rate of Excitation Energy Transfer from a Dye to a Metal Nanoparticle

Ms Sangeeta Saini *did her graduation and post graduation from Panjab University, Chandigarh. She is currently pursuing her Ph.D. in Solid State and Structural Chemistry Unit, Indian Institute of Science, Bangalore under the supervision of Professor Biman Bagchi.*

Shri Somnath Bhowmick *received B.Tech degree from Calcutta University and M.S. from Indian Institute of Science, Bangalore. He is currently a Ph. D. student at the Materials Research Centre, Indian Institute of Science, Bangalore.*

Dr. Vijay B. Shenoy *is a Faculty member at the Materials Research Centre, Indian Institute of Science, Bangalore. He received his B. Tech. degree from Indian Institute of Technology, Madras in 1992 and Ph.D. from Brown University, USA in 1998. He was awarded the Young Scientist Medal of the Indian National Science Academy in 2002 and the Young Engineer Award of the Indian National Academy of Engineering in 2004. His research interests include Theories of Strongly Correlated Electron Systems, Physics of Pattern Formation in Soft Films and Nanoscience Theory.*

Prof. Biman Bagchi *received his Ph.D. degree from Brown University, USA in 1981 with Professor Julian H. Gibbs as his advisor. He was Research Associate at the James Franck Institute, University of Chicago (1981-1983), where he worked with Professors David W. Oxtoby, Graham Fleming, and Stuart Rice, and the University of Maryland (with Robert Zwanzig) before returning to India in 1984 to join the faculty of the Indian Institute of Science, Bangalore, where he is currently the Amrut Mody Chair Professor of Chemical Sciences. He was awarded the Shanti Swarup Bhatnagar Prize in chemical sciences and is a Fellow of the Indian Academy of Sciences, Indian National Science Academy, National Academy of Sciences, India as well as the Third World Academy of Sciences. His research interests include molecular relaxation and transport in liquids, phase transitions, biophysical chemistry, supercooled liquids, and polymers.*

Abstract

Long range resonance energy transfer (RET) between a donor and an acceptor molecule is increasingly being used in many areas of biological and material science. The phenomenon is used to monitor the separations between different (bio) polymers/units of (bio) polymers and hence the

Ms. Sangeeta Saini and Prof. Biman Bagchi, Solid State and Structural Chemistry Unit, Indian Institute of Science, Bangalore 560 012
Shri Somnath Bhowmick and Dr. Vijay B. Shenoy, Materials Research Center, Indian Institute of Science, Bangalore 560 012;
E-mail:bbagchi@sscu.iisc.ernet.in

dynamics of various biomolecular processes. The technique is popularly termed as "spectroscopic ruler". In this work we examine the distance and orientation dependence of RET (i) between a nanometal particle (NMP) and a fluorescent dye and (ii) between two NMP. We show that in both the cases, the rate of RET follows a distance dependence of d^{-} where exponent approaches 6 at large d (FÖrster type dependence) but has a value varying from 3 - 4 at short to intermediate distance.

Introduction

The rate of fluorescence resonance energy transfer (FRET) k_{DA}, the non-radiative mode of energy transfer from a donor (excited state, D*) to an acceptor (A) within Förster formulation [1,2] is given by

$$k_{DA} \quad k_{rad} \quad \frac{R_F}{R}^{6} \qquad (1)$$

where k_{rad} is the radiative rate (typically less than 10^9 s^{-1}) and R_F is the well-known Förster radius given by the spectral overlap between the fluorescence spectrum of the donor and the absorption spectrum of the acceptor. The technique of FRET finds applications in most of the disciplines (chemistry, biology and material science) and is often designated as a "spectroscopic ruler" [3] because of strong distance dependence of the energy transfer rate. Undoubtedly, FRET has played a key role in understanding the conformational dynamics of single (bio) molecules in microscopic detail [4-7]. However, the conventional FRET (both donor and acceptor are dye molecules) can be used to measure separations typically in range of 20 – 80 Å. Beyond this distance, the energy transfer becomes too weak to be useful [8]. This limitation has motivated the use of RET systems involving dye molecules and the noble metal nanoparticles. These nanoparticles (Au, Ag) have prominent absorption spectrum in the visible region and are employed as either the acceptor, or more recently as both donor and the acceptor [9]. The absorption of light by nanoparticles is mainly dominated by the surface plasmon (SP) excitations [10,11]. In such RET systems, separations up to 700 Å can be monitored, which are about 10 times larger than the FÖrster distances, R_F. This feature makes these RET systems potentially extremely useful in many material and biomedical applications [12].

In the present paper we will discuss the distance and orientation dependence of energy transfer between different RET systems. In section II, we will consider the EET from a dye to a metal nanoparticle and in section III we will briefly discuss resonance energy transfer between two nanoparticles.

Excitation Energy Transfer from a Dye to a Metal Nanoparticle

A large number of theoretical and experimental studies exist on the rate of non-radiative energy transfer from a dye to both, a plane metallic surface [13-15] and a nanoparticle [16-20]. Nevertheless, only few of the studies explore the distance dependence of non-radiative energy transfer. In present section, we will discuss the dependence of the rate on the separation between a dye and a nanoparticle, the orientation of the dye molecule with respect to the distance vector R (Fig. 1) and the size of the nanoparticle.

First we briefly discuss the semi-classical approach adopted by us to calculate the non-radiative decay rate of a dye molecule in presence of a metallic nanoparticle [21]. Since the absorption spectrum of metal nanoparticles over a wide range of size is dominated by surface plasmon resonance. Therefore, the formalism invokes the transfer of excitation energy to the surface plasmon modes of the nanoparticle.

According to Fermi golden rule, the rate of energy transfer is given by

$$k_{DA} \quad \frac{2}{\hbar}|V_{DA}|^2 \sum_{M_D,N_D,M_A,N_A} f(E^e_{N_D})\, f(E^e_{M_A}) \left| \left\langle {}^{g}_{D};\ {}^{e}_{A} \middle| H_I \middle| {}^{e}_{D};\ {}^{g}_{A} \right\rangle \right|^2 (E^e_{N_D} \quad E^g_{M_A} \quad E^g_{M_D} \quad E^e_{N_A}) \qquad (2)$$

where

$$V_{DA} \quad \left| \left\langle {}^{g}_{M_D};\ {}^{e}_{N_A} \middle| H_I \middle| {}^{e}_{N_D};\ {}^{g}_{M_A} \right\rangle \right|^2 \qquad (3)$$

H_I is the interaction Hamiltonian and $\left\langle {}^{g}_{D};\ {}^{e}_{A} \middle| {}^{e}_{D};\ {}^{g}_{A} \right\rangle$ matrix elements are the nuclear overlap factors, and denote the electronic wave

functions. The delta function satisfies the condition of energy conservation. The sum is over all the possible vibrational states of donor molecule and the various other degrees of freedom of the nanoparticle (like the interaction with phonons, electron-hole pair interactions which broadens the absorption spectrum of the nanoparticle) weighed by their initial thermal distribution, $f(E^{e}_{N_D})$ and $f(E^{g}_{M_A})$ respectively. The delta function in Eq. (2) can be written as,

$$E^{e}_{N_D} \quad E^{g}_{M_A} \quad E^{g}_{M_D} \quad E^{e}_{N_A} \quad f(E^{e}_{N_D}) \quad dE \quad E^{e}_{N_D} \quad E^{g}_{M_D} \quad E \quad E^{g}_{M_A} \quad E^{e}_{N_A} \quad E \tag{4}$$

In the theoretical implementation of the scheme, the sharp resonance lines are replaced with Lorentzians of width 0.025 eV in order to account for the broadening caused by various degrees of freedom.

We model the dye molecule as a particle in a box. The corresponding charge density operator in terms of creation c_m and annihilation (c_m) operators is given by

$$d \quad \frac{2e}{L} \quad {}^{*}_{m,n}(r_D) \quad {}_{n}(r_D) c^{+}_{m} c_{n} \quad \frac{e}{L} \quad {}_{p} \quad c^{+}_{m} c_{m} \tag{5}$$

where s are the electronic wavefunctions which depend on r_D, the position vector of a point in the dye measured from its center, e is the magnitude of electron charge and 2L is the length of the 1D box. The second term accounts for the uniformly distributed positive charge background and ensures the overall charge neutrality of the dye molecule. The charge density operator for the nanoparticle is obtained using a following set of electrohydrodynamic equations:

$$\frac{}{t} \quad \frac{e}{m} \quad \frac{2}{n_0} \quad n$$

$$2 \quad \frac{en}{0}$$

$$2 \quad \frac{l}{n_0} \frac{}{t} n \tag{6}$$

Within this formalism the charge density operator for a nanoparticle is given by

$$(r_A) = \sum_{l,m} {}_{l,m}(r_A) = \sum_{l,m} A_{l,m} j_l (r_A) Y_{l,m} (,) \tag{7}$$

where $Y_{l,m}$ represent the spherical harmonics and $A_{l,m}$ is the amplitude operator given in terms of the plasmon Bosonic operators as

$$A_{l,m} \quad \frac{\hbar \quad {}_{l,m} \quad {}_{0}}{2a^3}^{2} \quad (a_{l,m} \quad a_{l,m})$$

$$\frac{2}{l,m} \frac{(2l \quad 1)}{2} j^{2}_{l+1} (\quad a) - j_{l-1} (\quad a) j_{l+1} (\quad a)^{1/2} \tag{8}$$

We study the rate of energy transfer between dye and the nanoparticle using two different interaction Hamiltonian. The full Coulombic interaction Hamiltonian is given by

$$H_I \quad \frac{1}{4 \quad {}_{0}} \quad dr_D \quad d^3 r_A \frac{(r_A) \quad (r_D)}{|R - r_A \quad r_D|} \tag{9}$$

while the interaction Hamiltonian within the dipole approximation is given by

$$H_I \quad \frac{1}{4 \quad {}_{0}} \quad \frac{{}_{D} \cdot {}_{A} \quad 3({}_{D}.d)({}_{A}.d)}{d^3} \tag{10}$$

where ${}_{D}$ and ${}_{A}$ are the dipole operators of the dye and the nanoparticle respectively. d is the distance between dye and the surface of the nanoparticle and is the corresponding unit vector (see Fig. 1)

The rate of energy transfer is calculated for a donor dye molecule emitting at 520 nm. The acceptor is a nanoparticle with plasma frequency ${}_{p}$ = 5.7 x 10^{15} s^{-1} (after Ref. 23; which fixes the value of the electron density n_0). The plasmon frequencies have strong size dependence for particles with a 7nm, and asymptotically reaches a plateau value (independent of the size of the nanoparticle) for larger particles. The frequencies of the surface modes are lower than ${}_{p}$; for a nanoparticle of radius 10 nm, the l=1 surface plasmon has an absorption spectrum centered around 590 nm, while the l=2 mode is centred around 450 nm. Both of these shift to smaller wavelengths with reduction in the size of the

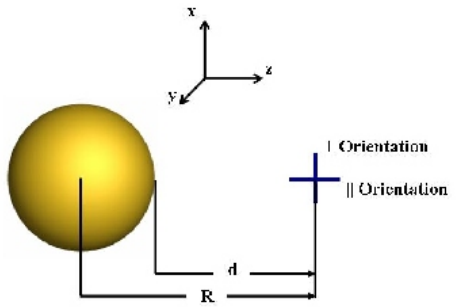

Fig. 1 A schematic illustration of the geometric arrangement of the spherical nanoparticle and the dye molecule in two different orientations, parallel and perpendicular, with respect to the distance vector R. d is the distance measured from the surface of the nanoparticle. The figure also shows the coordinate system employed in our calculations.

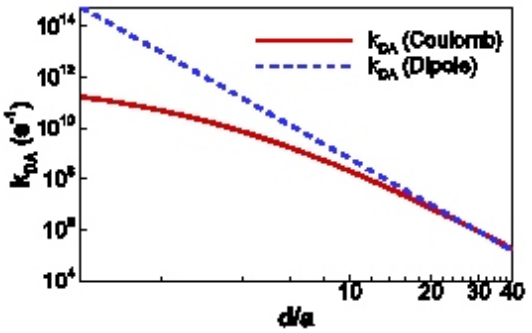

Fig. 2 The distance (d) dependence of the rate of energy transfer (k_{DA}) calculated using full Coulomb interaction (solid line) and the dipole-dipole approximation (FÖrster theory) (dashed line) for the parallel orientation for a nanoparticle of size (a) 3 nm.

nanoparticle. These considerations show that for a nanoparticle in the range of 5-30 nm radius, the l=1 (dipolar mode) is the predominant accepting mode for energy transfer with a dye emitting in the visible range from 500-600 nm (absorption spectrum of gold nanoparticles lie in this range).

Distance Dependence of Rate of Energy Transfer

The rate of energy transfer is calculated for both: the full Coulombic interaction and the dipole approximation using Eq. 2 where H_I is given by Eq.9 and Eq. 10 respectively. Fig. 2 illustrates that the rate of energy transfer (k_{DA}) is FÖrster type ($1/d^6$) at large separations compared to the radius of the nanoparticle. However, at small separations (d < 20a), it breaks down and at distances approximately d=a to d=4a, the rate varies as (1/d) where lies between 3 and 4. In a recent experimental study, Strouse et al. found that the rate of energy transfer from a dye, a FAM moiety, to an Au-nanoparticle (diameter = 1.4 nm) can be fitted to a ($1/d^4$) distance dependence [20]. These authors have suggested that this result may be understood as energy transfer from the dye to the surface modes of the nanoparticle - surface energy transfer (SET) [13,15]. However these theoretical studies are mainly for the interaction of a dye with a large metallic surface - surface of a metallic "half-space". Moreover our calculations show that if we plot rate of energy transfer against center to center distance R, we get ($1/R^6$) dependence over the entire range of separations. However if we plot k_{DA} against d, we find that at intermediate distances we have ($1/d^4$) dependence but asymptotically the rate dependence on distance is still FÖrster type.

Orientation Dependence of Rate of Energy Transfer

Because of the spherical symmetry of the nanoparticle, the orientation dependence is markedly different from that in two-dye system. In the latter case, depending on angle (defined as the angle between R and dye molecule, both being in the same plane), the normalized rate ($k_{DA}/k_{DA[max]}$) varies from 0 to 1 [24]. If the dyes are oriented perpendicular to each other with the dipole of one of them oriented along R (this corresponds to $=0^o$ for one dye and $=90^o$ for the other), then there is no energy transfer. On the other hand, when the dyes are parallel to each other, $k_{DA}/k_{DA[max]}$ is either 1 (both $=0^o$) or 0.25 (both $=90^o$). The scenario is different in case of nanoparticle-dye system. At large separations (d a), where the dipolar interaction Eq. (10) is accurate, the orientation dependence of the rate of energy transfer is governed solely by the

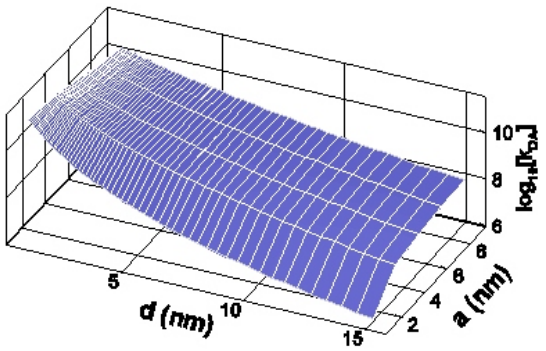

Fig. 3 Dependence of the rate of energy transfer on the orientation of the dye dipole moment $_D$ with respect to $\hat{d}$ [unit vector corresponding to $\hat{d}$ (see Fig. 4)]. The result shown is for a gold nanoparticle of radius 1 nm, calculated using the full Coulombic interaction Eq. (9)

second term ($_D.\hat{d}$)($_A.\hat{d}$). Since, the matrix element of $_A$is parallel to that of $_D$, it follows that the orientation dependence of the rate is completely determined by the angle between the donor dipole and the vector $\hat{d}$. Further, it follows that, in contrast to the conventional FRET, there is no orientation that forbids energy transfer, and at large separation the ratio of the largest rate of transfer to the smallest rate of transfer approaches 4. Interestingly, the orientation dependence becomes weaker at smaller distances (see Fig. 3).

Dependence of Energy Transfer Rate on the Size of Nanoparticle

The energy transfer rate from a nanoparticle to a given dye is governed by Coulombic overlap integral Eq. (3), the position (surface plasmon frequency) and width (inverse surface plasmon lifetime) of the absorption spectrum of the nanoparticle relative to those of the dye. For a given dye, all the three are, in general, functions of the nanoparticle size. We briefly discuss the size dependence at large separation distances (d,a). For large nanoparticles (a ~7 nm) since the plasmon frequencies are, to a very good approximation, independent of the size. Therefore, the energy transfer rate at large distances for large nanoparticles is determined entirely by the Coulombic overlap integral which we find to be proportional to the volume of the particle. For small nanoparticles both the plasmon frequency and lifetime depend on the size of the particle, hence the overlap of the absorption spectrum of the particle with the emission spectrum of the dye also contributes towards the size dependence of the rate. We have not studied the plasmon lifetime (inverse width of the absorption spectrum) in this work. Approximating the width of the absorption spectrum to be size independent (size dependence of the absorption spectrum has been studied using a time dependent density functional theory, for example, in Ref. 23), we have calculated the size dependence of the transfer rate at various distances as a function of nanoparticle size (see Fig. 4). These results agree with the asymptotics discussed above. Moreover, we find, interestingly, that at small separation distances, the energy transfer rate can even be non-monotonic with respect to the particle size (for small particles). A more detailed study including the size dependence of plasmon lifetimes is necessary to uncover the complete picture.

In brief, the present discussion addresses the important issues of distance and orientation dependence of the rate of excitation energy transfer from a dye to a metal nanoparticle. The results presented here show that for most applications of FRET involving metal nanoparticle, the energy transfer shall involve surface plasmons and the asymptotic distance dependence remains FÖrster-type, although $1/d^6$ dependence breaks down at separations < 20a. The orientation factor varies from 1 to 4 as the dye molecule is rotated along the dye-nanoparticle axis from the perpendicular to the parallel orientation. The formalism adapted predicts an asymptotic a^3 size dependence of the rate of energy transfer. The present formalism can be easily extended to address the problem of energy transfer between two nanoparticles of different sizes or different metals as is discussed in the next section. The details of the study discussed in present section can be found in Ref. 21.

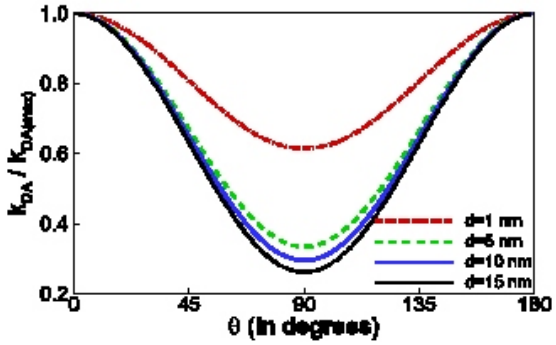

Fig. 4 Energy transfer rate as a function of the radius (a) of the nanoparticle and the distance (d) between the nanoparticle and the dye.

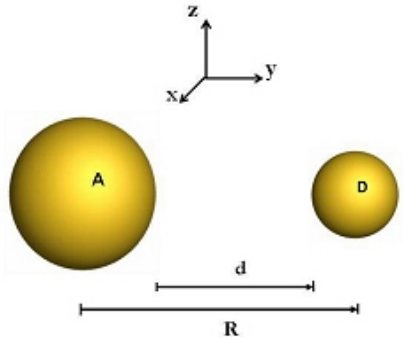

Fig. 5 A schematic illustration of the RET system involving two nanoparticles. The figure shows the coordinate system employed in calculation.

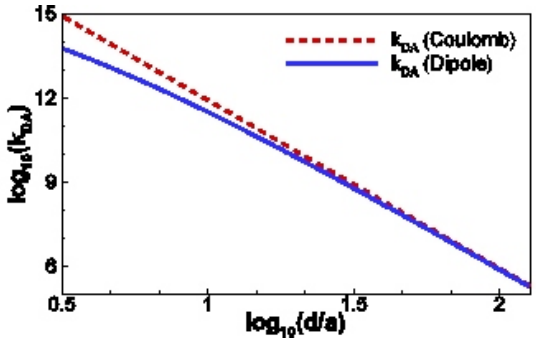

Fig. 6 The distance (d) dependence of the rate of energy transfer between two nanoparticle. The radius of the donor nanoparticle is taken to be 1.5 nm while that for the acceptor to be 2 nm. Note that the increase in size of the nanoparticles will not change the qualitative dependence of the rate on the distance.

Excitation Energy Transfer between Two Metal Nanoparticles

The use of nanoparticles both as donor and acceptor in resonance energy transfer significantly increases the range over which the separations can be monitored. These RET systems are popularly referred to as 'plasmon rulers'. The rate of energy transfer from one nanoparticle to the other depends on the separation between the two and the size and shape of the particles. In case of spherical particles the rate does not depend on the relative orientation of the nanoparticles. A recent experimental study demonstrated the plasmon coupling can be used to monitor separations of up to 70 nm between single pairs of gold and silver nanoparticles in vitro [10].

Here we report the results of our study on the rate of energy transfer between two nanoparticles based on the formalism discussed above. The full Coulombic interaction and the dipolar interaction Hamiltonian is again given by Eq. (9) and Eq. (10) respectively. However for full Coulombic interaction Hamiltonian both the integrations over donor and acceptor in the present case will be three dimensional.

Figure 5 shows the schematic representation of the system under study. For resonance energy transfer to take place we need to consider two different size of nanoparticle with acceptor being larger in size as compared to the donor. We consider the donor to be in first excited state corresponding to l = 1 mode while acceptor to be in the ground state i.e. no plasmon excitations. The distance dependence of the rate is shown in Fig. 6. We find that for an acceptor size of 2 nm, the rate of energy transfer in case of two nanoparticle system is greater than that for a dye-nanoparticle system. As a result large separations can be monitored with the former RET system. As discussed the rate of enegy transfer also depends on the size and shape of the nanoparticles. Though the qualitative dependence of the rate on distance will not change with the increase in the size of the nanoparticles but quantitative

behaviour will definitely change. The further details of the study will be reported elsewhere [25].

Conclusion

The success of RET as a spectroscopic ruler depends critically on our knowledge of the distance and the orientation dependence of the rate of energy transfer. The present study involving nanoparticle reveals that while asymptotically we do have a FÖrster type l/d^6 distance dependence, at short separations comparable to the size (a) and even for somewhat larger separations (4a), the rate varies as l/d with varying from 3-4. Also for two conjugated dye molecules the deviation from l/d^6 as been observed [24]. Note that d in case of dye and nanoparticle system refer to the distance from the surface to the center of the dye molecule while for two nanoparticle system it is surface to surface distance. We find that unlike in conventional FRET the ratio of rate (k/k_{max}) varies from 1 to 4 as the dye molecule is rotated along the dye-nanoparticle axis from the perpendicular to the parallel orientation. The formalism adapted predicts an asymptotic a^3 size dependence of the rate of energy transfer. We find that the range of separations that can be monitored substantially increases when "plasmon ruler" is employed. The rate also depends on the shape of the nanoparticle. However, the present study ignores the effects of vibrational relaxation in dye and also the electron dynamics. These effects will result in broadening of lineshapes which has been introduced here as an approximation. In future, we hope to extend the theory to explicitly take into account these broadening factors.

References

1. Th. FÖrster, Ann. Phys. (Leipzig) 2 (1948) 55.
2. Th. FÖrster, in O. Sinanoglu (Ed.), Modern Quantum Chemistry, Istanbul Lectures, Part III: Action of Light and Organic Crystals, Academic Press, New York, pp. 93-137.
3. L. Stryer, Science 162 (1968) 526.
4. E.A. Lipman, B. Schuler, O. Bakajin, and W.A. Eaton, Science 301 (2003) 1233.
5. T.A. Laurence, X. Kong, M. JÄger, and S. Weiss, Proc. Natl. Acad. Sci. 102 (2005) 17348.
6. B. Schuler, E.A. Lipman, and W.A. Eaton, Nature 419 (2002) 743.
7. D. Hu, J. Yu, and P.F. Barbara, J. Am. Chem. Soc. 121 (1999) 6936.
8. J.R. Lakowicz, Principles of florescence spectroscopy, 2nd ed., Kluwer Academic /Plenum Publisher , New York, 1999.
9. C. SÖnnichsen, B.M. Reinhard, J. Liphardt, and A.P. Alivisatos, Nat. Biotechnol. 23 (2005) 741.
10. U. Kreibig, and M. Vollmer, Optical Properties of Metal Clusters, Springer Publisher, Berlin, 1995.
11. C.F. Bohren, and D.R. Huffman, Absorption and Scattering of Light by Small Particles, Wiley Publisher, New York, 1983.
12. D.A. Stuart, A.J. Haes, C.R. Yonzon, E.M. Hicks, and R.P. Van Duyne, IEE Proc Nanobiotechnol 152 (2005) 13.
13. R.R. Chance, A. Prock, and R. Silbey, Adv. Chem. Phys. 37 (1978) 1.
14. W.H. Weber, and C.F. Eagen, Optics Letters 4 (1979) 236.
15. B.N.J. Persson, and N.D. Lang, Phys. Rev. B 26 (1982) 5409.
16. J. Gersten, and A. Nitzan, J. Chem. Phys. 75 (1981) 1139.
17. R. Ruppin, J. Chem. Phys. 76 (1982) 1681.
18. A. P. Alivisatos, D.H. Waldeck, and C.B. Harris, J. Chem. Phys. 82 (1985) 541.
19. E. Dulkeith, A.C. Morteani, T. Niedereichholz, T.A. Klar, J. Feldmann, S.A. Levi, F. C. J. M. van Veggel, D. N. Reinhoudt, M. MÖller, and D.I. Gittins, Phys. Rev. Lett. 89 (2002) 203002.
20. C. S. Yun, A. Javier, T. Jennings, M. Fisher, S. Hira, S. Peterson, B. Hopkins, N. O. Reich, and G.F. Strouse, J. Am. Chem. Soc. 127 (2005) 3115.
21. S. Bhowmick, S. Saini, V. B. Shenoy, and B. Bagchi, J. Chem. Phys. 125 (2006) 181102.
22. C. Kittel, Introduction to Solid State Physics, 7th ed., John Wiley and Sons, Inc.

23. E. Prodan, P. Nordlander, and N.J. Halas, Nano Lett. 3 (2003) 1411.

24. K. F. Wong, B. Bagchi, and P. J. Rossky, J. Phys. Chem. A 108 (2004) 5752.

25. S. Saini, S. Bhowmick, V. B. Shenoy, and B. Bagchi, (2006) Manuscript under preparation; Ibid. Journal of Photochemistry and Photobiology A: Chemistry (Special Issue), 2006 (In press)

NUCLEUS

The Nobel prize in chemistry for the year 1998

The Nobel prize in chemistry for the year 1998 was given jointly to Professor Walter Kohn and Professor John Anthony Pople for their revolutionary contribution in the field of quantum chemistry, viz. Prof. Kohn for his development of the density functional theory and Prof. Pople for his development of computational methods in quantum chemistry.

The experimental techniques are now being supplemented by the computer based calculations. Conventional calculations of the properties of molecules are based on a description of the motion of individual electrons. Such methods are therefore mathematically very complicated. Prof. Kohn showed that it is not necessary to consider the motion of each individual electron, the knowledge of average number of electrons located at any point in space is enough to calculate the properties of a molecule. This has led to a computationally simpler method 'The Density Functional Theory'. Calculations of large molecules became possible because of the simplicity of this method.

Prof. Kohn was born in 1923 into a middle class Jewish family in Vienna, Austria. He was inspired in physics and mathematics from his teachers Dr. Emil Nohel and Dr. Victor Sabbath. In the year 1957, he became a naturalized citizen of United States. He is currently a professor Emeritus at the University of California at Santa Barbara. He is also a member of the International Academy of Quantum Molecular Science.

Prof. Pople's major contribution was a theory of approximate molecular orbital (MO) calculations pi electron systems, which is now called Pariser-Parr-Pople method. Subsequently he developed the methods of Complete Neglect of Differential Overlap (CNDO) and Intermediate Neglect of Differential Overlap (INDO) for approximate MO calculations on three dimensional molecules. Prof. Pople has developed very sophisticated computational methods to calculate the molecular properties. These methods are based on the fundamental laws of quantum mechanics. He pioneered the design of the 'GAUSSIAN' computer program, a code for calculation of molecular properties and energetics.

Prof. Pople, born in 1925 in England, was a theoretical chemist. He moved to United States in 1960. He received his B.A. (in 1946) and doctorate (in 1951) degrees in mathematics from the Cambridge University in U.K. Interestingly his thesis is on a topic of chemistry 'The bonding structures of water'. No member of his family was involved in any scientific and technical activity. He was the first to attend a university from his family.

Compiled by A. Bhattacharya

IANCAS New Committee (2006-2008)

President
Dr. V.K. Manchanda
Head, RCD , BARC, Mumbai

Vice-Presidents
Dr. M.C. Chattopadhyaya
Univ. of Allahabad,

Dr.K.L.Ramakumar
Head, RACS, RC & I Group

General Secretary
Dr. G.A. Rama Rao
PDS, RC&IG,, BARC, Mumbai

Joint Secretary
Shri M.K. Saxena
RACS, RC&IG, BARC, Mumbai

Treasurer
Shri P.V. Joshi
RPhD, BARC, Mumbai

Joint Treasurer
Dr. (Mrs.) Veena Sagar
RACS, RC&IG, BARC, Mumbai

Editor
Dr. B.S. Tomar
RCD, BARC, Mumbai

Members
Dr. V. Venugopal (Ex-President)
Director, RC&I Group, BARC,Mumbai

Dr. P.K. Pujari (Ex-Secretary)
RCD, BARC

Dr.S.K.Agrawal
Head, FCD, BARC

Dr.H.C.Jain
Mumbai

Dr. P.C. Kalsi
RCD, BARC, Mumbai

Dr. S.B.Manohar
Mumbai

Dr.(Mrs.) Meera Venkatesh
Head, RPhD, BARC, Mumbai

Dr.Y.P.Naik
PDs, RC & I Group BARC

Dr. A. Ramaswami
Ex- BARC, Vashi, Navi Mumbai

Shri B.K. Sen
Head, PDS, RC&IG, BARC, Mumbai

Prof. Sushantha Lahiri
SINP, Kolkata

Prof. Umayoru Bhagan
S.T. Hindu College, Nagercoil

Dr.A.K.Bajpai
Govt. Model Sci. College, Jabalpur

IANCAS Outgoing Committee (2003-2005)

President
Dr.V.Venugopal
Director, RC & Group,BARC

Vice Presidents
Dr.V.K.Manchanda
Head, RCD, BARC

Dr.(Mrs.) Nilima Rajurkar
Univ.of Pune, Pune

General Secreatry
Dr.P.K.Pujari
RCD, BARC

Joint Secretary
Dr.(Mrs.) Hemlata Bagla
K.C.College, Mumbai

Treasurer
Dr.(Mrs.) Veena Sagar
RACS, BARC

Joint Treasurer
Sri P.V.Joshi
RPhD, BARC

Editor
Dr.G.A.Rama Rao
FCD, BARC

Members
Dr.S.B.Manohar (Ex.President)
Head, RCD,BARC

Dr.P.C.Kalsi
RCD,BARC

Sri R.V.Kamat
FCD, BARC

Dr.(Mrs.) Meera Venkatesh
RPhD, BARC

Dr. Raghunath Acharya
RCD, BARC

Sri V.V.Ramakrishna
FCD, BARC

Dr.R.K.Rastogi
FCD, BARC

Dr.A.V.R.Reddy
RCD, BARC

Dr.R.Swarup
Navi Mumbai

Dr V.N. Vaidya
FCD, BARC

Prof Satya Prakash
DEI, Agra

Dr G.R. K. Naidu
S.V. Univ. Tirupati

Dr Sivaprasad
BRIT, Vashi